STRUCTURAL AND BIOPHYSICAL STUDIES OF α-SYNUCLEIN: MOLECULAR INSIGHTS INTO AGGREGATION IN PARKINSON'S DISEASE

by

LIJUAN KANG

A Dissertation submitted to the

Graduate School-New Brunswick

Rutgers, The State University of New Jersey

In partial fulfillment of the requirements

For the degree of

Doctor of Philosophy

Graduate Program in Chemistry and Chemical Biology

Written under the direction of

Professor Jean Baum

And approved by

_____

_____

_____

_____

New Brunswick, New Jersey

[October, 2012]

ABSTRACT OF THE DISSERTATION

Structural and Biophysical Studies of α-Synuclein: Molecular Insights into Aggregation in Parkinson's Disease

By LIJUAN KANG

Dissertation Director:

Professor Jean Baum

α-Synuclein (αsyn), the main component of Lewy Body (LB), is the pathogenesis of Parkinson's disease (PD) as well as other synucleinopathies. αSyn is intrinsically disordered and its aggregation process is affected by sequence replacement and environment factors. In this dissertation, nuclear magnetic resonance (NMR) was employed to characterize the conformations of αsyn and its variants and Thioflavin T (ThT) fluorescence was utilized to identify aggregation kinetics. The correlation between aggregation kinetics and conformation revealed specific aggregation-prone conformations, thereby providing new insights into the molecular mechanism of αsyn aggregation and possible therapeutic targets for PD.

Investigation of key residues or regions determining the difference of aggregation between human and mouse αsyn reveals that the N terminal substitution A53T plays a key role in controlling the growth rates. The helical propensity of residues 6–31 and 50–

56 also have a good correlation with the aggregation growth rate. The low population of this aggregation-prone conformation in the equilibrium state leads to the proposal of possible selective molecular recognition mechanism for aggregation. The aggregation-prone mutant induces a population shift, which facilitates mutual conformational selection of the favored conformational states and leads to induced-fit structural rearrangement to the formation of stable fibril structures. Further studies on trifluoroethanol (TFE)-induced αsyn aggregation reveal a transient helical intermediate containing the same aggregation-prone region (residues 6–31) as human-mouse chimera proteins. Finally, the more physiological, acetylated forms of αsyn and A53T familial mutations are investigated. The study is the first identification of conformation and aggregation changes induced by acetylation on αsyn and its familial mutation. The results on the acetylated αsyn and A53T compared with the non-acetylated form confirm that the helical propensity in the particular region (residues 6–31) is important for fast αsyn aggregation.

Acknowledgements

I would like to express my great appreciation to my advisor, Prof. Jean Baum, for her continuous guidance and support. She guided me to this interesting and challenging scientific field. Without her precious advice and encouragement, my graduate research would have never been completed. In addition to research, she has also been a great mentor who provides unconditional support through my career development.

I would like to thank Prof. Ronald Levy, Prof. Sheena R. Radford, Prof. Allison E. Ashcroft, Prof. Michele Vendruscolo, Prof. David Talaga, and Prof. Masayori Inouye for their advice and insights. I also would like to thank Prof. Charalampos Kalodimos, Prof. Mary M. Mouradian for serving on the committee of the thesis proposal and defense.

I also wish to thank Dr. Seho Kim, Dr. Nagarajan Murali for their support in NMR experiments and helpful discussions, Mr. Valentin Starovoytov for his kind help with TEM, Prof. Gene Hall, Dr. David P. Remeta and Dr. Conceicao Minetti for their help with ThT fluorescence, Lucy A. Woods for collaboration in mass spectroscopy.

I am so grateful to all the former and current members of our laboratory. Dr. Yingjie Li, Dr. Jianxi Xiao, Dr. Kuen-Phon Wu and Dr. Yu-Jen Chen are acknowledged for their suggestions and advices in many aspects of my research. I'd like to thank Dr. Ana Monica Nunes, Gina M. Moriarty, Maria Janowska, Chitra Narayanan, Jackie Sikora, Robb Young, and Rayna Addabbo for their support and the joys they brought to our wonderful group.

Finally, I would like to express my deepest appreciations to my family. My mother, my father and my grandparents always encouraged me throughout graduate school. Thank you for your care and support for my whole life. My husband, Dr. Gao Shang, accompanied me going through the most difficult times, supported me in both my research and my life. I can never imagine what I would have accomplished without your love.

Table of Contents

Lists of Figures

Lists of Tables

Chapter 1 Introduction

1.1 Parkinson's Disease and α-Synuclein.

1.1.1 Parkinson's Disease.

Parkinson's Disease (PD) is a degenerative disorder of the central nervous system. The diagnostic hallmark of PD is Lewy body (LB), a cytoplasmic inclusion composed principally of α-synulein (αsyn), and the death of dopaminergic neuron cells in the substantia nigra, the midbrain. The root cause of the disease as well as the mechanism of neuron death still remains unknown. The disease was named after Dr. James Parkinson who first published the detailed description of PD in 1871 (Parkinson 1817). Motor symptoms during the early stages of the disease include tremor at rest, slowness of movement and rigidity. As the disease progresses, cognitive and behavioral problems may arise. Today, PD is the second most prevalent neurodegenerative disease in the world. It is estimated that ~0.3 % of the whole population in industrialized countries and ~1.5 million people in America are affected by PD. It is generally considered an age-related disease. The prevalence rises from 1% in populations over 60 years of age to 4% in those over 80 (de Lau and Breteler 2006). The mean age of onset is around 60 years; but 5–10% early onset PD cases begin between age of 20–50 (Samii, Nutt et al. 2004). As the global population ages, PD is expected to impose an increasing social and economic burden on our societies.

As early as the late 19th century, there was debate regarding whether the cause of PD was inherited or induced by environmental factors as discussed by the French neurologist Charcot (Charcot 1878) and English neurologist Gowers (Gowers 1888). Since then the

two opinions regarding genes versus environment took prevalence in turns as influenced by various discoveries along the way. The discovery of parkinsongenic neurotoxin known as 1-methyl-4-phenyl-1,2,3,6-tetrahydropyridine (MPTP), the exposure of which induces similar syndrome to those of PD (Langston, Ballard et al. 1983), tilted the interest to the environmental hypotheses and promoted studies on environmental toxins including pesticides (Petrovitch, Ross et al. 2002) (Tanner, Kamel et al. 2011) and heavy metals (Lai, Marion et al. 2002). The above mentioned hypotheses include free-radical hypothesis (Graham 1978), which is among the earliest theories and is still drawing great attention, excitotoxicity (Beal 1998), perturbation of energy production (Schulz and Beal 1994), nitrous oxide (Chabrier, Demerle-Pallardy et al. 1999), inflammations (Hirsch, Breidert et al. 2003; Wersinger and Sidhu 2006), etc. One decade after the discovery of MPTP, the scientific interest in PD has grown substantially from the genetic view, triggered by the discovery of several causative genes. Although most PD is idiopathic, 5–10% of patients are now known to have some forms of the disease caused by mutations of several specific genes (Lesage and Brice 2009). These genes code for αsyn (SNCA), parkin (PRKN), leucine-rich repeat kinase 2 (LRRK2), PTEN-induced putative kinase 1 (PINK1), DJ-1 and ATP13A2 (Lesage and Brice 2009). The discovery of triplication of SNCA in Spellman-Muenter kindred (most often known as Iowa kindred) implies the association of SNCA to familial PD (Singleton, Farrer et al. 2003). More significantly, wild-type αsyn itself could cause dopaminergic neuron cell death and formation of LB. Those monogenic cases directly link the genes with the molecular pathway of both familial and sporadic PD.

PD is complex; both genes and environmental factors provide insights into the pathogenesis and etiology of the disease. The molecular pathways identified directly in genetic cases or indirectly from environmental factors are crucial to understanding the molecular mechanism of PD and develop therapeutic cures. αSyn, the major component of LB, is critical to the pathophysiology of familial and sporadic PD. Recently it has attracted intensive attention and many studies have been carried out to understand its aggregation mechanism and cytotoxicity in dopaminergic neurons.

1.1.2 The pathogenic role of αsyn in PD.

Many findings implicate the role of αsyn in the pathogenesis of PD and other synucleinopathies characterized by filamentous αsyn lesions including dementia with Lewy bodies, multiple system atrophy, neuronal degeneration with brain iron accumulation type I, pure autonomic failure and REM sleep behavior disorder (Trojanowski and Lee 2003). Accumulation of evidence connecting αsyn to mechanisms underlying PD and other synucleinopathies gives rise to protein misfolding and aggregation hypothesis for the molecular mechanism shared by PD and related synucleinopathies. The determination of αsyn as the major component of LB using αsyn antibody established the critical role of αsyn in the pathogenesis of PD (Spillantini, Schmidt et al. 1997). This seminal finding, however, did not answer the causative relationship between αsyn and PD. The direct role of αsyn in the etiology of PD is revealed by genetic evidence. It was shown that early onset PD was induced in a small group of kindred by three familial mutations and SNCA gene mutiplication. A53T, occurring most frequently among the three familial mutations, was identified in

Mediterranean families (Polymeropoulos, Lavedan et al. 1997). A30P was found in a German family (Kruger, Kuhn et al. 1998) and E46K was discovered in a Spanish family (Zarranz, Alegre et al. 2004). The discovery of overexpression of αsyn due to gene triplication leading to early onset PD implicates the role of wild type αsyn in the etiology of familial PD. Therefore, the difference between wild-type and familial mutation αsyn as causative players for PD is quantitative rather than qualitative (Singleton, Farrer et al. 2003). Subsequent in vivo and in vitro studies further confirmed that αsyn plays an important role in the pathogenesis of PD and other synucleinopathies. Over-expression of αsyn and familial mutants in transgenic mice (Masliah, Rockenstein et al. 2001) and flies (Feany 2000) leads to similar symptoms reminiscent of PD. Cells transfected with αsyn followed by certain treatment might develop LB-like inclusions (Smith, Margolis et al. 2005; Bi, Zhang et al. 2011). Numerous in vitro studies on recombinant αsyn show formation of amyloid fibril and the process is modulated by familial point mutations (Conway, Harper et al. 1998) (Greenbaum, Graves et al. 2005) as well as environmental factors (Fink 2006). Therefore, these findings strongly suggest that misfolding and aggregation of αsyn is a critical component in the pathogenesis and etiology of PD and related synucleinopathies.

1.2 Structural Characterization of αSyn.

1.2.1 Synuclein family and physicochemical property of αsyn.

Synuclein is first discovered in Torpedo californica as a neuro-specific protein localized to the synapses and nuclei (Maroteaux, Campanelli et al. 1988). There are currently 250 DNA and protein sequences in the sequence databases (UniProtKB) with high homology

(sequence identity ≥30%) to αsyn. All synuclein sequences currently available can be assigned into three classes (α-, β- and γ-synuclein), which arise from three distinct genes in vertebrates (Lavedan 1998; Clayton and George 1999). β-Synuclein (βsyn) is the most conserved among the synuclein family. αSyn is the second most conserved with human and mouse αsyn sharing 95% identity. Compared to the first two proteins, γ-synuclein (γsyn) is the least conserved (Lavedan 1998). Both αsyn and βsyn are expressed predominantly in the brain and are particularly concentrated in the presynaptic termini of neurons (Jakes, Spillantini et al. 1994; Iwai, Masliah et al. 1995). γSyn has been identified in the peripheral nervous system and retina (George 2001); but its over-expression is associated with breast tumor development (Bruening, Giasson et al. 2000). In brain homogenates, αsyn mostly localizes to cytosolic fractions and also presents with membrane structures in various vesicle fraction, which suggest αsyn may be associated with synaptic vesicles (Irizarry, Kim et al. 1996; Lee, Choi et al. 2002). Recent studies have shown that αsyn may be involved in regulation of synaptic vesicle pools (Murphy, Rueter et al. 2000) and block vesicle trafficking (Outeiro and Lindquist 2003; Cooper, Gitler et al. 2006). Studies on synuclein knockout mouse strains revealed that αsyn has a role in modulation of neurotransmitter release (Liu, Ninan et al. 2004) and it appears that synucleins involved in fine tuning neuronal function rather than basic neuronal activity and viability (Chandra, Fornai et al. 2004). It has been shown that αsyn possesses typical characteristics of molecular chaperone and recent study suggests it may act as a non-classical chaperone that promotes the assembly of a SNARE-complex in neuronal synapse (Burre, Sharma et al. 2010).

Human αsyn is composed of 140 amino acid residues and can be divided into three regions (Figure 1.1). An N-terminal domain (residues 1-60) contains three familial mutation sites and includes four 11-residue imperfect repeats with a highly conserved hexamer KTKEGV like motif that forms α-helices in association with membranes (Bussel Jr., Ramlall et al. 2005). A central hydrophobic and amyloidogenic region (residues 61-95) forms the core of the amyloid fibril in αsyn fibril (Heise, Hoyer et al. 2005; Vilar, Chou et al. 2008). It is also known as the "non-Amyloid β component" (NAC) since it represents second intrinsic constitutes (~10%) in Alzheimer's plaque (Ueda, Fukushima et al. 1993). There are two additional KTKEGV like motifs residing in NAC and the interface of NAC and N-terminal region. The total of six imperfect repeats in first 95 residues result in variation in hydrophobicity and a periodicity characteristic of amphipathic lipid-binding α-helical domains of apolipoproteins (Clayton and George 1998). The C-terminal region is acidic and proline-rich (Kim, Paik et al. 2002) (residues 96-140). In the cellular environment, αsyn usually undergoes acetylation, phosphorylation and nitration modifications. It also contains three highly conserved tyrosine residues in both αsyn and βsyn (Uversky 2007). Under physiological conditions, αsyn carries nine negative charges with a pI of 4.7.

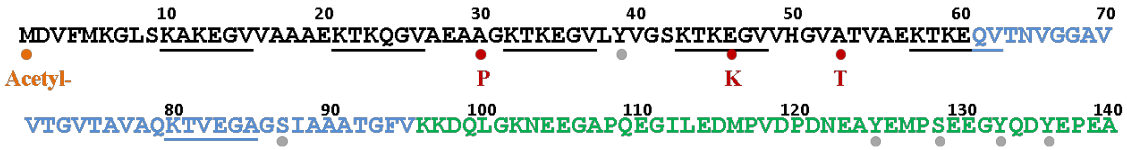

Figure 1.1 Human αsyn sequence and domains. N-terminal region is shown in black, NAC region is shown in blue, C-terminal region is shown in green. The six KTKEGV like motifs are underlined. Acetylation site is indicated by the orange dot. Familial mutations are indicated by the red dots. Phosphorylation and nitration modifications are indicated by the grey dots.

1.2.2 The intrinsically disordered state and NMR characterization.

Due to the absence of significant secondary structural propensity, αsyn is determined to be an intrinsically disordered protein (IDP) or natively unfolded protein under physiological conditions (Weinreb, Zhen et al. 1996). In contrast to the traditional paradigm relationship of 3D structure and function, IDPs or intrinsically disordered regions in the absence of 3D structure have been shown to perform numerous biological functions including molecular recognition, molecular assembly, protein modification and entropy chain activities (Dunker, Brown et al. 2002; Dunker, Silman et al. 2008). Early studies have shown that αsyn exhibits spectra of typical unfolded polypeptide with no or low content of secondary structure by far-UV circular dichroism (CD) and Fourier transform infrared spectroscopy (Uversky, Li et al. 2001). Analytical ultracentrifuge results show that αsyn sediments slower than its globular protein counterpart, which suggests αsyn is not compact (Weinreb, Zhen et al. 1996).

Fortunately, by employing NMR spectroscopy the more detailed, residue specific characteristic of αsyn is revealed. NMR is a powerful tool for investigation of IDPs and

opens a new era in characterizing them. The application of NMR in the investigation of αsyn conformational state has provided unparalleled atomic information. Pulse-field gradient NMR has shown that the hydrodynamic radius of αsyn is slightly more collapsed than a random coil of the same length (Morar, Olteanu et al. 2001), which suggests that compared with random coil, αsyn exhibits some residual structure (Uversky, Li et al. 2001). High-resolution NMR studies of ^{13}carbon chemical shifts has revealed secondary structure propensities in αsyn. Although αsyn is mostly unfolded, it exhibits a small helical propensity in the N-terminal region (Eliezer, Kutluay et al. 2001). Intra-molecular paramagnetic relaxation enhancement (PRE) experiments have shown long-range contact profiles of αsyn (Bertoncini, Jung et al. 2005). Inter-molecular PREs have determined the transient head-to-tail inter-molecular interactions (Wu and Baum 2010). ^{15}N backbone relaxation, which provides motional information of ps-μs and μs-ms timescale, has been used to reveal local clusters in the study on human and mouse αsyn at low temperature (Wu, Kim et al. 2008). Residual dipolar coupling have been used for defining local structural elements (Mohana-Borges, Goto et al. 2004) as well as long-range contacts (Bernado, Bertoncini et al. 2005; Salmon, Jensen et al. 2012). All these NMR experiments have been applied in the characterization of αsyn and its mutations under various conditions.

1.2.3 αSyn amyloid fibril structure.

αSyn amyloid fibril, the final disease state of aggregation, has also been well characterized. Amyloid fibrils share a common characteristic, which is a helical array of the β-sheet parallel to the long fibril axis with the β-strand perpendicular to this axis

despite the sequence and conformation of precursor protein (Serpell, Berriman et al. 2000). αSyn fibrils separated from the substantia nigra of PD patients displayed straight unbranched fibrils with a width of 5–10 nm and a length of 200–600 nm as determined by transmission electron microscopy (TEM) (Crowther, Daniel et al. 2000). Atomic force microscopy (AFM) image of αsyn fibrillation reveals three fibrillar species: protofilament ~3.8 nm, protofibril ~6.5 nm, and fibril ~9.8 nm. Fibrils are formed by intertwined protofibrils, which are formed by intertwined protofilaments. Both protofibrils and fibrils are present in the final mature phase (Khurana, Ionescu-Zanetti et al. 2003). Later high-resolution cryogenic electron microscopy (cryo-EM) indicates consistent results to AFM study (Vilar, Chou et al. 2008). The fully extended αsyn (~51nm), which is at least five times the fibril diameter and at least 10 times the protofilament diameter (Uversky, Li et al. 2001), would not satisfy the fibril dimension determined by EM and AFM. Thus, αsyn needs to be folded or part of the molecule is involved in fibril core or both to satisfy the fibril dimensions. Site-directed spin label electron paramagnetic resonance revealed that the αsyn fibril core is arranged in a parallel, in-register structure from residues 38–95 (Chen, Margittai et al. 2007). Studies by Vilar et al. showed the detailed residual specific information of αsyn fibrils by combination of hydrogen/deuterium exchange and solid-state NMR (Vilar, Chou et al. 2008). The fibril core ranges from residue 30–110 containing five β-strands with the N-terminal's ~30 residues heterogeneous and the C-terminal's ~30 residues flexible. Based on these results, the αsyn aggregation process involves structural rearrangement, folding and molecular association of the intrinsically disordered αsyn to a cross-β fibril structure.

1.3 αSyn Aggregation.

αSyn aggregation is a process where the unfolded monomer converts into cross-β structure amyloid fibrils. The initial stage of the dynamic ensemble of unfolded monomers (Eliezer, Kutluay et al. 2001) and the final stage of ordered amyloid fibrils (Vilar, Chou et al. 2008) have been well characterized, however, the conversion of αsyn from unfolded monomer to amyloid fibril is still not well understood. It has been proposed and demonstrated that transient oligomers (Wu and Baum 2010; Winner, Jappelli et al. 2011) and protofibrils (Lashuel, Petre et al. 2002) are present during αsyn aggregation (Figure 1.2A). Fibril formation is a complex process which involves the interplay of the microscopic processes of nucleation, elongation and fragmentation (Knowles, Waudby et al. 2009). At the macroscopic level, this phenomenon is typically characterized by the presence of a lag phase followed by an exponential growth phase and a final stable mature phase.

In vitro studies of αsyn are usually monitored by Thioflavin T (ThT) fluorescence (Figure 2B). ThT binds to the amyloid fibril not the monomer and gives a distinct spectral shift upon binding (Khurana, Ionescu-Zanetti et al. 2003). By monitoring fluorescent signals, the aggregation processes usually exhibit a sigmoidal shape. Two macroscopic parameters, apparent growth rates and lag time, are used to examine the aggregation process. However, they only approximate the microscopic processes of nucleation and elongation. NMR is a powerful tool to reveal the residue-specific information of intrinsically disordered proteins (Dyson and Wright 2004). A number of approaches have been developed to characterize secondary structural propensity and long range interactions including analysis of ^{13}C chemical shift, intra-molecular and inter-molecular

paramagnetic relaxation enhancement, residual dipolar couplings for partially folded states and disordered state at equilibrium state (Dyson and Wright 2004; Rezaei-Ghaleh, Blackledge et al. 2012). Computational simulation is a powerful complement to experimental studies of IDPs (Rauscher and Pomes 2010). Whereas experimental observations measure averages over the heterogeneous ensembles of protein conformations present in the sample, simulations allow one to visualize individual conformations, and thereby characterize the sub-ensembles present. Growth phase is usually measured by seeding assay and quartz crystal microbalance (QCM). Mature phase fibril morphology is usually characterized by TEM and AFM. Residue specific fibril structure is characterized by solid-state NMR and electron paramagnetic resonance (EPR).

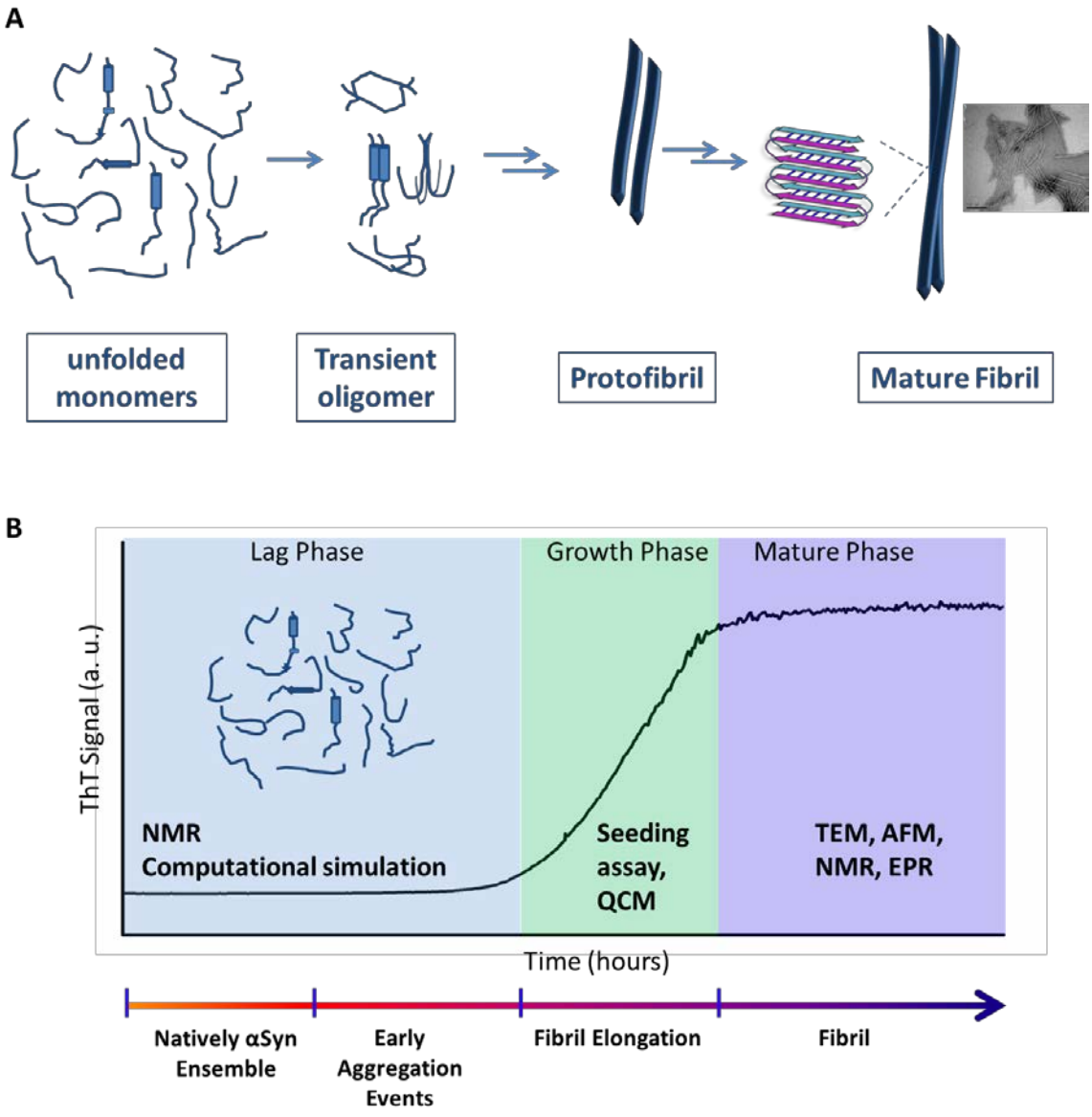

Figure 1.2 Schematic representation of αsyn aggregation. A. The possible aggregation pathway of αsyn converting from unfolded monomer to ordered fibril. B. The *in vitro* ThT fluorescence measurement of αsyn aggregation. Lag phase, growth phase and mature phase are shaded by light blue, green and purple separately. Techniques used to characterize the each phase are shown in each phase. The arrow at the bottom represents the species present in each phase.

1.4 Objectives

The relationship between αsyn aggregation and PD has been established for over a decade. With great effort of researchers, the field has grown into one of the most exciting and dynamic fields in PD research. The main focus of the field is to elucidate the molecular pathway for the conversion of αsyn from unfolded monomer to cross-β fibril structure. αSyn aggregation is a complex process. Although through years of investigation, there is consensus about the importance of the relationship between the conformational features of monomer and aggregation rates, there are still many different views on the critical conformational requirements for fibril initiation. The first section of this thesis focuses on solving this controversy by studying a carefully and systematically designed mutation set.

A few years ago, it was widely accepted that αsyn existed as IDP. Interestingly, the field experienced a heated debate last year on whether αsyn exists as a helical tetramer (Bartels, Choi et al. 2011; Wang, Perovic et al. 2011) or an unfolded monomer (Fauvet, Mbefo et al. 2012). The proposal of the tetramer made the already complex topic of αsyn aggregation even more complicated. In the midst of uncertain discussions, we have focused our attentions on the more physiological form of acetylated αsyn. The investigation of the more physiological form of αsyn will reveal important conformational and aggregation properties of αsyn which will provide insights in αsyn aggregation in the human central nervous system. The second part of this thesis focuses on the characterization of acetylated αsyn and its familial A53T variant.

1.4.1 αSyn aggregation and monomer conformational features.

Providing quantitative evidence that a direct link can be made between sequence, monomer structural propensities of αsyn and aggregation rates is critical to understanding the role of the monomer in aggregation and to deciding at which stage to target drugs for inhibition of aggregation. There is consensus that monomer conformational features are important to aggregation kinetics. However, there are conflicting proposals that the secondary structure propensities are critical to directing aggregation (Bertoncini, Rasia et al. 2007; Sung and Eliezer 2007; Abedini and Raleigh 2009; Rospigliosi, McClendon et al. 2009; Anderson, Ramlall et al. 2010) versus the view that release of long-range interactions that exposes the hydrophobic NAC region, which forms the core of the fibril, is the important aggregation initiator (Bertoncini, Fernandez et al. 2005; Bertoncini, Jung et al. 2005; Wu, Kim et al. 2008). More recently, there have been proposals that there is involvement of helical intermediates during the lag phase and that stabilization of helical conformations may accelerate the formation of β-sheet rich structure (Kirkitadze, Condron et al. 2001; Meng, Abedini et al. 2007; Williamson, Loria et al. 2009; Anderson, Ramlall et al. 2010; Sivanandam, Jayaraman et al. 2011). An alternative view based on physico-chemical properties such as the electrostatic charge and hydrophobicity (Chiti, Stefani et al. 2003; DuBay, Pawar et al. 2004; Rivers, Kumita et al. 2008; Brorsson, Bolognesi et al. 2010) suggests that for a disordered protein the local aggregation propensity within the amino acid sequence determines the aggregation rate irrespective of any transient structure observed in the monomeric form.

The controversy can only be resolved by a careful systematic analysis of the monomer conformational features and their relationship to aggregation kinetics. Design of mutations based on aggregation properties will provide information about the molecular

mechanism of αsyn fibril formation. Mouse αsyn, which differs from human αsyn at only seven positions, has been shown to form fibrils faster than human αsyn in previous studies (Rochet, Conway et al. 2000). However, the details of fibril assembly kinetics and the basis for the sequence dependent differences in fibrillation between human and mouse αsyn were not completely understood on. In the first part of my thesis work, a systematic set of human-mouse chimeras have been designed to pinpoint the residues or regions of the protein that result in faster fibrillation and are most sensitive to amino acid substitution. Then detailed NMR structural studies are carried out in order to reveal the relationship between the conformational properties of the monomers and the aggregation kinetics.

1.4.2 Acetylated αsyn and familial A53T mutation.

While a large body of evidence over many years has supported the characterization of αsyn as an intrinsically disordered monomer, a recent study by Bartels, et. al., in which αsyn was isolated from red blood cells, as well as neuronal and non-neuronal cell lines, reported that in its physiological form αsyn exists as a helical tetramer that is resistant to amyloid formation and has a mass corresponding to the sole modification of the monomer by an acetyl group (Bartels, Choi et al. 2011). Shortly thereafter, a GST recombinant αsyn protein purified from the micellar reagent ß-octyl glucoside (BOG) similarly showed the existence of a dynamic αsyn tetramer (Wang, Perovic et al. 2011). In response to these papers, Fauvet, et al. and an assemblage of groups went on to demonstrate that αsyn isolated from rodent and human nervous system tissues, and erythrocytes presents as an intrinsically disordered monomer. In this work, Fauvet, et al. was the first to address the role of the acetyl group, referred to in the Bartels paper, and

showed the acetylated and non-acetylated proteins migrate similarly on non-denaturing gels (Fauvet, Mbefo et al. 2012). A follow up report by Rhoades has indicated that recombinant acetylated αsyn (Ac-αsyn) is monomeric under physiological conditions; but that it may display a greater preference for helical structure and higher-order oligomerization states when purified in the presence of BOG (Trexler and Rhoades 2012).

It has been demonstrated that the soluble and insoluble fractions of brain tissues from patients suffering from Parkinson's and from dementia with Lewy bodies universally contain N-terminal Ac-αsyn.(Anderson, Walker et al. 2006; Ohrfelt, Zetterberg et al. 2011) While an uncommon modification to prokaryotic proteins, the N-termini of eukaryotes are often processed at the initiating amino acid with the addition of an acetyl group by N-acetyltransferase complexes (Polevoda and Sherman 2003). The role of N-terminal acetylation, however, is poorly understood, but has been suggested to affect the kinetic or thermal stability of proteins (Polevoda and Sherman 2000; Arnesen 2011). Because N-terminal Ac-αsyn is now believed to be the physiologically relevant species in the brain, it is critically important to characterize the conformational properties and fibrillation kinetics of this protein in order to understand how acetylation impacts on the mechanism of fibril formation and disease.

The second part of this thesis work focuses on the characterization of the acetylated αsyn and the comparison of its secondary structural propensity and the aggregation behavior with the non-acetylated αsyn. The acetylated familial mutation A53T is also characterized and compared to both its non-acetylated counterpart and the acetylated

αsyn. The results reveal intriguing insights about the function of acetyl group and interesting conformational features that are critical to aggregation kinetics.

1.5 Scope of this dissertation.

In this dissertation, sequence and environmental effects on αsyn aggregation have been investigated by various biophysical techniques. The main objective is to correlate aggregation kinetics changes to alterations in monomer conformational features induced by sequence or environmental factors, furthering our understanding of the molecular mechanism in PD and shedding light on the development of therapeutic targets for PD. Chapter 2 describes protocols to make αsyn and its variants, methods characterization of fibril assembly characterization and NMR strategies for structural and dynamic studies. Chapter 3 focuses on investigating key residues responsible for different aggregation properties of human and mouse αsyn with a systematically designed set of human-mouse chimera. Chapter 4 extends to conformations that are critical to increased aggregation kinetics in human-mouse chimera. Chapter 5 describes a detailed structural and dynamic study of trifluoroethanol induces helical intermediate, which could be on fibril pathway. Chapter 6 focuses on the effect of acetylation, a common eukaryotic co-translational modification, on αsyn and familial mutation A53T's aggregation and structural propensities. All the studies, which are concluded in Chapter 7, focus on conformational changes induced by sequence and environmental factors and ultimately the molecular mechanism of αsyn aggregation and PD.

Chapter 2 Methods, Materials and Experimental Procedures.

This chapter describes experimental procedures for site-directed mutagenesis, protein expression, and purification. For purification, recent suggestion that the boiling step denatures the αsyn leads to the comparison of 'mild' and 'harsh' purification methods. In this chapter, only the classic 'harsh' method is described. The advocate of 'mild' purification was accompanied the new interesting molecular target acetylated αsyn, the 'mild' purification method is described in Chapter 6.2.2.1. The study shows that αsyn purified from both 'mild' and 'harsh' purification has the same conformations (Chapter 6.2.2). Nuclear magnetic resonance (NMR) experiments including triple resonance assignment, ^{15}N relaxation dynamics, paramagnetic relaxation enhancement, residual dipolar couplings and pulse field gradient diffusion measurements are described. Methods for examining fibril assembly including Thioflavin T (ThT) fluorescence which measures fibril assembly kinetics and transmission electron microscopy (TEM) which examines fibril morphology are described.

2.1 Site-Directed Mutagenesis.

A pT7-7 plasmid containing human α-synuclein (αsyn) sequence (kindly supplied by Dr. Peter T. Lansbury) was used to overexpress αsyn in E. coli. In vitro site-directed mutagenesis is a valuable technique for studying structure-function relationship by introducing mutations to protein sequence.

2.1.1 Material and Instruments.

Accuprime Pfx DNA polymerase, rxn mix, 1 kb plus DNA ladder were purchased from Invitrogen. DpnI digestion enzyme was purchased from Invitrogen or New England Biolabs. QIAprep Miniprep was purchased from QIAGEN. Thermal cycler was purchased from Biometra.

2.1.2 Protocol.

1. Mutagenic primer: The online tool PrimerX (Lapid and Gao) is used to design primer and the primer was synthesized by GENEWIZ, Inc.
2. PCR:

Table 2.1. PCR protocol

Component	Volume	Final Conc.
10X AccuPrime Pfx rxn mix	5 µL	1X
Primer mix (10 pmol/ul)	1 µL+1 µL	0.3uM each
Template DNA (10 pg-200 ng)	1 µL	As required
AccuPrime Pfx DNA polymerase	0.4~1 µL	1.0-2.5 units
dH_2O(autoclave)	to 50 uL	

PCR thermal cycling:

Lid :105 °C (not too tight)

Initial denaturation: 2min 95 °C

Cycles (18)

a) seg 01min 95 °C

b) seg 01min 58 °C (usually 10 °C below the melting temperature calculated by IDT).

c) seg 10min 68 °C

Final extension 10min 68 °C; Final hold 4 °C; Total time: 3hr 52min

3. Use DpnI to digest the amplification products. Amount 1µL for at least 3 hr.
4. Analyze the products with and without DpnI digestion by agarose gel electrophoresis and visualize by ethidium bromide (EtBr) staining: 1% agarose gel with EtBr was used with 100 V for 1 hour 10 mins
5. Transformation to DH5α competent cells:

   (1) Transfer 3 µl of DpnI-treated PCR product and add it into 100 µl competent cell(DH5α)

   Optional control : verify the transformation efficiency of the competent cells.

   (2) Leave it on ice for 2–5 min.

   (3) Heat at 42 °C for 90 s.

   (4) Leave it on ice for 2 min.

   (5) Transfer 100 µl to the plate (with 50 mg/mL ampicillin), use L-shape stick to streak cell onto plate.

   (6) Incubate at 37 °C overnight.
6. Colonies selection and purification of plasmid.

   (1) Pick 3–4 colonies and dissolve in each tube containing 5 mL LB and ampicilin.

   (2) Shake at 37 °C overnight

   (3) Use QIAprep Miniprep to purify the plasmid and send to sequencing.

7. Cell line stock

   (1) Transform the correct sequence into DE3 competent cell following the transformation method mentioned before (Chapter 2.1.2.5).

   (2) Pick 1 colony to 5 mL tube and incubate overnight.

   (3) Mix 1 mL overnight LB cell culture and 0.4 ml 70 % sterilized glycerol. A good final glycerol concentration should be 15 % ~35 %.

   (4) Invert several times to make sure the solution is homogenous and store in – 80 $^{\circ}$C freezer.

2.2 Expression of αSyn and Variants.

αsyn and variants were expressed following the published protocol (Weinreb, Zhen et al. 1996) with some modifications.

2.2.1 Materials and Instrument.

All the isotopes were purchased from CIL, Sigma-Aldrich Isotec. Stock solutions and cells were prepared as follows:

1. –80 $^{\circ}$C stocked cell line (now, all αsyn and variants were kept in E.coli BL21 DE3 strain with ampicillin resistance except human beta and gamma synuclein which are with kanamycin resistance.)
2. sterile LB medium or 10 X M9 minimal medium (67.8 g Na_2HPO_4, 15 g KH_2PO_4, 2.5 g NaCl)
3. 50 mg/ml Ampicillin (stock concentration, 1000X)
4. 1M IPTG (stock concentration, 2.5 g in 10 ml dH_2O, 1000X ~ 2000X)

5. 50 mg/ml Thiamin (stock concentration, 1000X)
6. UV-VIS spectrometer (Beckman DU 640), Incubator Shaker Refrigerated (New Brunswick Scientific), Centrifuge (Sorvall Super T21 from Kendro)

2.2.2 Protocol.

1. Pick small piece of –80 °C stocked E.coli cell line by 200 µL tip and transfer to 25 mL LB medium with proper (50 µg/mL) amount of antibiotics, incubate in shaker at 37 ºC with 225–250 rpm for ~9 hour.
2. Prepare 500 mL sterile LB medium with proper antibiotics and transfer the overnight cultured E.coli BL21 DE3 strain to the 500 mL medium. Still incubate the E.coli in shaker, 37 °C with 225–250 rpm rate for several hours.
3. About 4 hours, check the optical density (OD) by using UV-VIS spectrometer. The measurement is done in wavelength 600 nm and distilled water is used as a blank. To do over-expression, when the OD_{600} values reach to 0.6 to 1.0, add IPTG to the culturing medium. The final concentration of IPTG is 0.50 – 1 mM . Keep the culturing medium in shaker with same temperature and same agitation speed for another 4 hours.
4. 4 hours after adding IPTG, collect the E.coli pellet by centrifugation with 8500 rpm for 15 minutes at 4 °C. For LB medium, supernatant looks like light beer and discard the supernatant solution to sink. Keep the pellet at –80 °C freezer to disrupt the cell wall for protein purification.

For ^{15}N and/or ^{13}C labeled sample, change step 2 in Chapter 2.2.2 to the following step:

1. Add 1 mL 1M $MgSO_4$, 50 uL 1M $CaCl_2$, 0.5 g $(^{15}NH_4)_2SO_4$ and 0.5 g ^{13}C glucose

(or 1 g ^{12}C glucose), 500 µL ampicillin, 500 µL thiamine to 500 mL M9 medium. I have noticed that M9 medium with a pH around 7.4 express better than lower pH.

2. The LB culturing medium in step 1 in Chapter 2.2.2 has to be removed, thus do centrifugation at in 4 °C at 3000 rpm for 15 min.
3. Discard the supernatant and re-suspend the E.coli pellet by M9 medium. Transfer the E.coli to M9 medium.
4. Do steps 3 and 4 in Chapter 2.2.2 .

2.3 Purification of αSyn and Variants.

αSyn and variants were purified following the published protocols with some modifications (Weinreb, Zhen et al. 1996).

2.3.1 Materials.

Required buffers are prepared as follows:

a. Lysis buffer: Phosphate saline buffer (PBS) : 10 mM Na_2HPO_4, 1.8 mM KH_2PO_4, 137 mM NaCl, 2.7 mM KCl, pH 7.4.
b. Ion exchange (IEX) buffer: Buffer A: 25 mM Tris-HCl, pH 7.7; Buffer B: 25 mM Tris-HCl and 500 mM NaCl, pH7.7
c. Emulsiflex C5 Homogenizer (AVESTIN), Centrifuge (Sorvall Super T21 from Kendro); Dialysis bags (Spectrum Laboratories), FPLC (GE healthcare), Anion exchange column Hitrap Q 5 mL (GE healthcare). All chemicals are purchased from Sigma.

2.3.2 Protocol.

1. Take the bottle having cell pellet from –80 °C freezer and run the bottom of bottle under tap water for a few minutes to thaw the pellet. Then take the cell pellet to the 50 mL falcon tube and add 30 ml lysis buffer, mix and dissolve the pellet by stirring at 4 ºC.
2. Break up the cells: Homogenize 3 times of the solution with the pressure 10 – 15,000 psi. Or sonicate the solution by putting in steel cap on ice and do sonication using the program with around 35% amplitude and 30 sec on and 30 sec off for 15 min.
3. Run centrifugation at 4 ºC, 12500–13000 rpm for 30 min. A black line usually is observed around the pellet which represents an efficient breakup of cell walls.
4. Transfer the supernatant to the 50 mL tube or a clean flask which has dry streptomycin sulfate (10 mg/mL) and a stir bar. Mix the protein crude and streptomycin sulfate by stirring at 4 °C (cold room) for 15 – 30 min.
5. Transfer the solution in step 4 to small centrifugation tube, run centrifugation with 12500 –13000 rpm for 30 minutes at 4 °C. Keep the supernatant solution. (Now, the synuclein protein is in the solution)
6. Transfer the supernatant to the 50 mL tube or another clean flask which has $(NH_4)_2SO_4$ (0.361 g/mL) and mix the two components in 4 °C (cold room) by stirring for 30 minutes after all the $(NH_4)_2SO_4$ are dissolved.
7. Repeat step 5, run centrifugation and collect the pellet for next step. (This time, synuclein protein is in pellet.)
8. Suspend the pellet by adding 10–15 mL PBS solution and transfer the whole

solution to 50 mL tube or a clean flask for next step. Use a stir machine to facilitate dissolving the pellet. Also, prepare a beaker with 100–250 mL tap water and heat it up to ~100 °C.

9. Do double boiling by putting the flask in the boiling water for 20 minutes. Most of background proteins will be heat denatured and synuclein protein is heat stable. Then, take the tube or flask out the double boiler and wait it cool down to near room temperature.
10. Repeat step 5.
11. Collect the supernatant and transfer it to a dialysis bag to dialyze against 10–25 mM Tris buffer for next day's FPLC.
12. FPLC: further separating negatively charged αsyn using anion exchange column Hitrap Q 5 mL. Step-wise gradient is used to elute αsyn (Figure 2.1) with 30%, 50% and 100% gradient and αsyn elutes at 50%.
13. Dialysis the protein against 10–20 mM ammonium bicarbonate (NH_4HCO_3). After 4 times dialysis, collect the solution and freeze it by liquid nitrogen for lyophilization.
14. Store the lyophilized protein in –80 °C freezer.

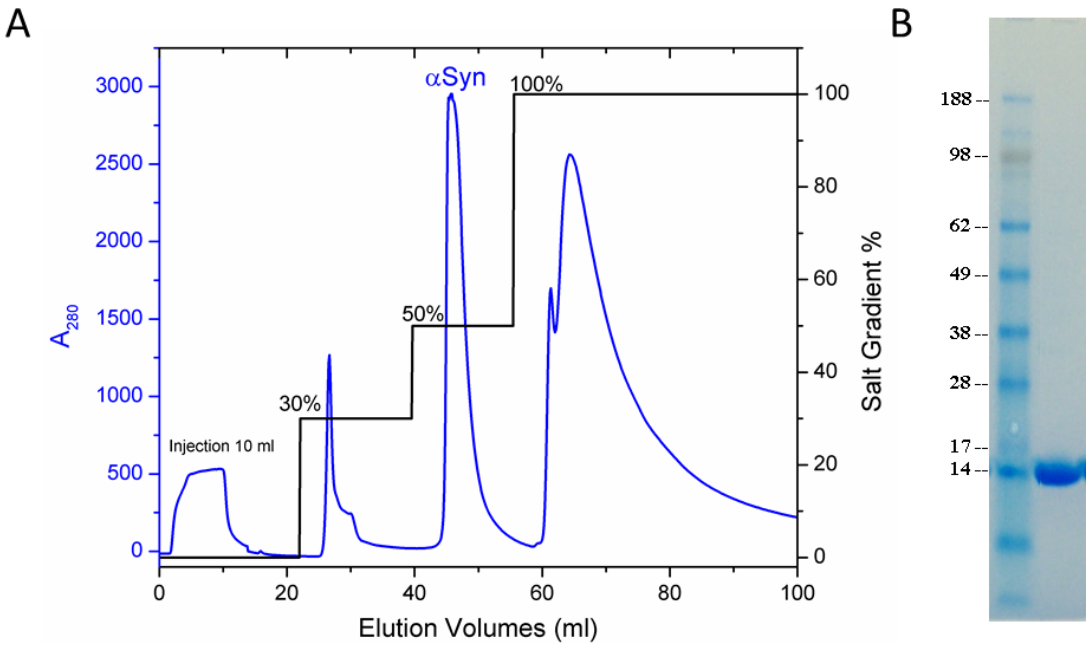

Figure 2.1 FPLC HitrapQ profiles of αsyn elution (A) and SDS-PAGE of αsyn (B).

2.4 NMR Experiments.

Here is a brief description of the NMR experiments used for characterization of αsyn and its variants, the detailed information are described in Wu, et al.(Wu 2010) .

2.4.1 NMR backbone assignment.

HNCACB/CBCACONH, HNCO/HN(CA)CO and HNN triple resonance experiments were used to obtain HN, ^{15}N ,$^{13}C^{\alpha}$,$^{13}C^{\beta}$ and ^{13}CO resonance assignments. Usually ~350 μM of ^{15}N and ^{13}C labeled αsyn or its variants in physiological condition could give good triple resonance spectrum in around 3 days with NMR parameters set up as in Table 2.2 on Varian 800 MHz and Bruker 700 MHz machine. As αsyn is unfolded with six conserved motif KTKEGV repeats, overlapping is a big problem during assignment. Conventional triple resonance experiments including HNCACB/CBCACONH,

HNCO/HN(CA)CO and HNCA/HN(CO)CA, which obtains ^{13}C-^{13}C connections of preceding (i-1) and succeeding (i) connections, could not solve the serious overlap. Hosur and his colleagues developed HNN and HN(C)N experiment which obtain ^{15}N-^{15}N connections of i-1, i and i+1 correlation and unlike ^{13}C-^{13}C connections which requires a pair of experiments, HNN or HN(C)N is capable of providing complete assignments separately (Panchal, Bhavesh et al. 2001). The combination of HNN with HNCACB/CBCACONH relieves the overlay assignment problem. NMRPipe (Delaglio, Grzesiek et al. 1995) is used to process and Sparky (Goddard and Kneller) is used for assignment.

Table 2.2 NMR parameters for triple resonance experiment

	HNCACB	CBCA(CO)NH	HNCO	HN(CA)CO	HNN
number of scans	8	8	4	8	8
number of points in ^{13}C or ^{15}N (ppm)	54	54	44	44	42
sweep width indirect ^{13}C or ^{15}N (ppm)	70	70	6	6	26
number of points in ^{15}N	32	32	32	32	36
sweep width indirect ^{13}C (ppm)	26	26	26	26	26
number of points	1024	1024	1024	1024	1024
sweep width (ppm)	9	9	9	9	9
Time (hours)	19	18	7.5	15	16

2.4.2 NMR relaxation experiments.

All NMR ^{15}N backbone relaxation data were recorded on Varian 800 MHz, Varian 600 MHz, Bruker 700 MHz, Bruker 600 MHz using different pulse sequences including longitudinal relation rate R_1 (Farrow, Muhandiram et al. 1994), transverse relaxation rates

R_2^{CPMG} (Farrow, Muhandiram et al. 1994), steady state heteronuclear NOE (Farrow, Muhandiram et al. 1994), and $^1H^N$ transverse relaxation ($^1H^N$ R_2) (Donaldson, Skrynnikov et al. 2001) (Table 2.3). Dr. Seho Kim made the in-house pulse sequence for $^1H^N$ R_2. All the data are stored as a pseudo 3D format and the interleaved FID acquired on Varian were separated using a macro written in C language obtained from Dr. Lewis Kay while the interleaved FID acquired on Bruker were separated using 'rser2d' command in Topspin. Individual FIDs were then processed by NMRPipe (Delaglio, Grzesiek et al. 1995) and was analyzed by Sparky using a single exponential decaying function plugged in (Goddard and Kneller). The detailed fitting methods are described by Farrow et al.(Farrow, Muhandiram et al. 1994).

Table 2.3 NMR parameters for relaxation experiment

Type	Relxation Time	Data Point	Recycle delay
R_1	10 – 1800 ms	≥ 9	2 s
R_2^{CPMG}	10 – 250 ms	≥ 9	2 s
NOE	3 s	2	2 s
$^1H^N$ R_2	6 – 52 ms	7	2 s

2.4.3 MTSL spin label reaction and PRE measurement.

Site-directed mutagenesis was applied on variants of interest to introduce cysteine mutations at A19C, A90C and G132C for spin labeling. A19C and G132C for wild type αsyn are made by Dr. David Fela. Detailed method was described by Bertoncini, et al. (Bertoncini, Jung et al. 2005). 5–10 mg of lyophilized cysteine variants of αsyn or its

variants was dissolved in 1–2 mL PBS (10 mM Na_2HPO_4, 1.8 mM KH_2PO_4, 137 mM NaCl, 2.7 mM KCl, pH 7.4) buffer with DTT (20 times molar ratio) for around 4 hours at 4 °C to remove all cys-cys dimers. Proteins with A19C mutation are dissolved in PBS plus 4M urea first for ~2 hours and then treated with DTT (20 times molar ratio) for ~2 hours. The sample was then injected into a desalting column (GE Hiprep 26/10 desalting) to separate αsyn or its variant and DTT. αSyn usually elutes after 10 mL and immediately after elution (1-oxy-2,2,5,5-tetra-methyl-3-pyrroline-3-methyl)-methanesulfonate (MTSL) (Toronto Research Chemicals, Ontario, Canada) is added into αsyn or its variant fraction. Spin label reaction was performed at 4 °C for o/n in dark (Wu, Kim et al. 2008) and the labeled protein was either exchanged to desired buffer or dialyzed against 10–20 mM ammonium bicarbonate (NH_4HCO_3) and lyophilized. PRE can be simply obtained by calculating the intensity ratio of cross-peaks in ^{1}H-^{15}N HSQC under paramagnetic and diamagnetic conditions. Detailed intra-molecular PRE and inter-molecular PRE are described in Chapter 4.2.3.

2.4.4 Residual dipolar coupling experiments.

The bicelle medium developed by Rukert et al. (Ruckert and Otting 2000) was used to measure RDC. C8E5 and 1-octanol are purchased from Sigma.

Preparation 10 % C8E5 stock medium with 500 µL final volume with the molar ratio of C8E5 (50 µL): octanol (14 µL) = 1.59 :

i. 50 µL C8E5 is mixed with 400 µL of PBS and 50 µL D_2O. The solution is clear.
ii. Add 4 µL of octanol solution. Vortex the mixture and the solution will be foamy.

iii. Add another 3 µL of octanol. Vortex longer than 10 min and the solution will be cloudy.

iv. Add another 3 µL of octanol. Bubbles will be generated. Vortex the solution and it will become clear.

v. Wait for at least 2 hours and double check the whether the solution is clear.

Dilute the media with PBS to the final concentration of C8E5 to 5%. Check the quadrupolar D_2O splitting Hz. The optimum value is around 22 – 25 Hz. Then mix the protein sample solution with media to reach the final C8E5 concentration of 5 %. The quadrupolar D_2O is very sensitive to pH, salt concentration, etc. If using different buffer, the molar ratio of C8E5 and octanol needs to be adjusted. It is common that RDC samples made by same protocol have different splitting Hz. Normalization based on splitting Hz are usually applied when comparing RDC data.

To obtain the RDC backbone amide protons (D^{NH}), two ^{1}H-^{15}N HSQC spectra using IPAP (in phase-anti phase) pulse train without decoupling are needed (Ottiger, Delaglio et al. 1998). One is acquired with alignment media which provides $J_{NH}+D_{NH}$, the other is not which provide J_{NH}. The subtraction of the two values will give D_{NH}.

2.4.5 Translational diffusion coefficient.

Translational diffusion coefficient were measured by Pulse-Field Gradient NMR (PFG-NMR) incorporated with longitudinal Eddy current pulse schemes and convection compensation (Li, Kim et al. 2005). Samples containing internal standard 1,4-dioxan (~ 100 time of sample concentration) are dissolved in desired buffer (e.x. PBS). 25 1D PFG-NMR spectra are acquired over a range of gradient strengths of 2 to 17 G/cm or 5 to 50

G/cm for 1,4-dioxane or αsyn, respectively. To avoid strong water signals interfering with protein signal, sample are prepared in 100 % D_2O carried out by lyophilization of desired buffer and re-dissolved in 100 % D_2O. Methyl groups (0 – 2.3 ppm) are used to perform volume integration and further analysis. Peak volumes of 1,4-dioxane and αsyn are integrated using VnmrJ (Varian, Inc.) and are used to calculate D_{trans} following the equation:

$$I = I_0 e^{-2D_{tran}\gamma^2 G^2 \delta^2 \left(\Delta + \frac{2}{3}\delta + \frac{3}{4}\tau\right)}$$

where γ is proton gyromagnetic ratio (26752.22 s^{-1} gauss $^{-1}$), δ, Δ, and τ are time delays used for data collection and factor 2 is included if pulse train of convection compensation is used. Since αsyn and 1,4 dioxane is dissolved in one solution, the viscosity effect on D_{trans} of αsyn and dioxane can be ignored in Stokes-Einstein equation, therefore D_{tran} αsyn can be calculated:

$R_h^{asyn} D_{trans}^{asyn} = \frac{k_B T}{6\pi\eta} = R_h^{dioxane} D_{trans}^{dioxane}$, where $R_h^{dioxane}$ is 2.12 Å.

2.5 Methods for examining fibril assembly.

2.5.1 Thioflavin T fluorescence assay for fibril formation.

Protein was thawed and exchanged to desired buffer using Amicon 10k MWCO centrifugal filter (Millipore) for three times or dissolved in desired buffer and buffer exchange once. The solution was filtered through Amicon 100k MWCO centrifugal filter (Millipore) to remove the big aggregates and the final protein concentration was around desired concentration (ε_{280}=5120 M^{-1} cm^{-1}) with 20 μM ThioflavinT for fluorescence measurements. 100 μL of the mixture was then pipetted into a well of the 96-well clear-bottom black-wall plate (Costar) which was compressed air (Falcon, Dust off) cleaned

before use and sealed with clear sealing film (Axygen) to prevent the evaporation during incubation. Measurements were recorded at desired temperatures with linear shaking at 600 rpm with excitation at 440 nm and emission at 480 nm. ThT fluorescence was recorded at 30-min intervals using a POLARstar Omega reader (BMG, Inc.). The data were fitted using the Boltzmann function, modified Boltzmann function (Nielsen, Frokjaer et al. 2001), linear fit (Routledge, Tartaglia et al. 2009) or exponential fit (Chiti, Taddei et al. 2002).

(1) Boltzmann function fit (Figure 2.2 A):

$$y = A2 + \frac{A1-A2}{1+e^{(x-x0)/dx}}$$

where y is fluorescence intensity, A2 is the final value, A1 is the initial value, x_0 is half time, dx width is the change in time corresponding to the most significant change in ThT value ($1/k_{app}$). Lag time is calculated by x_0-2*dx.

(2) Modified Boltzmann function fit (Figure 2.2B):

$$y = (a + bx) + \frac{c + dx}{1 + e^{\frac{x0-x}{dx}}}$$

where y is fluorescence intensity, x_0 is half time, dx width is the change in time corresponding to the most significant change in ThT value ($1/k_{app}$). Lag time is calculated by x_0-2*dx. The function is used when kinetics curve does not have classical sigmoidal curve shape, for example, the baseline or final value of sigmoidal curve is changing linearly.

(3) Linear fit. (Figure 2.2C)

All the data were first normalized to final ThT signal and the resulting curves were used for analysis of lag time and apparent growth rate. The growth rate was obtained by fitting

a line to the slope of the growth phase from 30% to 70% and the lag time was determined from intersect. The linear fit is usually used as an alternative to the modified Bolzmann fit. The function is used when kinetics curve does not have classical sigmoidal curve shape, for example, the baseline or final value of sigmoidal curve is changing and exhibit irregular shape.

$$y = ax + b$$

where y is fluorescence intensity, a is the apparent growth rate (k_{app}) and – b/a is the lag time.

(4) Exponential fit (Figure 2.2D)

Some of aggregation kinetics does not exhibit sigmoidal curves. One example is trifluoroethanol (TFE) induced human muscle acylphosphatase (AcP) aggregation(Chiti, Taddei et al. 2002). TFE induced αsyn also exhibit exponential curve and is fitted by equation as follows:

$$y = q + Ae^{-kx}$$

where y is fluorescence intensity, k value provides a quantitative measure of the apparent growth rate (k_{app}).

(5) Data normalization

The data were normalized by applying the initial value as 0 and final value as 100. The initial value is A1 for Bolzmann function fit and the beginning point for curves does not obey Bolzmann function. The final value is A2 for Bolzmann function fit and the transition point between growth phase and mature phase in other fit. The formula used for fit is as follows:

$$y = \frac{(x-A1)*100}{A2-A1}$$

where y is the normalized data, x is the raw data, A1 is the initial value, A2 is the final value.

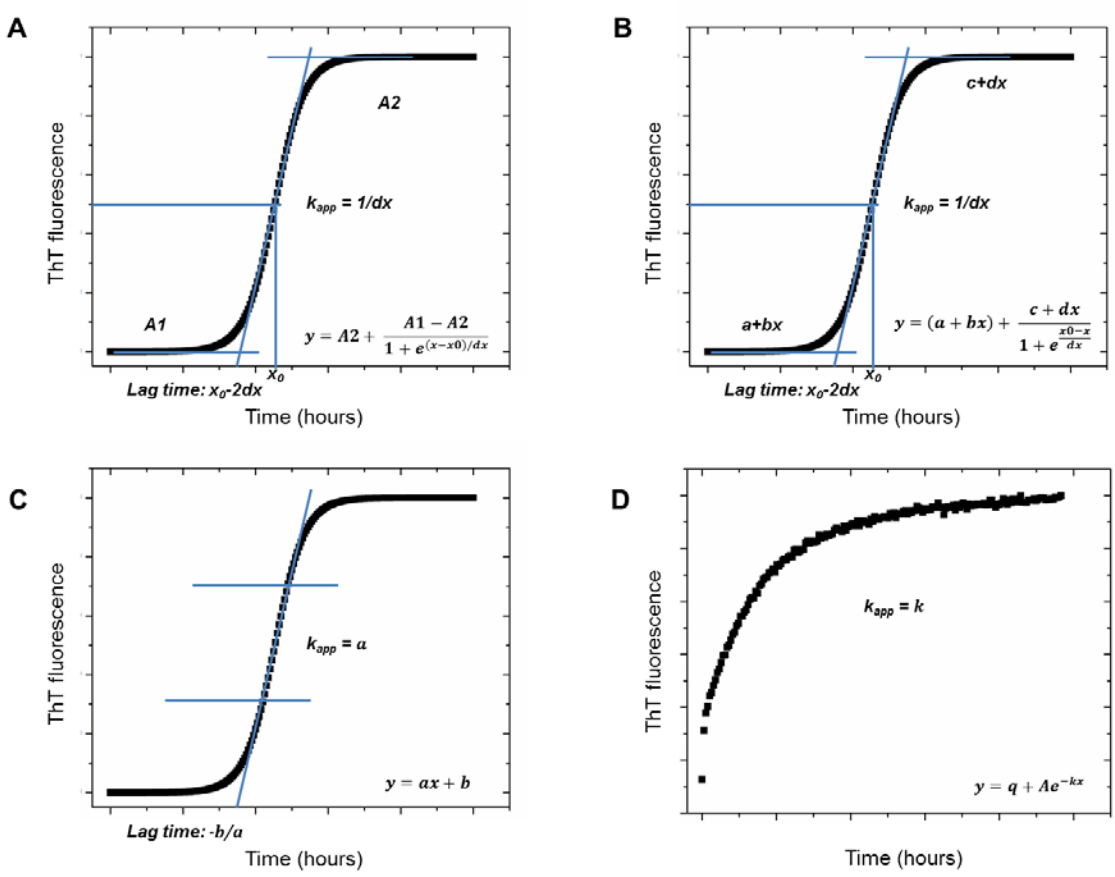

Figure 2.2. Fluorescence fitting functions. (A) Boltzmann function fit; (B) modified Boltzmann function fit; (C) Linear fit; (D) Exponential fit, especially in TFE induced αsyn aggregation.

2.5.2 Factors affecting ThT fluorescence assay.

By recording the fluorescence signal of ThT, a dye which gives a fluorescence shift by binding to fibril structure, the fibril assembly kinetics is monitored. This method is widely used for studying fibril assembly kinetics. Typically fibril assembly is a sigmoidal process with a nucleation forming lag phase, exponential increase growth phase and a

stable mature phase (Figure 2.3). ThT fluorescence assay is very sensitive to agitation, protein preparation protocol, evaporation, pre-seeding, etc. Also it has been suggested that even for indistinguishable samples, ThT fluorescence exhibited big variation, which implies intrinsic stochastic behavior of protein aggregation (Waudby 2009). Without agitation αsyn can not start fibril assembly for months. Also a big body of evidence has suggested aggregation surface such as mica surfaces, pyrolytic graphite (Hoyer, Cherny et al. 2004)and agitation material such as glass ball, Teflon ball (Pronchik, He et al. 2010) play an important role in αsyn aggregation. Shaking and stirring in quartz cuvette have been investigated and it often encounters the problem of fibrils clustering in the solution-air interface which can not be detected in the light path. After using a pipet to remix the solution, sometime fluorescent intensity can increase folds. The big variability exists in this method such as low-speed mixing, the limited number of samples which can be examined at one time (at most three or four), large protein consumption have promoted the developing of a more automated, fast-speed, efficient sample screening method. By using the fluorescence plate reader which can examine 96 samples at a time with maximum shaking speed of 1300 rpm and statistical analysis, the situation have been largely improved and at the same time it revealed the stochastic property of the fibril assembly process. For one sample that is aliquot distributed to several wells, the final ThT fluorescence value can be very different and fibril assembly kinetics can have a wide distribution.

Here is shown an example of fibril assembly of human αsyn expressed and purified using same protocol (Chapter 2.2, 2.3) (Figure 2.3). Two batches of protein purified at different times are examined and in one batch one repeat was done in different time. HHH-1-1 and

HHH-1-2 represent protein from the same batch but done in different times. HHH-2 represents protein from a different batch. The results suggest a great variability of final ThT value (Table 2.4). Samples from the same batches have similar lag times and k_{app}. However, samples from different batches display distinct aggregation kinetics with around two times faster than the other batch. The possible reason for the difference may come from the difference in small quantity of impurity existing in different batches. However, as mentioned before, for aliquots of a single sample significantly different lag times and k_{app} are observed (data not shown). Hortschansky et al. reported notable examples of stochastic kinetics for Aβ 1–40 and related peptide (Hortschansky, Schroeckh et al. 2005). The stochastic kinetics may imply many microscopic pathways during aggregation processes and more investigation on the origin of fluctuations should be carried out which may lead to important biological significance of protein self-assembly.

Table 2.4 Fibril assembly kinetics for αsyn in different time

	Lag Time	Lag (error)	k_{app}	k_{app} (error)	Used data set	Total data sets
HHH-1-1	93.51	11.12	0.07	0.01	9	12
HHH-1-2	98.12	14.27	0.12	0.06	8	9
HHH-2	53.48	15.79	0.22	0.07	12	12

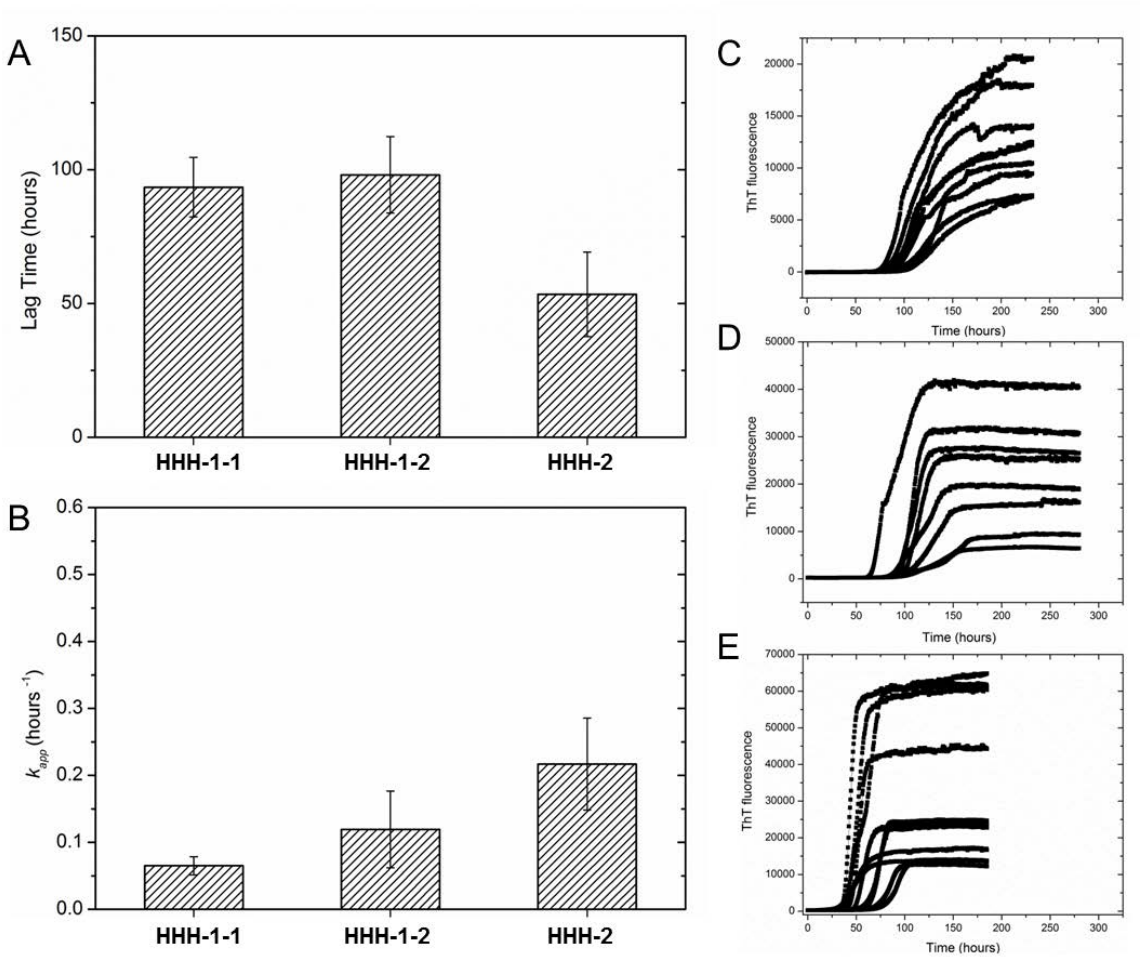

Figure 2.3 Three trials of fibril assembly kinetics of human αsyn (HHH).

HHH-1-1 and HHH-1-2 represent protein from the same batch but done in different times. HHH-2 represents protein from a different batch. A. Lag time of HHH; B. k_{app} of HHH; C. Raw fluorescence data of HHH-1-1; D. Raw fluorescence data of HHH-1-2; E. Raw fluorescence data of HHH-2.

2.5.3 Methods for examining fibril morphology by TEM.

Negative straining TEM was performed using single droplet procedure (Harris and Horne, 1991) at ambient temperature. Micrographs were recorded at a magnification of 100,000× with a JEM-100CXII manufactured by JEOL in electron imaging facility and

thanks Valentin Starovoytov for assistance with the TEM pictures. All the chemicals are purchased from Sigma.

(1) Carbon-coated FCF300-Cu grids(Electron Microscopy Sciences, Hatfield, PA) are glow-discharged overnight under UV light with shining side facing up, which renders the grids hydrophilic and adsorptive.

(2) Freshly prepare staining solutions: 1% uranyl acetate (10 mg/mL) or the molybadate solution with 5% ammonium molybadate (w/v) + 1% Trehalose (0.1% , 0.5%) in DI H_2O

(3) A drop of each vertexed sample (~5 µL, for my case, the buffer from pH 2.5 to pH 7.4) placed on a piece of parafilm or wax film. One grid with shining side down is put onto the sample droplet for one minute.

(4) Remove excess sample solution with a filter paper.

(5) Filter staining solution with 0.22 µm filter and put a staining solution droplet on parafilm or wax film.

(6) The grid with shining side down is put onto the staining solution droplet for another one minute.

(7) Repeat step 5 and dry the grid at room temperature.

Chapter 3. The A53T Mutation is Key in Defining the Differences in the Aggregation Kinetics of Human and Mouse α-Synuclein

3.1 Introduction.

Mouse αsyn, which differs from human αsyn at only seven positions has been shown to form fibrils significantly faster than human αsyn in previous studies.(Rochet, Conway et al. 2000) However, the detailed fibril assembly kinetics and the basis for the sequence dependent differences in fibrillation between human and mouse are not yet understood in detail.

In this work we designed a systematic set of human-mouse chimeras to pinpoint the residues or regions of the protein that result in faster fibrillation and are most sensitive to amino acid substitution. Kinetic measurements by ThT fluorescence experiments show that the identity of the N terminal substitution A53T plays a key role in controlling elongation rates. Furthermore, we found the presence of specific local differences in secondary structure propensity at this position, as derived from a chemical shift analysis of the monomeric forms, which suggests a link between secondary structure propensity around residue 53 and aggregation rates.

3.2 Method and Material.

3.2.1 Mutagenesis, Protein Expression and Purification.

αsyn variants were produced by site-directed mutagenesis . The method for site-directed mutagenesis, expression and purification of recombinant wild type and mutant αsyn were as previously described (Chapter 2. 1–2.3).

3.2.2 Biophysical characterization of αsyn and its aggregation.

ThT fluorescence assay, fibril morphology examination and NMR chemical shift measurement is shown in Chapter 2.5 and 2.4.1 separately.

3.3 Results and Discussion.

3.3.1 Design of human-mouse chimeras.

αSyn is an IDP characterized by a low sequence complexity, low overall hydrophobicity and high net charge.(Uversky 2003) The amino acid sequence of this protein can be divided into three regions: an N-terminal region (residues 1-60) with a highly conserved KTKEGV motif;(Weinreb, Zhen et al. 1996) a NAC region (residues 61-95) composed of a central hydrophobic region that has been proposed to be important for aggregation; and a highly acidic C-terminal region (residues 96-140). The distribution of substitutions between human and mouse is asymmetric along the sequence with a single substitution (A53T) in the N-terminal region, a single substitution (S87N) in the NAC region and five substitutions (L100M, N103G, A107Y, D121G and N122S) in the C terminal region (Figure 3.1). The A53T substitution in mouse is the same as the mutation that results in early onset disease in humans and is considered to be a reversion to residues found in lower organisms.(Rochet, Conway et al. 2000) We analyzed in this work systematic variations of the different substituting residues to provide insight into the critical residues or regions that lead to faster nucleation and elongation of mouse versus human αsyn.

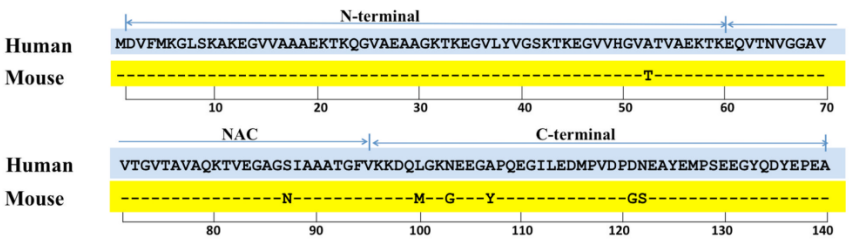

Figure 3.1. Sequence alignment of human and mouse αsyn. Conserved residues are represented by dashed lines in the mouse sequence. Residue numbers are shown below the sequence and the N, NAC and C-terminal regions are identified above the sequence.

Table 3.1. αSyn human-mouse variants.

αSyn Variants	Name
Human	HHH
Human A53T	MHH
Human S87N	HMH
Human L100M-N103G-A107Y-D121G-N122S	HHM
Human A53T-S87N	MMH
HumanA53T-L100M-N103G-A107Y-D121G-N122S	MHM
HumanS87N-L100M-N103G-A107Y-D121G-N122S	HMM
HumanA53T-S87N-L100M-N103G-A107Y-D121G-N122S (Mouse)	MMM

Sequence variants of human αsyn were designed by preparing a series of single-point mutations and domain chimeras. Starting with the human sequence as a control and denoting this sequence as HHH corresponding to human N-terminal, human NAC and human C-terminal, we prepared an additional seven variants in which each variant is composed of a combination of the three regions described above taken from mouse (M)

or human (H) αsyn (Table 3.1). The variants contain either one substitution of the human to mouse region (for example MHH, HMH or HHM) or two substitutions (HMM, MHM or MMH) or all three substitutions (MMM) corresponding to the mouse sequence. The notation M or H is used for each region independently of the number of substitutions within the region, even if the N-terminal and NAC regions contain a single substitution while the C-terminal contains five substitutions.

3.3.2 Fibril morphology of human-mouse chimeras.

All the variants were found to form amyloid fibrils (Figure 3.2.) within 8 days in a plate reader at 37 °C under linear 600 rpm shaking. Typically, for human αsyn and all the other variants, the fibril widths are around 10 nm and lengths vary from around 20 nm to 2 μm. The fibrils are always helically twisted or stuck together, however, for HMM, HHH and HHM long single fibrils prevail. Both straight and curved fibrils are observed. It is not clear whether the curved morphology is due to plasticity or the artifacts during drying on TEM grids.

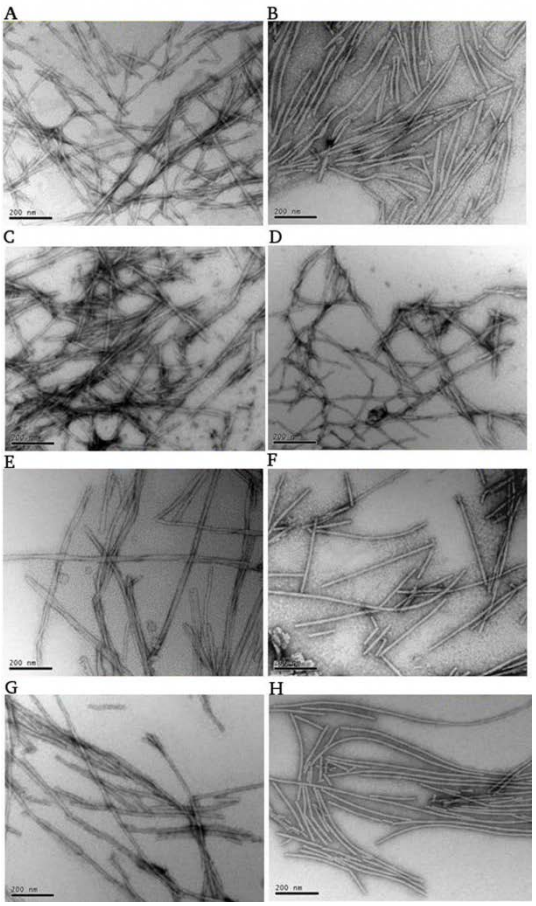

Figure 3.2 Negatively stained electron micrographs of the end products of fibril formation of the αsyn variants considered in this work. MMH (A), MHH (B), MHM (C), MMM (D), HMH (E), HMM (F), HHH (G) and HHM (H) are shown in each panel. The scale bar is 200 nm.

3.3.3 Fibril assembly kinetics: growth rates.

To assess the effect of each mutational variant on the kinetics of fibril assembly, the growth rates and the lag times of all the variants were obtained from the fibril assembly process monitored by ThT fluorescence as a probe of the aggregation process. The kinetics of all the variants were recorded with multiple replicates simultaneously under physiological conditions with shaking (See Materials and Methods). All eight variants

were measured at the same time and normalized data were used to determine the mean and standard deviation of the apparent growth rate and the lag time of each variant (Figure 3.3).

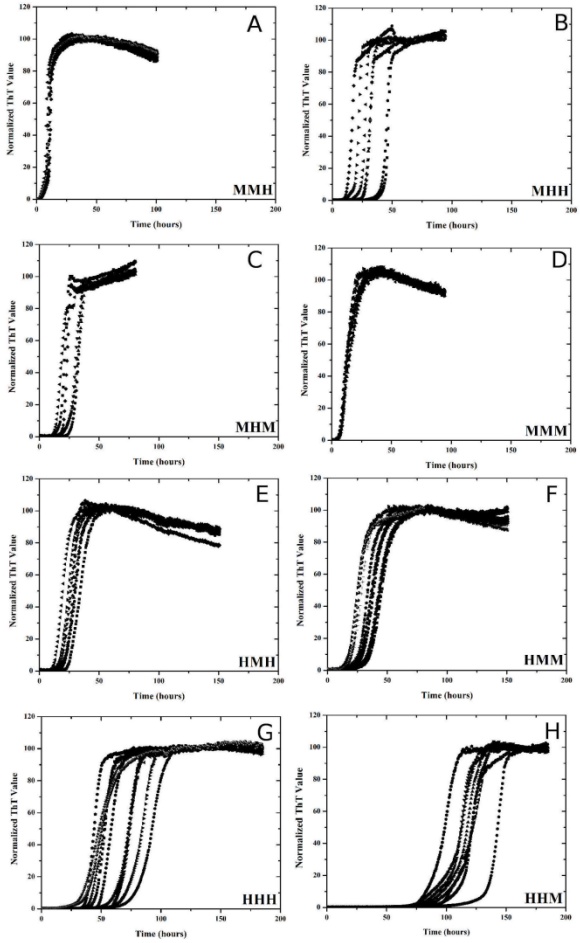

Figure 3.3 The normalized time course fibril growth curves for all the αsyn variants. MMH (A), MHH (B), MHM (C), MMM (D), HMH (E), HMM (F), HHH (G) and HHM (H) are shown in each panel.

Five-fold differences in apparent growth rates were observed for the eight variants (Figure 3.4.A.). From Figure 3.4.B., it is clear that the A53T substitution is the dominant factor in modulating the growth rates. Qualitatively the growth rates can be divided into

two groups: one group contains the human A53 residue at the N-terminal (HMH, HMM, HHH and HHM) and has slower growth rates (Figure 3.5.B); a second group contains the mouse T53 residue (MMM, MHM, MHH and MMH) and has faster growth rates. For the group containing the human A53 residue, the apparent growth rates of the four variants are very similar to one another suggesting that other substitutions within the NAC and C-terminal region do not play a role in modulating the rates of growth. For the group containing the mouse T53 residue the growth rates of the four variants have a fivefold difference across the range. These results show that the growth rates in this group are sensitive not only to the mutation at position 53, but also to the human-mouse substitutions in the rest of the αsyn sequence. The 53T variants that contain a human C-terminal sequence (MHH, MMH) have faster growth rates than the 53T variants with the mouse C-terminal sequence (MHM, MMM) suggesting that the C-terminal sequence plays a secondary role in modulating the growth when residue 53 is a Thr. In contrast, substitutions in the NAC region do not impact on growth rates in a systematic way. Taken together, these data suggest that 1) Ala at position 53 is critical to slowing down the growth rates in the human-mouse chimeras; 2) Thr at position 53 results in faster growth rates in all the cases examined; the single A53T human to mouse mutation that results in early onset disease in humans has faster growth rates than mouse αsyn suggesting that the additional NAC or C-terminal substitutions in mouse may be compensatory mutations that slow down growth rates.

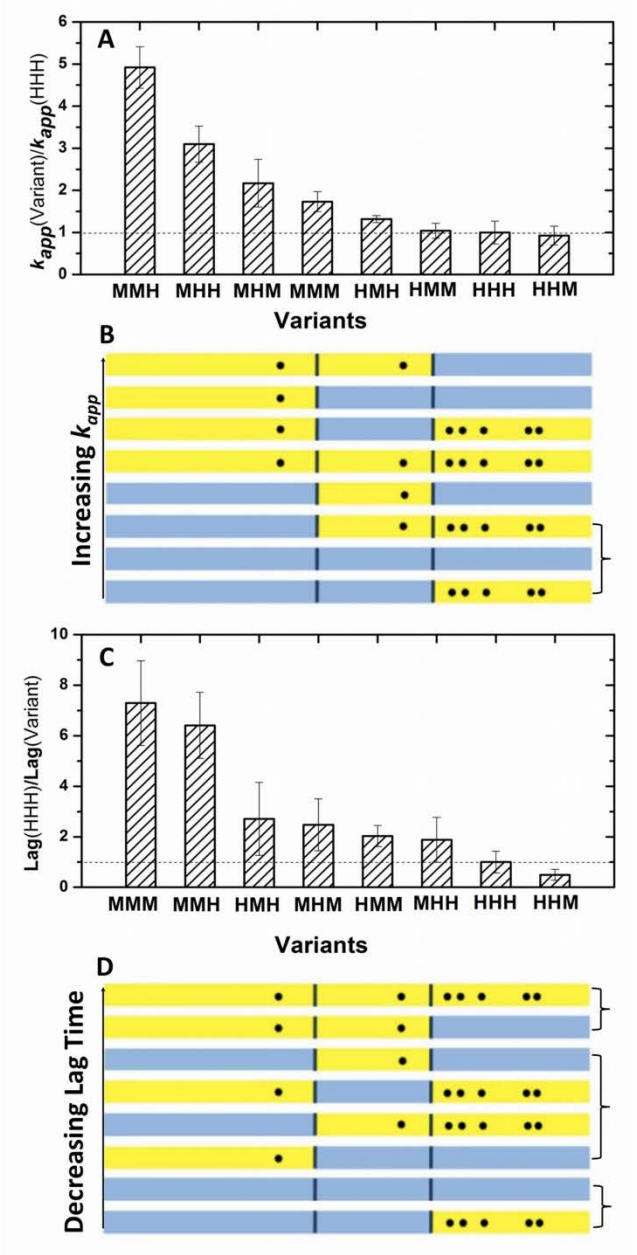

Figure 3.4. Fluorescence kinetic analysis of αsyn and its variants. (A) The ratio of apparent growth rates of αsyn variants over that of human αsyn (HHH). (B) Schematic representation of variant sequences in the order of the slowest to the fastest growth rates. The variants are color coded with the mouse region in yellow and the human region in blue. Dots represent substitutions from human to mouse αsyn. The bracket indicates the variants that have equivalent growth rates within the error bars. (C) The ratio of lag time

of human αsyn (HHH) over that of αsyn variants. (D) Schematic representation of variant sequences in order of the longest to the shortest lag time. Color code and dots are the same as in (B). The bracket indicates the variants that have equivalent lag times within the error bars.

3.3.4 Fibril assembly kinetics: lag times .

We investigated the length of the lag phase for the eight human to mouse variants. The average lag time varied from 8 to 110 hours with the shortest lag time attributed to MMM and MMH and the longest to HHH and HHM (Figure 3.4.C). Variants with intermediate lag times include HMH, MHM, MHH and HMM. The lag time results are consistent with the previous observation by Rochet et al.(Rochet, Conway et al. 2000) that mouse αsyn (MMM) has a much shorter lag time than human αsyn (HHH) and human A53T (MHH). The data presented here suggest that two regions, the N-terminal and NAC region, of the sequence play a significant role in determining the length of the lag phase (Figure 3.4.D). Qualitatively the data can be divided into three groups. The longest lag time arises when the N-terminal and NAC region simultaneously contain the human residues 53A and 87S; the shortest lag time arises when both the N-terminal and NAC region contain the mouse residues 53T and 87N. Variants that contain either human and mouse sequences in the N-terminal and NAC result in intermediate lag times. In order to determine whether simultaneous mutations of residues 53 and 87 act in synergy, a statistical analysis has been performed to see whether the lag time of MMH, for instance, is what we expect if it is assumed that the effects of the HHH to HMH and MHH to MMH substitutions are independent. In Figure 3.5, we perform a factorial analysis in which the ratios of the lag

times for the substitutions of HHH to HMH and MHH to MMH are compared. If the effects of the substitutions are independent of one another then the ratios are expected to be similar. Here the ratios are very different and the slopes connecting these points are not parallel suggesting that the simultaneous A53T and S87N substitutions have a synergistic effect on the lag time and do not act independently. Similar results are seen when comparing the ratios of variants that contain the mouse C-terminal substitutions (HHM to HMM and MHM to MMM). These data indicate that substitutions at residues 53 and 87 act in synergy if they are made simultaneously and that the sequence composition of the N terminal and NAC regions act cooperatively during the lag time.

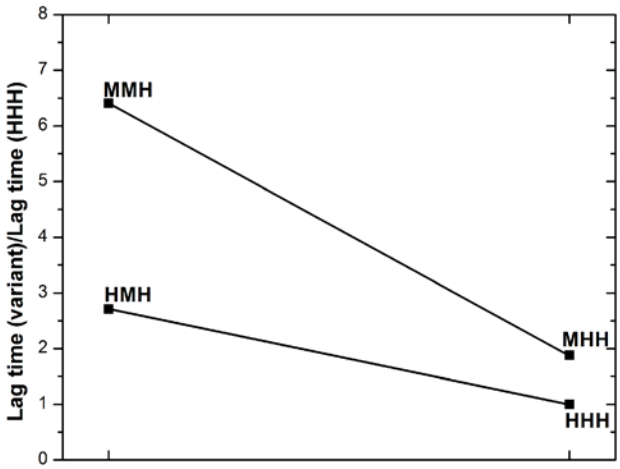

Figure 3.5. Factorial design analysis of the effect of A53T and S87N on lag time.

3.3.5 Different residues govern growth rates and lag times.

The correlation between growth rates and lag times is analyzed to provide insight into whether sequence substitutions affect these two phases similarly. A plot of the growth rates versus lag times indicates that there is no correlation between the two parameters (Figure 3.6.). Previous studies have shown that polypeptide chains such as insulin,

glucagon, Aβ peptide variants(Fandrich 2007) and β2-microglobulin(Platt, Routledge et al. 2008) have a high correlation between lag times and growth rates whereas a recent study on amyloid formation of Apolipoprotein C-II(Ryan, Teoh et al. 2010) has revealed that DHPC affects only the lag time but not the growth rate of this process. The data presented here suggest that aggregation of αsyn is complex and that different regions of the protein are involved in different stages of the aggregation process. We show that the N-terminal A53T substitution plays a dominant role in altering the growth rates but that lag time is influenced by the N-terminal A53T and the NAC S87N substitution in synergy.

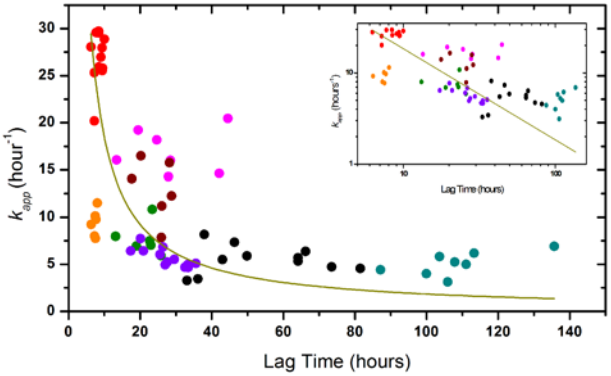

Figure 3.6. The correlation between lag time and kapp .The colors are MMH (•), MHH (•), MHM (•), MMM (•), HMH (•), HMM (•), HHH (•), HHM (•). The fit $k_{app}=a/(T_{lag})$ lead to an adjusted r-square 0.04. Inset is the log-log plot of the same data set.

3.3.6 Evolutionary assay.

To understand the functional significance of the A53T and S87N mutations we have investigated the conservation at positions 53 and 87 across different species using UniProt (www.uniprot.org) (Table 3.2). Thr is found at position 53 in many other species

including New World primates and it has been hypothesized that the T53A mutation may be an evolutionary adaptation in humans to minimize the risk of PD(Hamilton 2004). Our data support this view as A53 plays a dominant role in controlling the growth rates in human/mouse chimeras. In addition, further analysis of the 27 complete sequences from different species indicates that the A53T and S87N point mutations have less diversity than the other five residues in the C-terminal region as shown in Table 3.2. Thus the mutation in the NAC region at position 87, which has been shown in our studies to be a second key residue in minimizing the duration of the lag phase, may have functional significance. The sequence determinants of the lag times and growth rates in the αsyn human-mouse variants may provide a starting point for the design of aggregation inhibitors that target those regions of the protein.

Table 3.2 The alignment of 27 complete αsyn sequences generated by BLAST and aligned with ClustalW2. The common name and primary access number of each sequence is shown in the first column. Human and mouse αsyn are highlighted with blue and yellow separately. The seven different residues between human and mouse αsyn are marked in red.

Zebra Finch (Q4JHT6)	1	----------MDVFMKGLSKAKEGVVAAAEK	21
Zebra Finch (B5G014)	1	----------MDVFMKGLSKAKEGVVAAAEK	21
Zebra Finch (B5G015)	1	----------MDVFMKGLSKAKEGVVAAAEK	21
Island canary (Q91448)	1	----------MDVFMKGLSKAKEGVVAAAEK	21
Chicken (Q9I9H1)	1	----------MDVFMKGLNKAKEGVVAAAEK	21
Rat (P37377)	1	----------MDVFMKGLSKAKEGVVAAAEK	21
Mouse (O55042)	1	----------MDVFMKGLSKAKEGVVAAAEK	21
Common woolly monkey (P61141)	1	----------MDVFMKGLSKAKEGVVAAAEK	21
Black-handed spider monkey (P61138)	1	----------MDVFMKGLSKAKEGVVAAAEK	21
Red-chested mustached tamarin (P61147)	1	----------MDVFMKGLSKAKEGVVAAAEK	21
Common squirrel monkey (D0FH84)	1	----------MDVFMKGLSKAKEGVVAAAEK	21

Rhesus macaque (P61143)	1	----------MDVFMKGLSKAKEGVVAAAEK	21
Crab-eating macaque (P61142)	1	----------MDVFMKGLSKAKEGVVAAAEK	21
Red guenon (P61139)	1	----------MDVFMKGLSKAKEGVVAAAEK	21
Lowland gorilla (P61140)	1	----------MDVFMKGLSKAKEGVVAAAEK	21
Human (P37840-3)	1	----------MDVFMKGLSKAKEGVVAAAEK	21
Human (P37840)	1	----------MDVFMKGLSKAKEGVVAAAEK	21
Pygmy chimpanzee (P61144)	1	----------MDVFMKGLSKAKEGVVAAAEK	21
Chimpanzee (P61145)	1	----------MDVFMKGLSKAKEGVVAAAEK	21
Sumatran orangutan (P61146)	1	----------MDVFMKGLSKAKEGVVAAAEK	21
Pig (Q3I5G7)	1	----------MDVFMKGLSKAKEGVVAAAEK	21
Bovin (Q3T0G8)	1	----------MDVFMKGLSKAKEGVVAAAEK	21
Human (P37840-2)	1	----------MDVFMKGLSKAKEGVVAAAEK	21
African clawed frog (Q7SZ02)	1	----------MDVFMKGLSKAKEGVVAAAEK	21
Zebra finch (B5G012)	1	----------MDVFMKGLSKAKEGVVAAAEK	21
Japanese pufferfish (Q3LU31)	1	----------MDAFMKGFSKAKDGVVAAAEK	21
Northern pike (C1BYT3)	1	MGTGYQVLQGADCIAGFEISRAKAVNWAVMDALMKGFSKAKDGVVAAAEM	50

Zebra Finch (Q4JHT6)	22	TKQGVAEAAGKTKEGVLYVGSRTKEGVVHGVTTVAEKTKEQVSNVGGAVV	71
Zebra Finch (B5G014)	22	TKQGVAEAAGKTKEGGVYVGSRTKEGVVHGVTTVAEKTKEQVSNVGGAVV	71
Zebra Finch (B5G015)	22	TKQGVAEAAGKTKEGVLYVGSRTKEGVVHGVTTVAEKTKEQVFFVPPAVV	71
Island canary (Q91448)	22	TKQGVAEAAGKTKEGVLYVGSRTKEGVVHGVTTVAEKTKEQVSNVGGAVV	71
Chicken (Q9I9H1)	22	TKQGVAEAAGKTKEGVLYVGSRTKEGVVHGVTTVAEKTKEQVSNVGGAVV	71
Rat (P37377)	22	TKQGVAEAAGKTKEGVLYVGSKTKEGVVHGVTTVAEKTKEQVTNVGGAVV	71
Mouse (O55042)	22	TKQGVAEAAGKTKEGVLYVGSKTKEGVVHGVTTVAEKTKEQVTNVGGAVV	71
Common woolly monkey (P61141)	22	TKQGVAEAAGKTKEGVLYVGSKTKEGVVHGVTTVAEKTKEQVTSVGGAVV	71
Black-handed spider monkey (P61138)	22	TKQGVAEAAGKTKEGVLYVGSKTKEGVVHGVTTVAEKTKEQVTSVGGAVV	71
Red-chested mustached tamarin (P61147)	22	TKQGVAEAAGKTKEGVLYVGSKTKEGVVHGVTTVAEKTKEQVTNVGGAVV	71
Common squirrel monkey (D0FH84)	22	TKQGVAEAAGKTKEGVLYVGSKTKEGVVHGVATVAEKTKEQVTNVGGAVV	71
Rhesus macaque (P61143)	22	TKQGVAEAAGKTKEGVLYVGSKTKEGVVHGVATVAEKTKEQVTNVGGAVV	71
Crab-eating macaque (P61142)	22	TKQGVAEAAGKTKEGVLYVGSKTKEGVVHGVATVAEKTKEQVTNVGGAVV	71
Red guenon (P61139)	22	TKQGVAEAAGKTKEGVLYVGSKTKEGVVHGVATVAEKTKEQVTNVGGAVV	71
Lowland gorilla (P61140)	22	TKQGVAEAAGKTKEGVLYVGSKTKEGVVHGVATVAEKTKEQVTNVGGAVV	71
Human (P37840-3)	22	TKQGVAEAAGKTKEGVLYV----------VAEKTKEQVTNVGGAVV	57
Human (P37840)	22	TKQGVAEAAGKTKEGVLYVGSKTKEGVVHGVATVAEKTKEQVTNVGGAVV	71
Pygmy chimpanzee (P61144)	22	TKQGVAEAAGKTKEGVLYVGSKTKEGVVHGVATVAEKTKEQVTNVGGAVV	71
Chimpanzee (P61145)	22	TKQGVAEAAGKTKEGVLYVGSKTKEGVVHGVATVAEKTKEQVTNVGGAVV	71
Sumatran orangutan (P61146)	22	TKQGVAEAAGKTKEGVLYVGSKTKEGVVHGVATVAEKTKEQVTNVGGAVV	71
Pig (Q3I5G7)	22	TKQGVAEAAGKTKEGVLYVGSKTKEGVVHGVTTVAEKTKEQVTNVGEAVV	71
Bovin (Q3T0G8)	22	TKQGVAEAAGRTKEGVLYVGSKTKEGVVHGVTTVAEKTKEQVTNVGEAVV	71
Human (P37840-2)	22	TKQGVAEAAGKTKEGVLYVGSKTKEGVVHGVATVAEKTKEQVTNVGGAVV	71

African clawed frog (Q7SZ02)	22	TKQGVAEAAGKTKEGVLYVGSKTKEGVVHGVTTVAEKTKEQVSNVGGAVV	71
Zebra finch (B5G012)	22	TKQGVAEAAGKTKEGVLYVGSRTKEGVVHGVTTVAEKTKEQVSNVGGAVV	71
Japanese pufferfish (Q3LU31)	22	TKQGVTGAAEMTKDGVMFVGTKTKDG----VTVVAGKTVSGVSQVGGAMV	67
Northern pike (C1BYT3)	51	TKQGVTGAAEMTKDGVIFVGNKTKDG----VTTVAGKTVSGVSHVGGAMV	96

Zebra Finch (Q4JHT6)	72	TGVTAVAQKTVEGAGNIAAATGLVKKDQLAKQNEEGFLQEGMVNNTG-VA	120
Zebra Finch (B5G014)	72	TGVTAVAQKTVEGAGNIAAATGLVKKDQLAKQNEEGFLQEGMVNNTG-VA	120
Zebra Finch (B5G015)	72	TGVTAKTQKTVEGAGNIAAATGLAKKDQLAKQNEEGFLQEGMVNNTG-VA	120
Island canary (Q91448)	72	TGVTAVAQKTVEGAGNIAAATGLVKKDQLAKQNEEGFLQEGMVNNTG-AA	120
Chicken (Q9I9H1)	72	TGVTAVAQKTVEGAGNIAAATGLVKKDQLAKQNEEGFLQEGMVNNTD-IP	120
Rat (P37377)	72	TGVTAVAQKTVEGAGNIAAATGFVKKDQMGKG-EEGYPQEGILEDM---P	117
Mouse (O55042)	72	TGVTAVAQKTVEGAGNIAAATGFVKKDQMGKG-EEGYPQEGILEDM---P	117
Common woolly monkey (P61141)	72	TGVTAVAQKTVEGAGNIAAATGFVKKDHSGKS-EEGAPQEGILEDM---P	117
Black-handed spider monkey (P61138)	72	TGVTAVAQKTVEGAGNIAAATGFVKKDHSGKS-EEGAPQEGILEDM---P	117
Red-chested mustached tamarin (P61147)	72	TGVTAVAQKTVEGAGNIAAATGFVRKDHLGKS-EEGAPQEGILEDM---P	117
Common squirrel monkey (D0FH84)	72	TGVTAVAQKTVEGAGNIAAATGFVKKDHLGKS-EEGAPQEGILEDM---P	117
Rhesus macaque (P61143)	72	TGVTAVAQKTVEGAGSIAAATGFIKKDQLGKN-EEGAPQEGILQDM---P	117
Crab-eating macaque (P61142)	72	TGVTAVAQKTVEGAGSIAAATGFIKKDQLGKN-EEGAPQEGILQDM---P	117
Red guenon (P61139)	72	TGVTAVAQKTVEGAGSIAAATGFVKKDQLGKN-EEGAPQEGILQDM---P	117
Lowland gorilla (P61140)	72	TGVTAVAQKTVEGAGSIAAATGFVKKDQLGKN-EEGAPQEGILEDM---P	117
Human (P37840-3)	58	TGVTAVAQKTVEGAGSIAAATGFVKKDQLGKN-EEGAPQEGILEDM---P	103
Human (P37840)	72	TGVTAVAQKTVEGAGSIAAATGFVKKDQLGKN-EEGAPQEGILEDM---P	117
Pygmy chimpanzee (P61144)	72	TGVTAVAQKTVEGAGSIAAATGFVKKDQLGKN-EEGAPQEGILEDM---P	117
Chimpanzee (P61145)	72	TGVTAVAQKTVEGAGSIAAATGFVKKDQLGKN-EEGAPQEGILEDM---P	117
Sumatran orangutan (P61146)	72	TGVTAVAQKTVEGAGSIAAATGFVKKDQLGKN-EEGATQEGILEDM---P	117
Pig (Q3I5G7)	72	TGVTAVAQKTVEGAGSIAAATGFGKKDQLGKN-EEGAPQEGILEDM---P	117
Bovin (Q3T0G8)	72	TGVTAVAQKTVEGAGSIAAATGFGKKDHMGKG-EEGASQEGILEDM---P	117
Human (P37840-2)	72	TGVTAVAQKTVEGAGSIAAATGFVKKDQLGK----------	102
African clawed frog (Q7SZ02)	72	TGVTAVAHKTVEGAGNFAAATGLVKKDQKNES---GFGPEGTMENSENMP	118
Zebra finch (B5G012)	72	TGVTAVAQKTVEGAGNIAASHWLGEEGPVGQT-------E----------	104
Japanese pufferfish (Q3LU31)	68	TGVTAVAQKTVESAGSIAAATGLVKKEPGKQG-DDAAAPEN-MAES----	111
Northern pike (C1BYT3)	97	TGVTAVAHKTVEGAGNIAAATGLVKKDPAKQE-EDTLSKDSPVKES----	141

Zebra Finch (Q4JHT6)	121	VDPENEAYEMPPEEEYQDYEPEA	143
Zebra Finch (B5G014)	121	VDPENEAYEMPPEEEYQDYEPEA	143
Zebra Finch (B5G015)	121	VDPENEAYEMPPEEEYQDYEPEA	143
Island canary (Q91448)	121	VDPDNEAYEMPPEEEYQDYEPEA	143
Chicken (Q9I9H1)	121	VDPENEAYEMPPEEEYQDYEPEA	143
Rat (P37377)	118	VDPSSEAYEMPSEEGYQDYEPEA	140

Mouse (O55042)	118	VDPGSEAYEMPSEEGYQDYEPEA	140
Common woolly monkey (P61141)	118	VDPDNEAYEMPSEEGYQDYEPEA	140
Black-handed spider monkey (P61138)	118	VDPDNEAYEMPSEEGYQDYEPEA	140
Red-chested mustached tamarin (P61147)	118	VDP----------	120
Common squirrel monkey (D0FH84)	118	VDPDNEAYEMPSEEGYQDYEPEA	140
Rhesus macaque (P61143)	118	VDPDNEAYEMPSEEGYQDYEPEA	140
Crab-eating macaque (P61142)	118	VDPDNEAYEMPSEEGYQDYEPEA	140
Red guenon (P61139)	118	VDPDNEAYEMPSEEGYQDYEPEA	140
Lowland gorilla (P61140)	118	VDPDNEAYEMPSEEGYQDYEPEA	140
Human (P37840-3)	104	VDPDNEAYEMPSEEGYQDYEPEA	126
Human (P37840)	118	VDPDNEAYEMPSEEGYQDYEPEA	140
Pygmy chimpanzee (P61144)	118	VDPDNEAYEMPSEEGYQDYEPEA	140
Chimpanzee (P61145)	118	VDPDNEAYEMPSEEGYQDYEPEA	140
Sumatran orangutan (P61146)	118	VDPDNEAYEMPSEEGYQDYEPEA	140
Pig (Q3I5G7)	118	VDPDNEAYEMPSEEGYQDYEPEA	140
Bovin (Q3T0G8)	118	VDPDNEAYEMPSEEGYQDYEPEA	140
Human (P37840-2)	103	----------EGYQDYEPEA	112
African clawed frog (Q7SZ02)	119	VNPNNETYEMPPEEEYQDYDPEA	141
Zebra finch (B5G012)	105	----------	
Japanese pufferfish (Q3LU31)	112	--PDVTDPAEATEEDADD-----	127
Northern pike (C1BYT3)	142	--PVDTEGGNTTAEGHSDGY---	159

3.3.7 Backbone assignment of αsyn and its variants.

The ^{1}H-^{15}N HSQC of human αsyn and its variants are well resolved and the mutations effect are pretty local (Figure 3.7 and Figure 3.8). The backbone assignments of all the variants were performed using a series triple resonance experiment at 288K in physiological condition (PBS, pH 7.4). At pH 7.4 , amide hydrogen exchange rate is high which results in weaker signal for Gly and Ser residues and no observation of 1M and 2D. Overlaps were very serious for certain segments of KTK(E/Q)GV repeats and several double repeats (AA, VV, GG and EE). Although with the help of HNN experiment the amide chemical shift could be assigned, most of residues in overlapped region have the same amide chemical shift and could not be used in relaxation analysis. For all the

variant, ~ 128 resonances of 135 assignable residues have been assigned with the overlapped residues and ~ 118 resonances of 135 assignable residues have been assigned without overlapped residues.

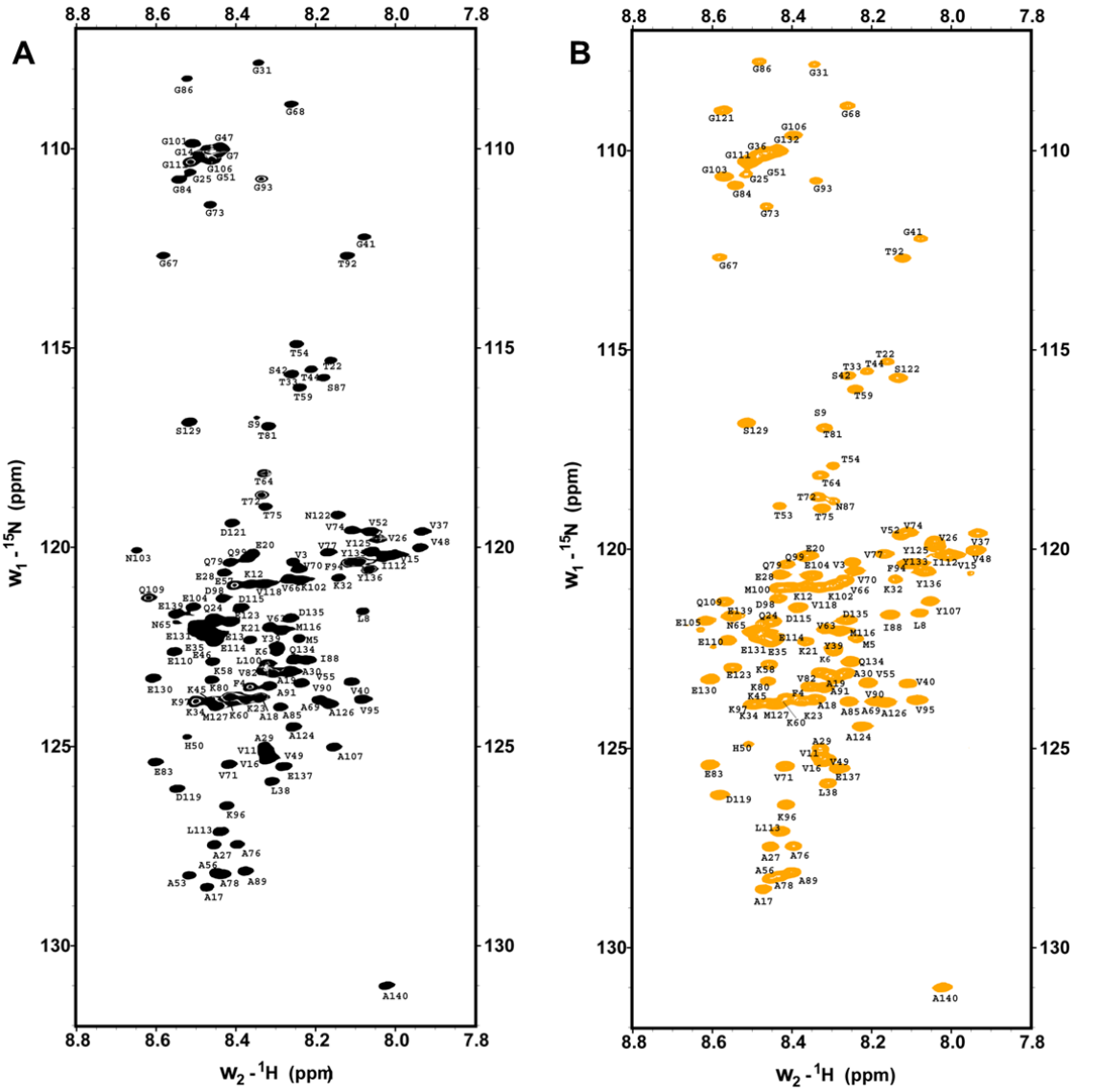

Figure 3.7 ^{1}H-^{15}N HSQC spectra of all the human-mouse variants. A. HHH (black) ; B. MMM (yellow);

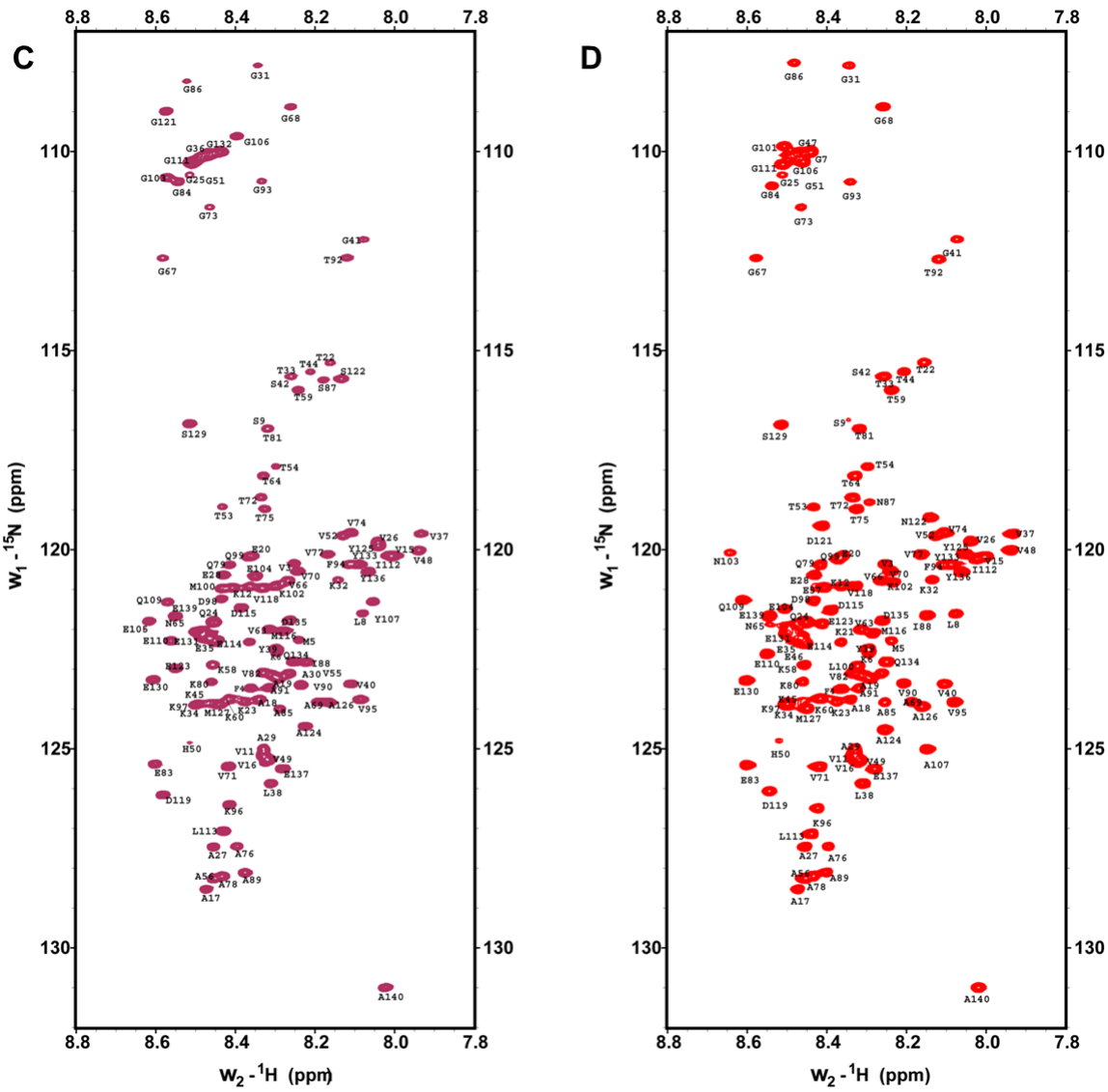

Figure 3.7 ^{1}H-^{15}N HSQC spectra of all the human-mouse variants. C. MHM (maroon) ; D. MMH (red).

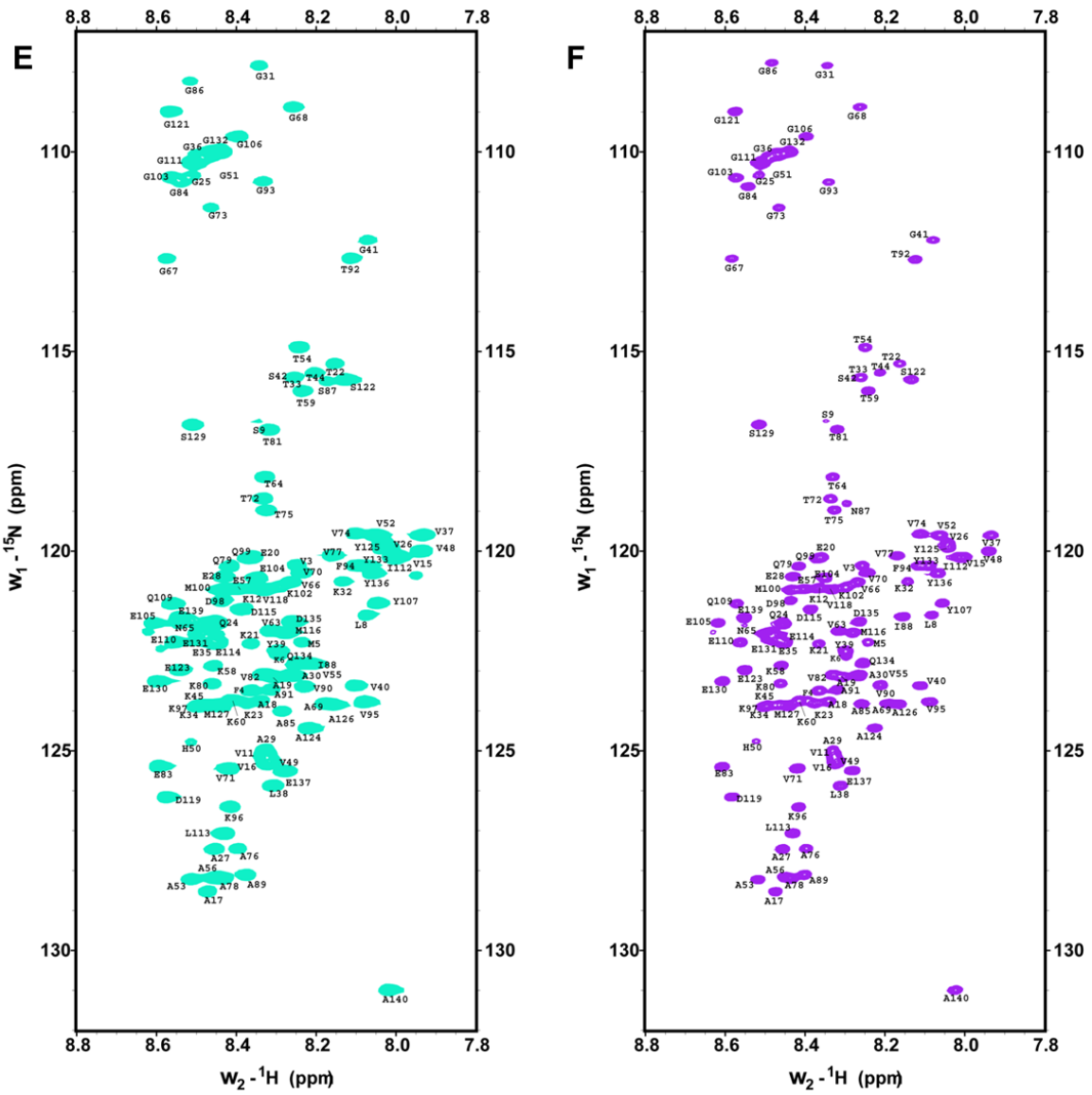

Figure 3.7 ^{1}H-^{15}N HSQC spectra of all the human-mouse variants. E. HHM (cyan) ; F. HMM (purple).

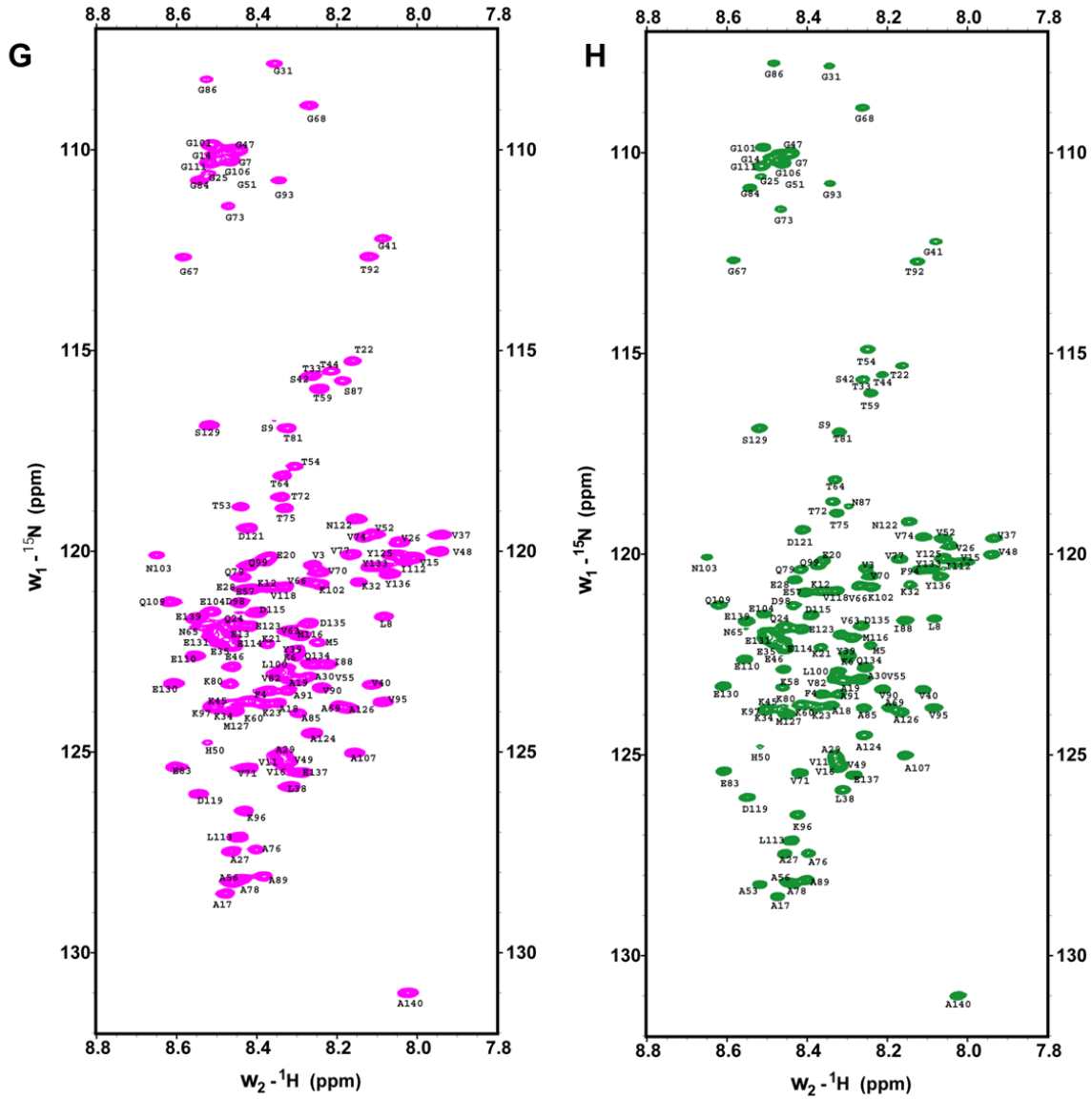

Figure 3.7 ^{1}H-^{15}N HSQC spectra of all the human-mouse variants. G. MHH (margenta) ; F. HMH (green).

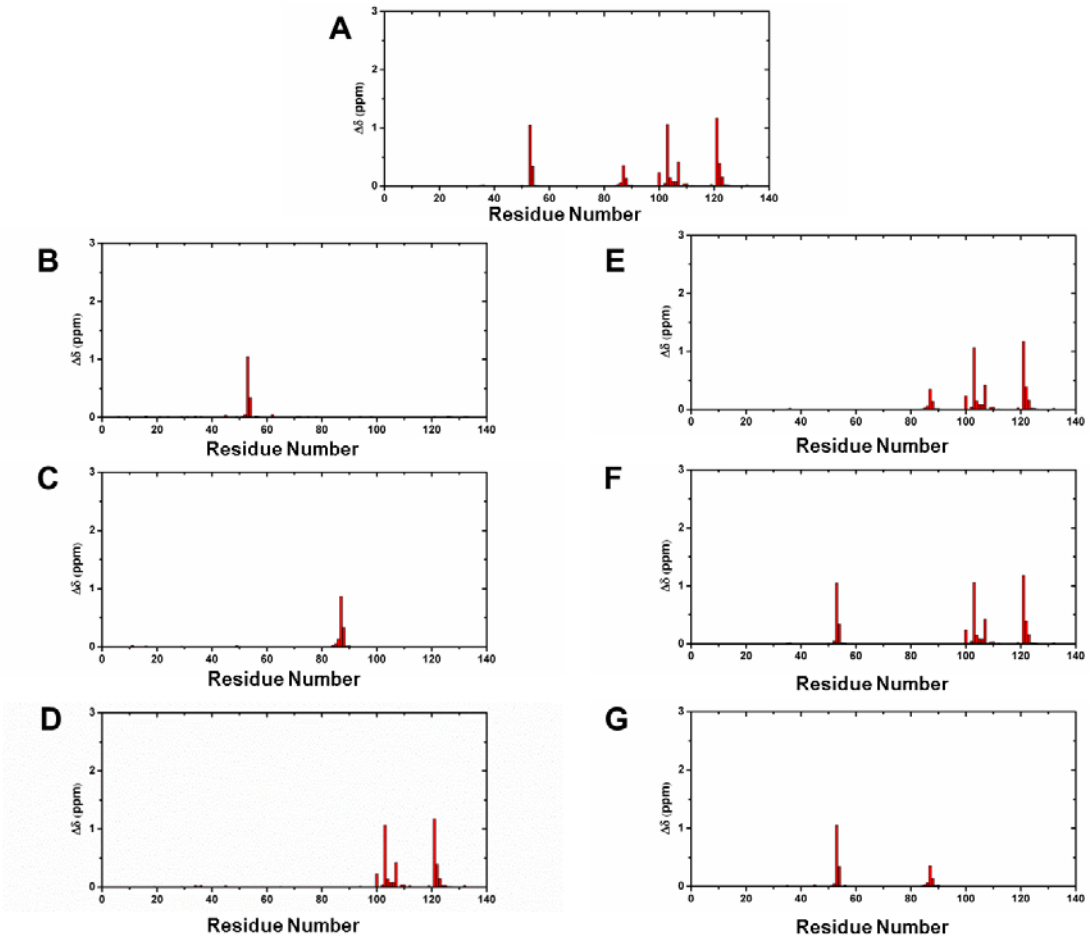

Figure 3.8 Backbone amide chemical shift changes between variants and HHH. The Δδ(ppm) is calculated by the expression $((\Delta H)^2+(0.159*\Delta^{15}N)^2)^{½}$(Liokatis, Dose et al. 2010). A. MMM vs. HHH; B. MHH vs. HHH; C. HMH vs. HHH; D. HHM vs. HHH; E. HMM vs. HHH; F. MHM vs. HHH; G. HHM vs. HHH.

3.3.8 Local differences in secondary structure propensities.

3.3.8.1 Using SSP to calculate secondary structure propensity**.**

It has been proposed that aggregation propensities are strongly influenced by conformational properties, including secondary structure propensities and long-range contacts.(Bussell and Eliezer 2001; Bertoncini, Jung et al. 2005; Marsh, Singh et al. 2006; Wu, Weinstock et al. 2009) Previous NMR(Wu, Kim et al. 2008) and CD(Rochet,

Conway et al. 2000) studies have indicated that human and mouse αsyn are IDPs in the monomer form with conformations that are more compact than would be expected for a fully unfolded protein. NMR chemical shifts are sensitive indicators of secondary structure propensities of IDPs and have been analyzed to determine the differences in the conformational propensities of the eight variants described here. We use secondary structure propensity (SSP) scores(Marsh, Singh et al. 2006) with $^{13}C^{\alpha}$ and $^{13}C^{\beta}$ chemical shifts as input and a 5 residue sliding window to define a residue-specific secondary structure propensity. SSP scores were obtained for all variants and Figure 3.9 indicates that scores along the sequence are quite similar to one another except for the region around position 53. In this region, the SSP scores are divided into two groups of four variants each defined by whether residue 53 is an Ala or a Thr. For the group that has A53 (HHH, HHM, HMH, HMM) the SSP scores are negative suggesting that the conformational ensemble in this local region is sampling more β-sheet conformations on average. The group that contains a Thr at position 53 (MHH, MHM, MMH, MMM) has more positive SSP values suggesting more local helical conformation on average in the ensemble.

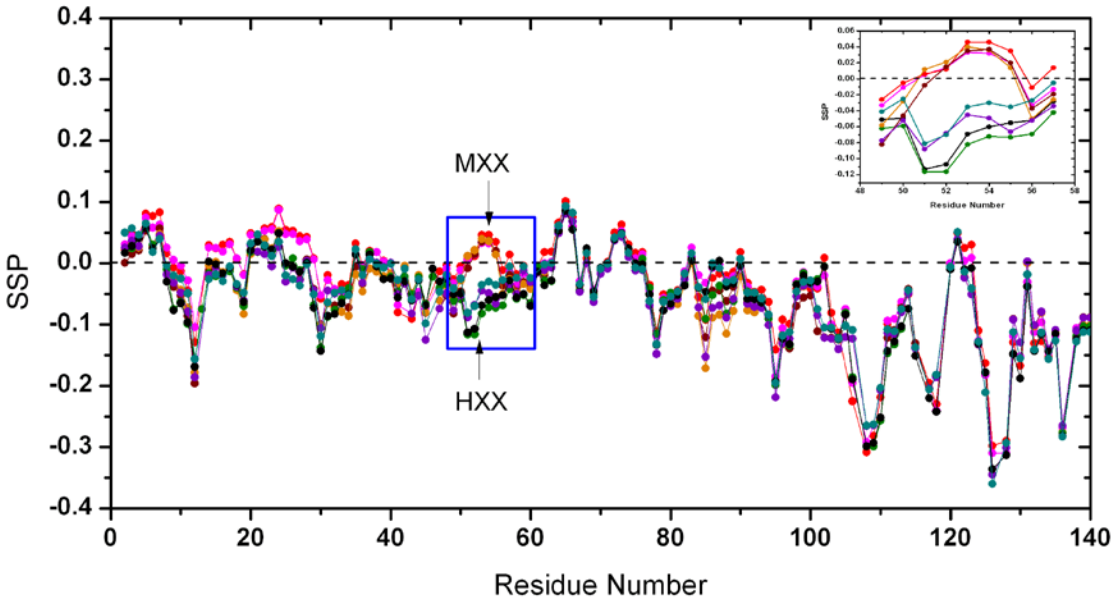

Figure 3.9 SSP scores calculated using 13Cα and 13Cβ chemical shifts as a function of residue for all the αsyn human-mouse variants. The colors are MMH (•), MHH (•), MHM (•), MMM (•), HMH (•), HMM (•), HHH (•), HHM (•). The region around position 53 is boxed and MXX represents the class of variants that have the mouse N-terminal sequence (MHH, MHM, MMH, MMM) and HXX represents the class of variants that contain the human N-terminal sequence (HHH, HHM, HMH, HMM). The inset is an enlarged region from residue 49 to 57.

The importance of the results presented here lies in the fact that there are systematic local differences in secondary structure propensities at and around position 53 as function of the amino acid type that occupies it. It is difficult to interpret SSP scores at any position along the sequence in terms of the absolute population of secondary structure elements as the scores represent ensemble-averaged values over a distribution. The SSP value does not uniquely define the α and β content within the distribution. Strikingly, the identity of position 53 as Ala or Thr is also responsible for regulating the growth rates in the human-

mouse chimeras. The results on this series of eight human-mouse chimeras suggest that the growth rates of the human-mouse chimeras may be directly influenced by the secondary structure propensities at position 53 and that growth rates are correlated to local secondary structure propensities of the monomer conformational ensemble. Previous studies of PD-linked mutations A30P, A53T and E46K that have different fibrillation or aggregation rates have also shown small changes in local chemical shifts(Bussell and Eliezer 2001; Rospigliosi, McClendon et al. 2009) supporting the results presented here that local secondary structure propensities may be correlated to the kinetics of aggregation.

3.3.8.2 Using δ2D to calculate secondary structure populations.

δ2D is developed by Dr. Vendruscolo's group (Camilloni, De Simone et al. 2012) and is used to characterize population of secondary elements consisting of α-helix, β-sheet, random coil and polyproline II using chemical shift. The δ2D value for all the variants are calculated and on average α-helical is ~4%, β-sheet is ~ 15%, random coil is ~73%, polyproline II is ~12%. The region around residue 53 which is determined to have distinct change of SSP also have different secondary structure populations (Figure 3.10). However, it shows that MXX have increased β-sheet population, decreased polyproline II population, increased coil population from residue 55~57, decreased coil population from 52~54 and no trend in α-helix. It is interesting to note that SSP shows that for MXX increased helical propensity is observed while δ2D shows that increased sheet population is observed for region around 53. The discrepancy between the two programs can come from the fact that SSP calculates two secondary elements and δ2D calculate four

secondary elements. The difference in definition of the propensities or populations may cause the discrepancy when interpreting the same chemical shift data.

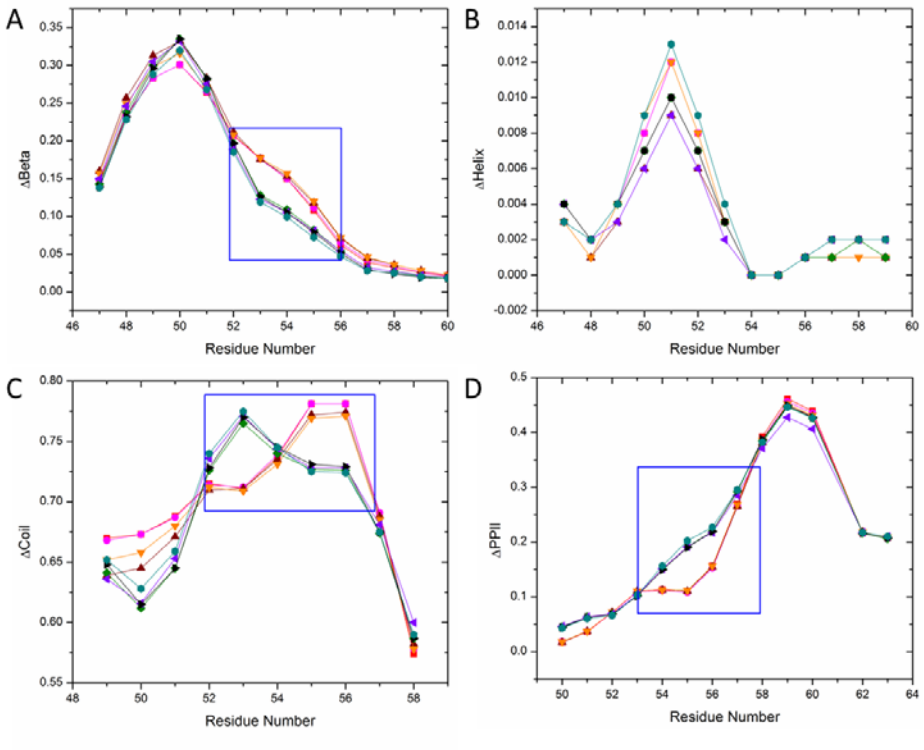

Figure 3.10 δ2D values for all the variants around residue 53. δ2D was calculated using $^{13}C^{\alpha}$ and $^{13}C^{\beta}$ chemical shifts as a function of residue for all the αsyn human-mouse variants around residue 53. The colors are MMH (•), MHH (•), MHM (•), MMM (•), HMH (•), HMM (•), HHH (•), HHM (•).

3.3.8 Conclusions.

We have designed a systematic series of human-mouse αsyn variants to study the role of naturally occurring substitutions on the in vitro fibril assembly kinetics and have determined that the N-terminal A53T substitution, which is known to cause early-onset PD both in humans and in transgenic mice(Williamson, Loria et al. 2009), plays a dominant role relative to the other substitutions in the NAC and C-terminal regions in

speeding up the fibril assembly kinetics of mouse relative to human αsyn. Seen from a different perspective, the mutational variants that contain Ala at position 53 all have similar growth rates implying that this residue serves as a control mechanism for fibrillar aggregation. Indeed, an NMR chemical shift analysis suggests that the growth process is controlled by the nature of the secondary structure propensity in this region. These data support the notion that the presence of Ala at position 53 may be an evolutionary adaptation to minimize PD in humans and suggest that the monomer conformation, in particular the critical N-terminal region, may provide new targets for drug therapy in αsyn.

Chapter 4. Secondary Structure Propensity Determines the Aggregation Kinetics of Human and Mouse α-Synuclein Variants

4.1 Introduction.

The conversion of αsyn from the normally soluble form to large aggregates including amyloid fibrils has been extensively studied (Uversky and Eliezer 2009). Aggregation studies in vitro using Thioflavin T (ThT) fluorescence have shown that the monomer form of αsyn undergoes a nucleation-dependent conversion to a cross-β rich oligomeric and high-order fibril form whose morphology resembles that found in the diseased state (Serpell, Berriman et al. 2000; Fink 2006). There is consensus from many different laboratories about the existence of a relationship between monomer conformational features and aggregation kinetics, however, at this stage there are differing views on the critical conformational requirements for fibril initiation. There are conflicting proposals that secondary structure propensities are critical to directing aggregation (Bertoncini, Rasia et al. 2007; Sung and Eliezer 2007; Abedini and Raleigh 2009; Rospigliosi, McClendon et al. 2009; Anderson, Ramlall et al. 2010) versus the view that release of long-range interactions that exposes the hydrophobic NAC region, which forms the core of the fibril, is the important aggregation initiator (Bertoncini, Fernandez et al. 2005; Bertoncini, Jung et al. 2005; Wu, Kim et al. 2008). Here we investigate the link between monomer structural propensities of αsyn and aggregation kinetics to identify the role of the monomer in aggregation.

In the previous chapter (Rochet, Conway et al. 2000), we studied eight human-mouse variants: human αsyn (HHH), human A53T (MHH), human S87N (HMH), human A53T-

S87N (MMH), human L100M-N103G-A107Y-D121G-N122S (HHM), human A53T-L100M-N103G-A107Y-D121G-N122S (MHM), human S87N-L100M-N103G-A107Y-D121G-N122S (HMM) and mouse αsyn, which is human A53T-S87N-L100M-N103G-A107Y-D121G-N122S (MMM) and showed that the A53T substitution is the key residue in controlling the growth rate of these variants and that both A53T and S87N substitutions play a key role in defining the lag time (Kang, Wu et al. 2011). Here we perform a detailed NMR structural study in order to reveal the relationship between the conformational properties of the monomers and the aggregation kinetics. We find that all eight human-mouse variants exhibit similar long-range contacts and hydrodynamic radii but have distinct although small differences in secondary structure propensities which correlate well with growth rates and lag times. The analysis of the effect of mutations on secondary structure propensity throughout the sequence identified three pivotal regions, residue 6–31 (I) and 50–56 (II) in N-terminal region and residue 84–89 (III) in NAC region. The results suggest that increased helical propensity and decreased sheet propensity in regions (I) and (II) may induce the increased growth rate while the combination of increased helical propensity and decreased sheet propensity in regions (I) and (II) and increased sheet propensity in region (III) are related to shortened lag time in human-mouse αsyn variants. The results points out the importance of secondary structure propensity in affecting aggregation.

4.2 Material and methods.

4.2.1 αSyn expression and purification.

All eight human-mouse variants were prepared as Chapter 2.1–2.3 described.

4.2.2 Secondary chemical shift measurement.

The chemical shift of all the variants were obtained as previously described at 15 °C at pH 7.4 phosphate buffer saline (PBS) as Chapter 2.4.1 described. $^{13}C_{\alpha}$ and $^{13}C_{\beta}$ were used to do the secondary structure propensity score (SSP) (Marsh, Singh et al. 2006) calculation with residue window of 5 and random coil reference from Zhang et al.(Zhang, Neal et al. 2003).

4.2.3. Intramolecular and intermolecular PRE measurement.

For intramolecular PRE experiment, MTSL-labeled freeze-dried αsyn variants was dissolved in PBS buffer and went through 100 kD filter to remove small invisible aggregates. The final concentration was 50–100 μM and was divided to equal volume for experiments at paramagnetic (oxidized) and diamagnetic (reduced) state. Addition of 10 mM L-ascorbate was applied for generating diamagnetic samples and the sample was incubated at lease 4 hours in 4 °C. The L-ascorbate treated sample then went through 10 kD filter for buffer exchange to remove excess L-ascorbate. PRE effects were measured by ^{1}H-^{15}N HSQC spectrum in the presence and absence of MTSL spin labeling at 15 °C in PBS at pH 7.4 in 600 MHz Varian or Bruker spectrometers. Theoretical PRE curves were calculated by using XPLOR-NIH to generate MTSL-attached fully extended structures (Schwieters, Kuszewski et al. 2003). For intermolecular PRE experiment, equivalent ^{14}N-labeled MTSL-conjugated protein and ^{15}N-labeled protein were dissolved in MES buffer (10 mM MES, 100 mM NaCl) and went through 100 kD filter to remove the small invisible aggregates. Then the sample was concentrated to 1100 μM and mixed to a final volume of ~350 μL. The sample was then transferred to Shigemi tube to

perform ^{1}H R_2 experiment on NMR. Paramagnetic $^{1}H^{N}$ R_2 data of different mixed samples were acquired at 15 °C on a Varian 800 MHz spectrometer using an in-house pulse sequence modified from best Nhsqc. The PRE on $^{1}H^{N}$ is calculated by: $^{1}H^{N}$ $\Gamma_2 = R_2^{para} - R_2^{dia}$. Seven relaxation delays (6 ms, 10 ms, 16 ms, 24 ms, 32 ms, 42 ms and 52 ms) with 2 seconds recycle delay were used for all R_2 measurements.

4.2.4 Hydrodynamic radius measurement.

Methods for measuring hydrodynamic radius were done as previously described in Chapter 2.4.5. In brief, the hydrodynamic radius was calculated through the translational diffusion coefficients, which was measured by in-house PFG-NMR experiments (Li, Kim et al. 2005). Samples containing 300 μM αsyn variants and 35 mM 1,4-dioxane were dissolved in PBS at pH 7.4 (100% D_2O). The experiments were performed on all eight variants at 15 °C on 600 MHz Varian spectrometers.

4.2.5 Amide hydrogen exchange experiment.

The sample is prepared by dissolving lyophilized ^{15}N-labeled αsyn variants in PBS buffer with 100 kD filtration. A final concentration is 250 μM with 10 % D_2O and the amide hydrogen exchange was measured by CLEANEX experiment (Hwang, van Zijl et al. 1998) at 15 °C on 600 MHz Varian spectrometers. Time zero is acquired first with 3 seconds recycle delay in one experiment and 10 relaxation delays ranging from 5 ms to 24 ms are acquired in another experiment with 2 seconds recycle delay. The data was fitted to

$$\frac{V}{V_0} = \frac{k}{(R_{1A,app}+k-R_{1B,app})} \times [e^{(-R_{1B,app}\times t)} - e^{-(R_{1A,app}+k)\times t)}] \qquad \text{(Eq. 4.1.)}$$

where $R_{1B,app}$ is 0.6 s^{-1}, V_0 is the peak height for time zero and V is the peak height for relaxation delay, peak height was used instead of peak volume as the serious overlay of αsyn spectrum. Statistical software R is used to fit the data and k is the amide exchange rate.

4.2.6 Residual dipolar coupling experiments.

The detailed method for making alignment media and measurement of RDC is described in Chapter 2.4.4. 5% C8E5 and 1-octanol were mixed in PBS buffer at pH 7.4. The molar ratio of C8E5 and 1-octanol is 1.05. The quadrupolar deuterium splitting constants are around 23.9 Hz for all the variants. The RDC value is normalized based on splitting constants of HHH. The sample was prepared by dissolving lyophilized protein in PBS buffer and filtered through 100 kD. The final concentration is around ~250 μM. High-resolution HSQC_IPAP spectra in the absence or in the presence of an alignment medium were collected at 15 °C with complex points of 2048 (t2) × 512 (t1) and 16 transient scans.

4.3 Results.

4.3.1 The mean hydrophobicity and mean charge for all the variants.

There have been shown that the intrinsic effect of mutations on unfolded polypeptide chain is to a great extent controlled by the physicochemical properties including hydrophobicity, secondary structure propensity and charge (Chiti, Stefani et al. 2003). The mean hydrophobicity is calculated by script created by Chitra Narayanan using Cowan-Whittaker hydropathy indices (Cowan and Whittaker 1990). The mean hydrophobicity and mean charge for all the variants are shown in Table 4.1. Although the differences of the mean hydrophobicity between variants are small, the correlation

between mean hydrophobicity and growth rate are good with correlation coefficient of -0.74 (Figure 4.1.). The correlation between mean hydrophobicity and lag times are not observed. For net charge, among eight variants, four of them are with D121G mutation and carry -8 net charges instead of -9. There is no correlation between mean net charge and growth rate as well as lag times.

Table 4.1 The mean hydrophobicity and mean charge

	Mean Hydrophobicity	Mean Charge
MMH	0.5588	0.0643
MHH	0.5595	0.0643
MHM	0.5619	0.0571
MMM	0.5613	0.0571
HMH	0.5600	0.0643
HMM	0.5625	0.0571
HHH	0.5607	0.0643
HHM	0.5631	0.0571

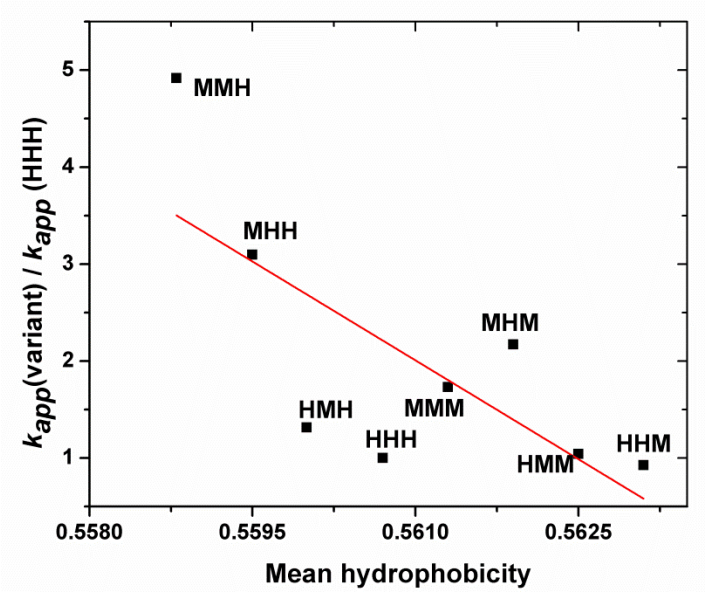

Figure 4.1. The correlation between the mean hydrophobicity and growth rate k_{app} ratio.

4.3.2 The effect of mutations on secondary structure propensities.

SSP provides a quantitative way to characterize the secondary structural propensity of unfolded protein with a value between 0 and 1 for helical propensity and a value between -1 and 0 for sheet propensity (Marsh, Singh et al. 2006). For all the variants the on average helical propensity is ~1% and sheet propensity is ~5%. We performed a detailed analysis SSP on αsyn variants to quantitatively define both the local and long-range effects of mutations secondary structure changes (Figure 4.2). The analysis is performed by: (1) varying the sequence in one region (N-terminal, NAC and C-terminal region) and then fixing the sequences in the other two regions; (2) taking the sum of the differences of the SSP for these four pairs of variants. For example, the effect of the A53T mutation in the N-terminal is the sum of the SSP differences for all the (MX'X''- HX'X'') variants consisting of (MMM-HMM), (MMH-HMH), (MHM-HHM) and (MHH-HHH) where the NAC and C-terminal regions are kept fixed while the N-terminal varies between the human H and mouse M. The result (Figure 4.2) shows that (1) the mutation in the N-terminal or A53T mutation not only increases SSP at and around residue 53, that is region (I), but also increases SSP values at residues 6~31 in the beginning of the N-terminal region; there is relatively smaller effect of the A53T mutation on the rest of the sequence. The increased SSP in region (I) and (II) denotes increased helical propensity or decreased sheet propensity; (2) the mutation in the NAC region or S87N mutation, which is represented by the sum of the SSP differences for all the (X'MX''-X'HX'') variants consisting of (MMM-MHM), (MMH-MHH), (HMM-HHM) and (HMH-HHH), has only a very limited local effect with decreased SSP which denotes increased sheet propensity

in region (III); (3) the mutations in the C-terminal or L100M-N103G-A107Y-D121G-N122S mutation, which are represented by the sum of the SSP differences for all the (X'X''M-X'X''H) variants consisting of (MMM-MMH), (MHM-MHH), (HHM-HHH) and (MHM-MHH), not only induces a distinct local pattern around the mutation point but also induces decreased SSP which denotes decreased helical propensity or increased sheet propensity in the N-terminal and NAC region especially in regions (I) and (III). It is interesting that the N-terminal mutation and the C-terminal mutations have opposite effects on SSP around region (I) and that the NAC mutation and the C-terminal mutations induce similar effect on SSP in region (III).

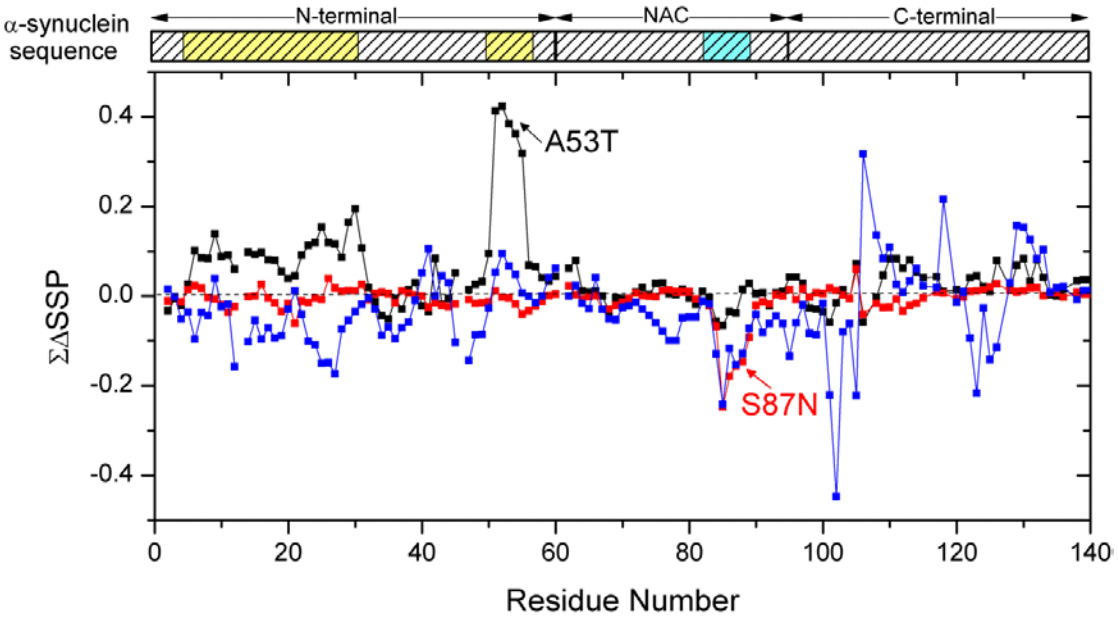

Figure 4.2 The mutations effect on secondary structure propensity. The sum of the SSP differences for all the (MX'X''-HX'X'') variants consisting of (MMM-HMM), (MMH-HMH), (MHM-HHM) and (MHH-HHH) with fixed NAC and C-terminal region in each pair represents the effects of the mutation in N-terminal or A53T mutation (black). The sum of the SSP differences for all the (X'MX''-X'HX'') variants consisting of (MMM-MHM), (MMH-MHH), (HMM-HHM) and (HMH-HHH) with fixed N-terminal and C-terminal region (red); the sum of the SSP differences for all the (X'X''M-X'X''H) variants consisting of (MMM-MMH), (MHM-MHH), (HHM-HHH) and (MHM-MHH) with fixed N-terminal and NAC region in each pair represents the effects of the five mutations in C-terminal (blue).

4.3.2 Correlation of secondary structure propensity with growth rate.

We performed a quantitative analysis which evaluates the correlation between the averaged helical and sheet propensity in regions (I), (II) and the growth rate. The results show a good positive correlation between averaged helical propensity represented by positive SSP in regions (I), (II) and growth rate and concurrently a good negative correlation between averaged sheet propensity represented by negative SSP in regions (I), (II) and growth rate. The correlation coefficient for averaged helical propensity ratio against that of HHH and growth rate ratio against that of HHH has a positive correlation coefficient of 0.96 (Figure 4.3A) and the averaged sheet propensity ratio against that of HHH and growth rate ratio against that of HHH has a negative correlation coefficient of -0.84 (Figure 4.3B). The data also suggests that the increased averaged helical propensity ratio and decreased sheet propensity ratio is comparable to the increased growth rate ratio; for example the averaged helical propensity of MMH is 4.37 times of that of HHH and the averaged sheet propensity of MMH is 4.42 times of that of HHH with a growth rate 4.91 times of that of HHH. However, it is noteworthy that the averaged helical propensity increase between MMH and HHH is 2.27 %. Although the values are small, the averaged helical propensity is intrinsically small for unfolded αsyn so the increase of 2.27% of actually counts for 77% of averaged helical propensity and averaged sheet propensity in said region above.

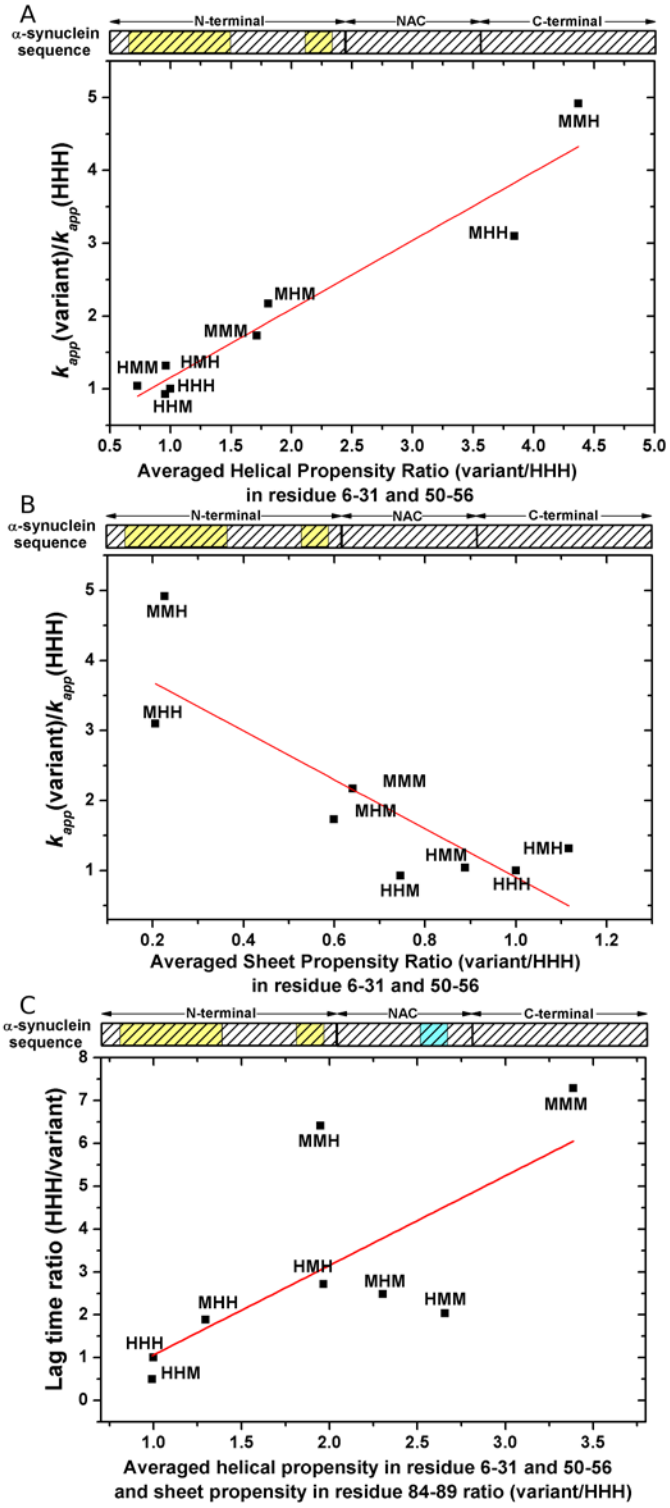

Figure 4.3. Correlation between variants SSP and growth rate as well as lag time. A. Correlation between the variants' averaged helical propensity ratio against that of HHH calculated by averaging the positive SSP values in the residues 6–31 and 50–56 and the

variants' growth rate ratio against that of HHH represented by k_{app}(variant)/k_{app}(HHH) for all eight variants. Correlation coefficient = 0.96. B. Correlation between the variants' averaged sheet propensity against that of HHH calculated by averaging the negative SSP values in residues 6–31 and 50–56 and the variants' growth rate ratio against that of HHH represented by k_{app}(variant)/k_{app}(HHH) of all eight variants. Correlation coefficient = -0.84. C. Correlation between the combination of averaged helical propensity in residue 6–31, residue 50–56 and averaged sheet propensity in residue 84–89 ratio against that of HHH calculated by adding up the average of the positive SSP values in residue 6–31, residue 50–56 and the average of the negative SSP values in residue 84–89 and the variants' lag time ratio between HHH and variants represented by lag time ratio (HHH/variant) for all eight variants. Correlation coefficient = 0.71.

4.3.3 Correlation of secondary structure propensity with lag time.

Previous results (Kang, Wu et al. 2011) show that A53T and S87N act synergistically the lag time, based on our SSP analysis we propose that the combination of the helical propensity in region (I) and (II) and the sheet propensity in region (III) correlate with the lag time. The results show that a good positive correlation between the combination of averaged helical propensity represented by positive SSP in region (I), (II) and sheet propensity represented by negative SSP in region (III) and lag time. The correlation coefficient for combined averaged helical propensity in residue 6–31, residue 50–56 and sheet propensity in residue 84–89 ratio against that of HHH and lag time ratio of HHH against that of variant has a positive correlation coefficient of 0.71 (Figure 4.3.C). Although the variant HHH has 7.29 times longer lag time than variant MMM, the

combined secondary structure propensity for MMM is only 3.39 time of that of HHH. It is surprising to learn that the lag time is sensitive to slight change of the secondary structure propensity. The positive good correlation between combination of helical propensity in region (I), (II) and sheet propensity in region (III) and lag time suggests that in human-mouse αsyn variants small helical propensity before and in the beginning of the fibril core region and sheet propensity in fibril core region accelerate monomer forming the oligomers during lag phase.

4.3.3 All the variants have similar long-range contacts and molecular dimensions.

It has been proposed that aggregation propensities are strongly influenced by conformational properties of the monomer, including secondary structure propensities and/or long-range contacts (Bussell and Eliezer 2001; Bertoncini, Jung et al. 2005; Marsh, Singh et al. 2006; Wu, Weinstock et al. 2009). We evaluate the long-range contacts in these series of variants by using paramagnetic relaxation enhancement (PRE) effects, which can detect a spatial proximity around 25 Å or less between a given residue and the spin label site. Previous studies have shown that A53T, which is MHH, has similar PRE profiles to human wild type (Rospigliosi, McClendon et al. 2009). Here we examine the PRE contacts of the other three variants in the fast growth rate group (MMH, MHM, MMM) with HHH using the N-terminal A19C and C-terminal G132C probes. The PRE profiles of the variants were similar to HHH. By averaging I_{ox}/I_{red} for MMH, MHM, MMM represented by MXX, we show that MXX have similar long-range contacts to HHH with the A19C probe showing a large reduction of I_{ox}/I_{red} ~0.3 around residue 40 and a generic diminished intensity throughout the rest of the entire sequence with an

average of I_{ox}/I_{red} ~0.8; the G132C probe showing a relatively large reduction of I_{ox}/I_{red} ~0.6 around residue 40 and 90 and general reduced intensity throughout the rest of the sequence with an average of I_{ox}/I_{red} ~0.8 (Figure 4.4 A, B). Our results show that the long range contacts do not correlate with aggregation rates in this series of mutants and that faster growth rate variants have similar long-range contacts. We performed diffusion experiments to evaluate the molecular dimension of the variants and the results show that the hydrodynamic radii for all the variants are similar and around 30Å (Figure 4.4.C). Based on PRE and diffusion experiments our results show that all the variants exhibit similar long-range contacts and molecular dimensions suggesting that different aggregation properties of variants do not arise from global conformational features in this context.

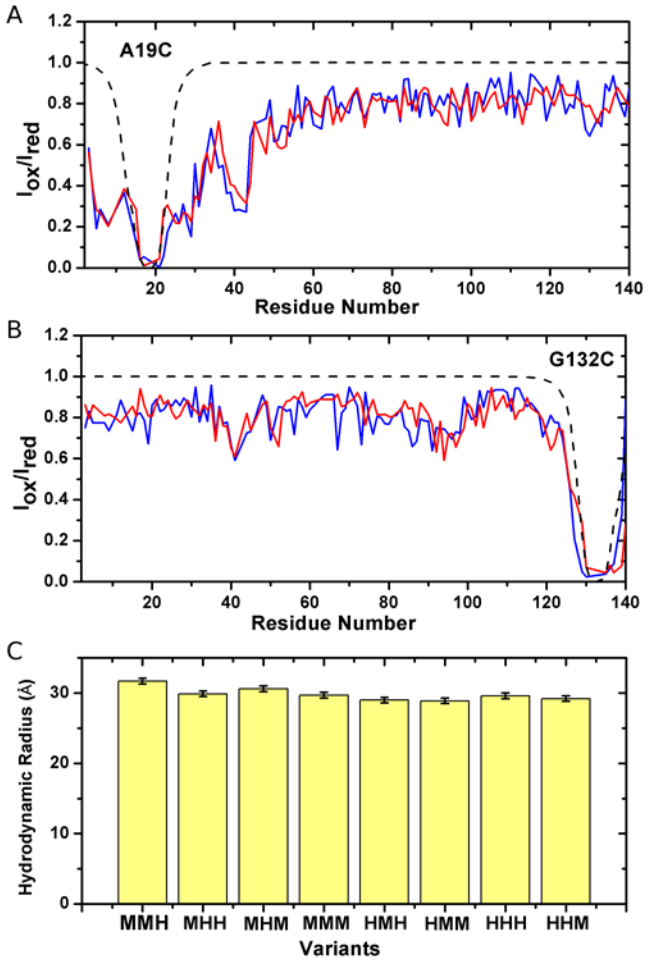

Figure 4.4. Intra-molecular PRE profiles and hydrodynamic radius for variants. A, B Intra-molecular PRE profiles of HHH (blue) and an average of MXX (red) profiles of A19C probe (A) and G132C probe (B). MXX is the average of MHM, MMH and MMM. C. Hydrodynamic radius of all the variants.

4.3.4 MHH maintains major head-to-tail intermolecular interaction with increased contacts.

The intermolecular interaction of MHH and HHH are measured as previously described using intermolecular PRE measurement with ^{1}H R_2 relaxation experiment and mixed spin labeled sample (Wu and Baum 2010). As at pH 7.4 the relaxation is largely affected by

hydrogen exchange, the experiments are carried out at pH 6.0 to reduce hydrogen exchange while still close to physiological condition. The residual $^{1}H^{N}$ Γ_2 value of MHH and HHH are shown in Figure. 4.5 and the characterized intermolecular interactions are (1) A19C to C-terminal residues 110–140; (2) A90C to residue 34–50 and (3) G132C to residues 1–20 and 35–50. Small differences are observed majorly in N-terminal region. MHH have decreased A19C to residues 6–28, increased A90C to residues 6–28, 37–50 and increased G132C to 17–30, 37–43, 52–59 and 76–95. It is interesting to note that residues 37–43, 52–59, 90–95 are among the five β-strands identified in the mature αsyn fibril. Previous study has shown that HHH have weak antiparallel head-to-tail intermolecular interaction in near physiological condition (Wu and Baum 2010). The interactions probably originate from 5–10% dimer population in this condition as observed by ESI-IMS-MS. The head-to-tail transient intermolecular contacts are different from the parallel arrangement of monomer in fibril, which suggests that the antiparallel dimer is not on fibril assembly pathway but rather belongs to the early stage equilibrium state maintained by the electrostatic forces. Although the antiparallel head-to-tail electrostatic interactions is the dominate forces in intermolecular dimer, the change of the intermolecular interactions in residues 6–28 as well as three β-strands regions in early stage equilibrium state in MHH may suggest the start of rearrangement.

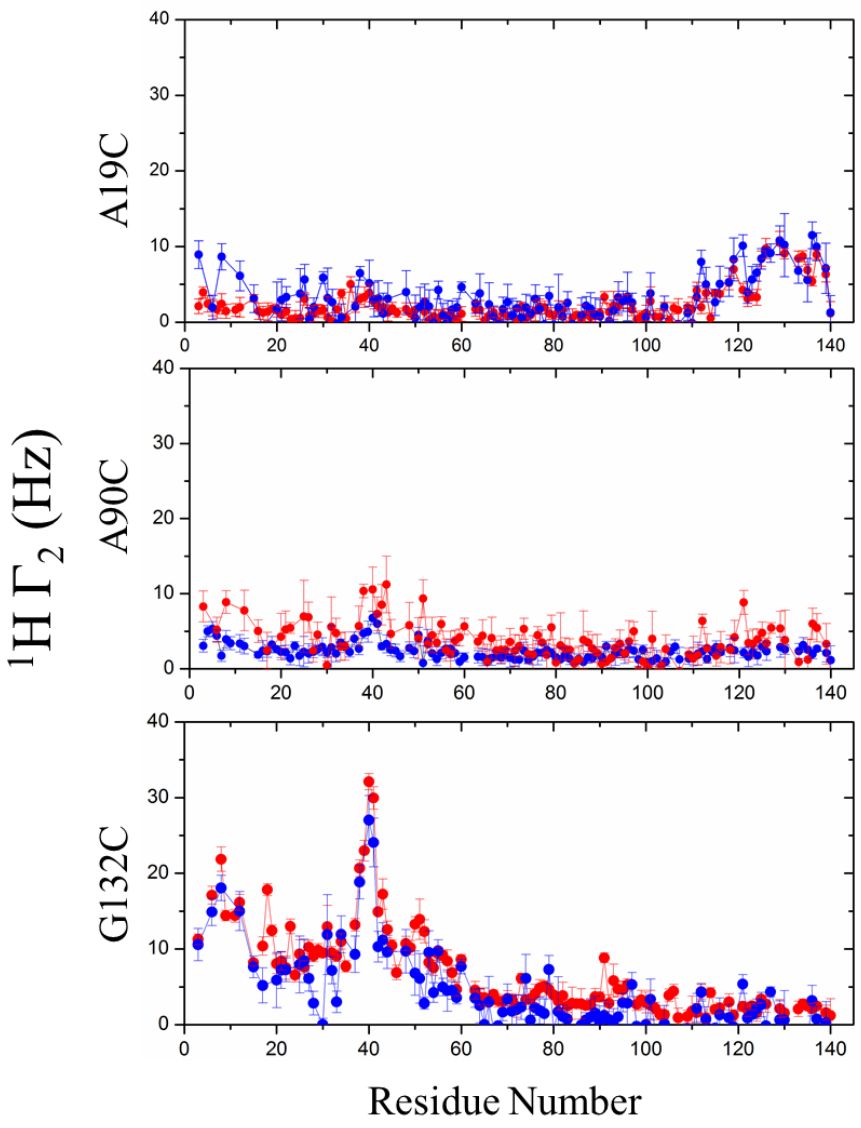

Figure 4.5. The intermolecular PRE profiles for HHH (blue) and MHH (red).

4.3.5 All the variants have similar amide hydrogen exchange rate.

Amide hydrogen exchange can provide information about residue solvent accessibility and reveal protein conformational information. CLEANEX pulse (Hwang, van Zijl et al. 1998) measures k_{HX} independently of pH and is believed to give accurate values. Here we examine the hydrogen exchange (HX) for the fast growth rate group (MMH, MHM,

MMM, MHH) with HHH. For HHH (Figure 4.6), the acidic C-terminal has much lower HX rate than rest of the protein which is consistent with what Croke et. al. observed (Croke, Sallum et al. 2008). The slow HX in C-terminal may be due to negative charges protect it from HX. It is also interesting to note that the HX profile is depending on sequence. Val residues in N-terminal and NAC show small exchange rates similar to residues from C-terminal region which is consistent with slow exchange rate of Val (Bai, Milne et al. 1993) and Gly residues show fast HX in N-terminal and NAC regions. As the great dependence on amino acid intrinsic exchange rate, the k_{HX} profile of the variants MXX, which is the average of MMH, MHM, MMM, MHH, is expected to be similar to HHH (Figure 4.6).

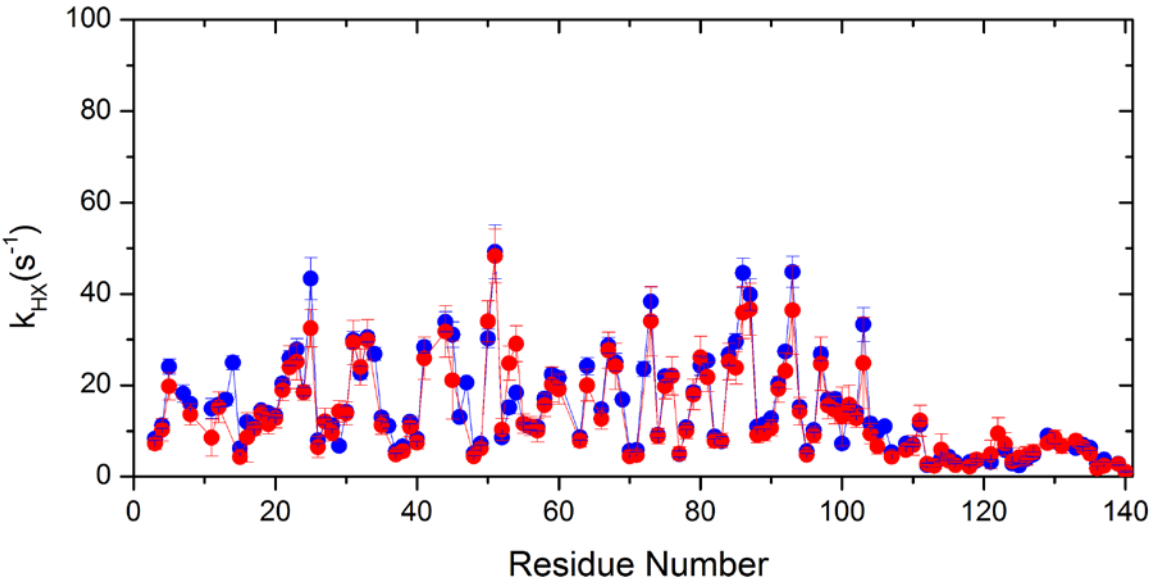

Figure 4.6. The amide hydrogen exchange rate k_{HX} for HHH (blue) and MXX (red) which is the average of MHH, MHM, MMM and MMH.

4.3.6 RDC profiles for all the variants.

Residual dipolar coupling (RDC) can provide important structure and dynamic information (Prestegard, Bougault et al. 2004). Dissolving protein in dilute liquid crystalline makes one bond inter-nuclear dipolar not averaged to zero and can be measured by liquid state NMR. A mixture of PEG/alcohol is used as the alignment media because it is cheap and can be used in a wide range of pH and temperatures. αSyn N-H RDC profile (Figure. 4.7) is distinct from smooth bell-shape like distribution predicted from unfolded polypeptide based on random flight chain model (Obolensky, Schlepckow et al. 2007), which implies that αsyn has more residual structure and long range interactions than random coil polypeptide. It is interesting to note that RDC and secondary structure propensity have good correlation with increased RDC correlate with sheet propensity in SSP (Figures. 4.7), especially in NAC and C-terminal region. Previous studies have shown that RDC contains information of residual structure and correlates well with secondary structure propensities in tau, denatured apomyoglobin (Mohana-Borges, Goto et al. 2004; Mukrasch, Markwick et al. 2007) and C-terminal of αsyn (Sung and Eliezer 2007). All the variants exhibit similar correlation between RDC and SSP. The mutations' effects on RDC profile are shown separately in comparison with wild type (Figure 4.8). All the variants have little differences in D^{NH} from that of HHH with an average deviation of 1–2 Hz .

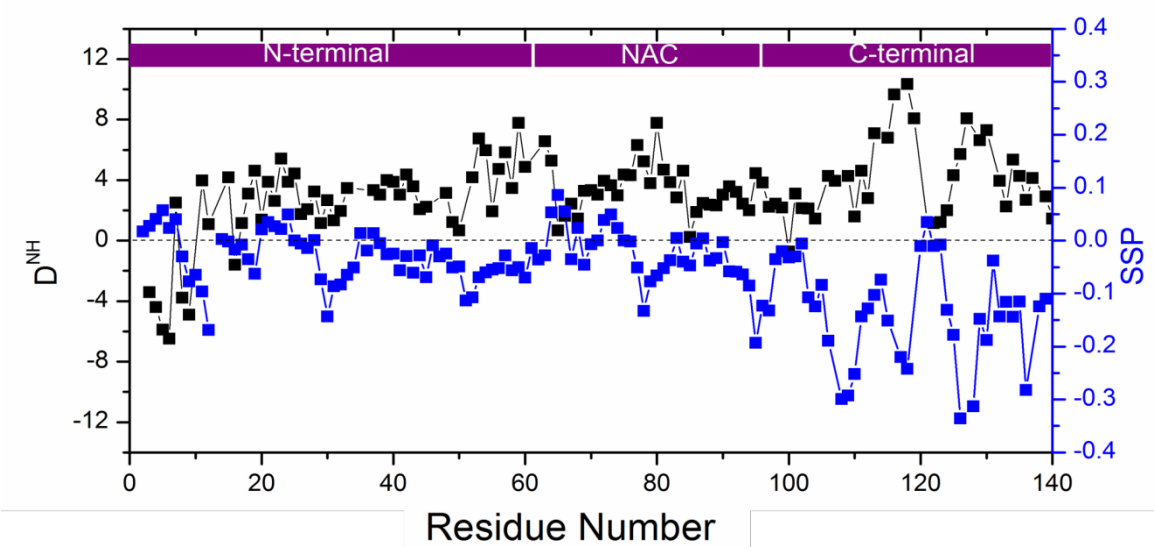

Figure 4.7 A good correlation is observed for HHH D^{NH} and SSP values.

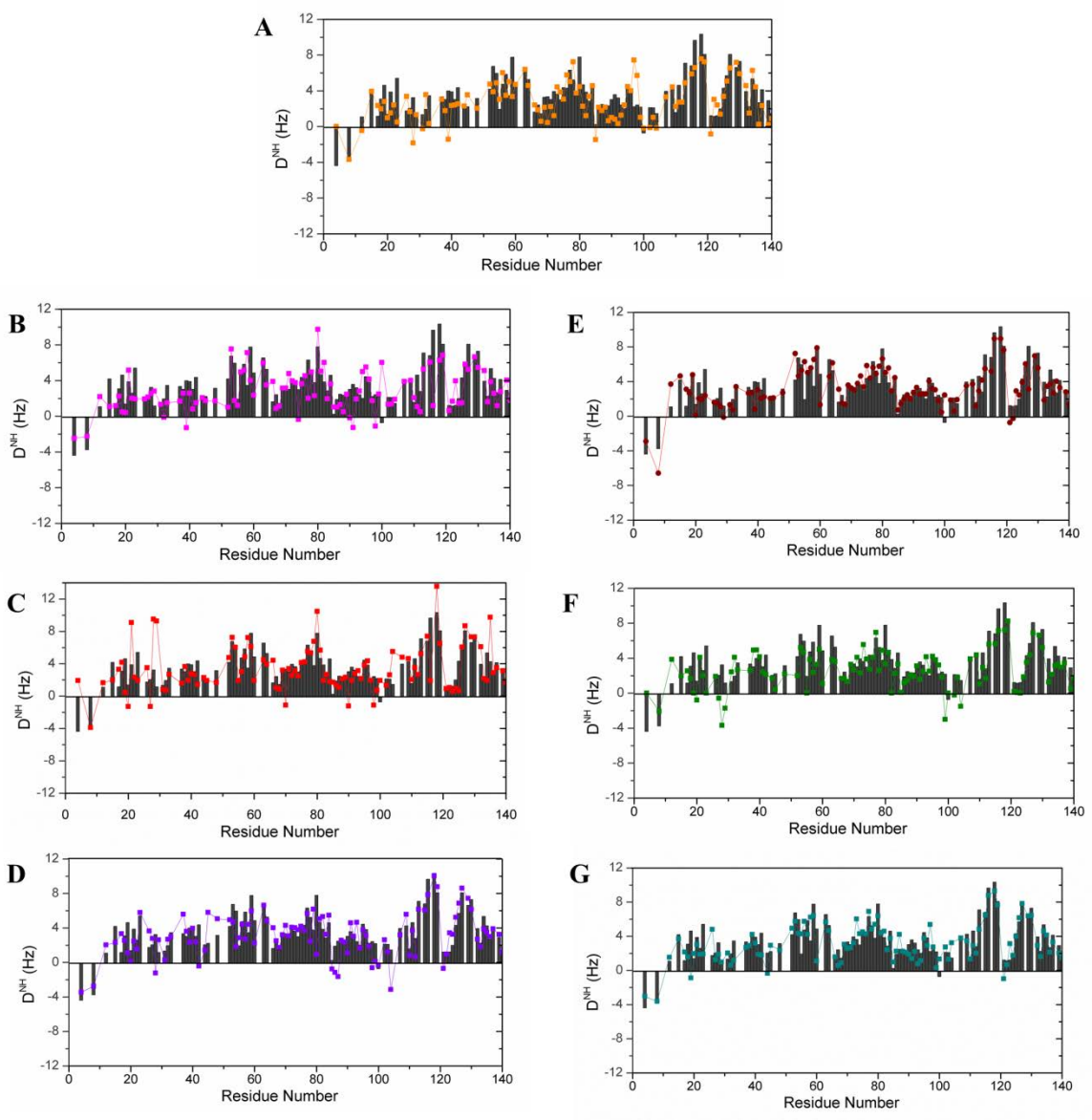

Figure 4.8 RDC profile for all the variants. A. RDC profile for MMM (orange dot) vs HHH (black bar); B. RDC profile for MHH (magenta dot) vs HHH (black bar); C. RDC profile for MMH (red dot) vs HHH (black bar); D. RDC profile for HMM (purple dot) vs HHH (black bar); E. RDC profile for MHM (wine dot) vs HHH (black bar); F. RDC profile for HMH (green dot) vs HHH (black bar); G. RDC profile for HHM (dark cyan dot) vs HHH (black bar).

4.4 Discussions.

The relationship between monomer conformation features and aggregation kinetics are important for studying protein misfolding and have been investigated by many different laboratories, however, there are many differing views on the critical conformational requirements for fibril initiation. There are conflicting proposals that secondary structure propensities are critical to directing aggregation (Bertoncini, Rasia et al. 2007; Sung and Eliezer 2007; Abedini and Raleigh 2009; Rospigliosi, McClendon et al. 2009; Anderson, Ramlall et al. 2010) versus the view that release of long-range interactions that exposes the hydrophobic NAC region, which forms the core of the fibril, is the important aggregation initiator (Bertoncini, Fernandez et al. 2005; Bertoncini, Jung et al. 2005; Wu, Kim et al. 2008). This study identifies via systematic mutations that secondary structure propensity not long-range contacts or molecular dimension play a key role in affecting the aggregation kinetics of human-mouse αsyn variants. The mutations disturb both local and long-range secondary structure propensity, however, do not affect long range interactions as detected by intra-molecular PRE and molecular dimensions as determined by hydrodynamic radius.

It is important to note that in spite of very small changes in magnitude of secondary structure propensities, aggregation rates are extremely sensitive to the small changes in secondary structure propensity. Theses results are different from previous results in which changes in environmental factors such as low pH affect large global conformational changes leading to faster aggregation rates. What could be the possible mechanism that enables small conformational alterations influencing greatly the aggregation kinetics? The selective molecular recognition mechanism, which starts from

mutual conformational selection, followed by population shift to favored conformational state and induce-fit optimization (Ma and Nussinov 2012), may be an appropriate representation. During aggregation where nucleation and elongation are in process, the disordered monomers sample large heterogeneous ensembles within which conformational searching and selection between monomers, higher order oligomers and fibrils are going on. Mutations that increase the population of the aggregation-prone state lead to faster aggregation kinetics. In the case of αsyn the more aggregation prone state is represented by increased helical propensity in regions (I) and (II) and sheet propensity in region (III) by SSP values (Figure 4.9).

Among three regions that are important to fibril assembly kinetics, region (I) belongs to noncore region which includes residues 1–29 and 111–140 (Vilar, Chou et al. 2008). Previously there are studies showing mutations in noncore region such as A29E (Volles and Lansbury 2007), Y135A, Y133A, Y136A (Ulrih, Barry et al. 2008), plus2, del2 (Kessler, Rochet et al. 2003) and so on affect fibril assembly kinetics. One recent paper systematically studying the effect of noncore mutations on TTR1 revealed that its functional variants which are mutated in noncore residues influence fibril assembly kinetics. These findings suggest the important role noncore residue played during fibril assembly. Based on our results the transient small helical propensity sampled in noncore region (I) may initiate or facility molecular association and conversion to fibril structure. It has been proposed that the mechanism by which the fibril formation is accelerated is by having helix mediated self-association which leads to a high concentration of amyloidogenic sequence which later convert to β-sheet structure and form β-sheet assemblies (Abedini and Raleigh 2009; Abedini and Raleigh 2009; Liu, Prabhakar et al.

2010). The identification of transient helical intermediates involving N-terminal of αsyn induced by TFE is one example of this mechanism (Anderson, Ramlall et al. 2010). Our observations that the increased small SSP value in N-terminal regions (I) and (II) may represent the formation of aggregation prone conformation with transient helix in these regions and the association of those helixes will facilitate the alignment of fibril core and later conversion to cross-β structure.

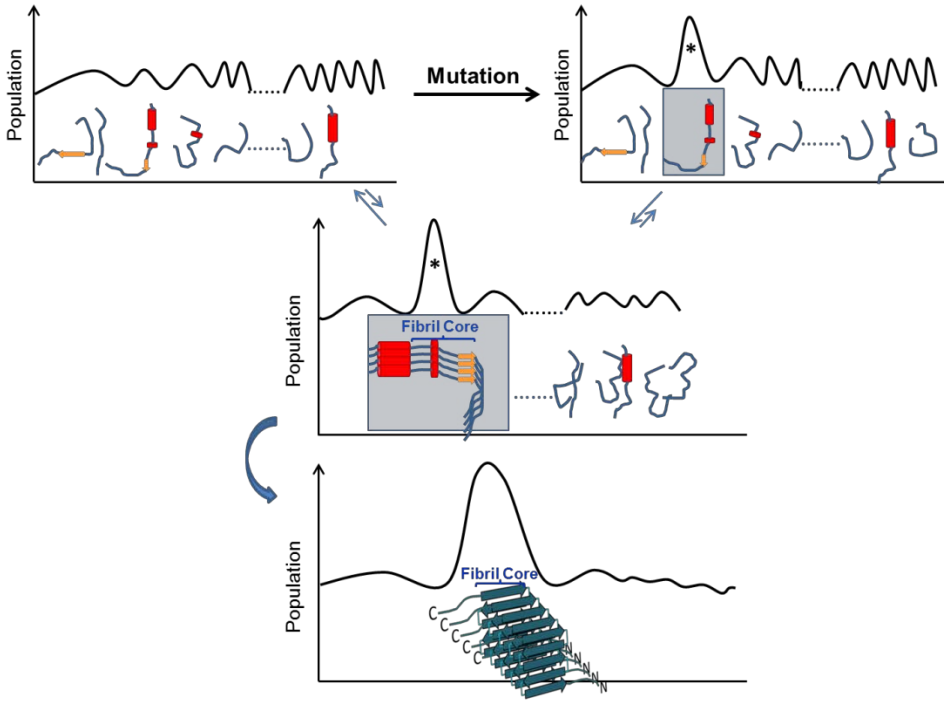

Figure 4.9 Conformational selection and population shift mechanism for human-mouse αsyn variants fibril assembly. The idea for schematic representation of mechanism comes from Ma et. al.(Ma and Nussinov 2012). The populations of various species in aggregation process are represented by black curves. Mutations increase the population of aggregation-prone conformations, which initiate the aggregation process and further shift the equilibrium population by formation of low energy transient oligomer intermediate and the final fibril structure which is the final stable conformation. Without mutation, it takes long time to find aggregation-prone conformation and shift the equilibrium toward fibril.

Chapter 5. Trifluoroethanol induced α-synuclein aggregation

5.1 Introduction.

Trifluoroethanol (TFE) is well-known for its ability to destruct rigid native structure and induce α-helix (Buck 1998). For amyloid proteins, different concentrations of TFE can induce or inhibit amyloid fibril formation by changing polar and hydrophobic interactions (Otzen 2010). For αsyn, low concentrations of TFE induce transient helical propensity and increases aggregation rates; while high concentration of TFE induces higher helical propensity or fully formed helix and inhibits aggregation(Munishkina, Phelan et al. 2003). A recent study has identified the on-pathway helical intermediate in TFE-induced αsyn aggregation (Anderson, Ramlall et al. 2010). However, there is no atomic information about this on-pathway intermediate. Hereby using state-of-art NMR along with ThT fluorescence and TEM, we reveal that the TFE-induced increased helical propensity in first 30 residues and around residue 55 to 65 and within those helical regions residues 1 to 8, 16 to 26 (2^{nd} repeat KTKQGV) and 58 to 64 (5^{th} repeat KTKEQV) are involved in head-to-head inter-molecular interactions. The head-to-head transient helix interaction is consistent with a proposal of helix induced aggregation (Abedini and Raleigh 2009). As αsyn is well-known to populate highly or partly formed helix when associate with membrane (Eliezer, Kutluay et al. 2001) and this study may imply the relevant aggregation pathway.

5.2 Material and Methods.

Protein expression and purification was done as described in Chapter 2.2 and 2.3. Fibril assembly was done as described in Chapter 2.5.1 with exponential fit. TEM was done as described in Chapter 2.5.2. NMR was done as described in Chapter 2.4.1. All the samples were prepared in 10 mM MES, 100 mM NaCl buffer.

5.3 Results and Discussion.

5.3.1 TFE-induced αsyn aggregation.

Previous studies have shown that TFE concentration between 10% to 20% induce the partly helical intermediate conformation of αsyn which leads to formation of short, flexible, β-sheet-rich fibrillar species (Anderson, Ramlall et al. 2010). Another study has shown that αsyn aggregation is inhibited with TFE higher than 15% (Munishkina, Phelan et al. 2003). To investigate the aggregation-prone conditions, a TFE concentration of 10% was used. A series of concentrations was used to investigate the effect of concentration with 10% TFE. The fibril assembly assay was performed at 15 ℃ without shaking to correlate with NMR study. The fibril assembly kinetics was performed with a series of different protein concentrations from 50 μM to 375 μM. All the concentrations exhibit exponential growth with depletion of the lag phase and there is a linear correlation between concentration and aggregation rates (Figure 5.1). All the conditions reach mature phase within 50 hours. Normally αsyn aggregation needs rigorous shaking at high temperature to form fibril. The same sample without TFE takes ~50 hours to pass the lag phase and ~100 hours to reach the mature phase at 37 °C with 600 rpm shaking (Figure xx salt). Addition of 10% TFE dramatically changes the aggregation kinetics. After the kinetics reach the mature phase, the additional shaking at 15 °C and at 37 °C did not

increase the ThT fluorescence. Final products are examined by TEM. Instead of classical straight fibrils, the short and flexible fibrils with a width around 10 nm (Figure 5.1A, inset) are dominated in αsyn aggregates with 10 % TFE without shaking at 15 °C, which is in consistent with what Anderson, et. al. observed (Anderson, Ramlall et al. 2010).

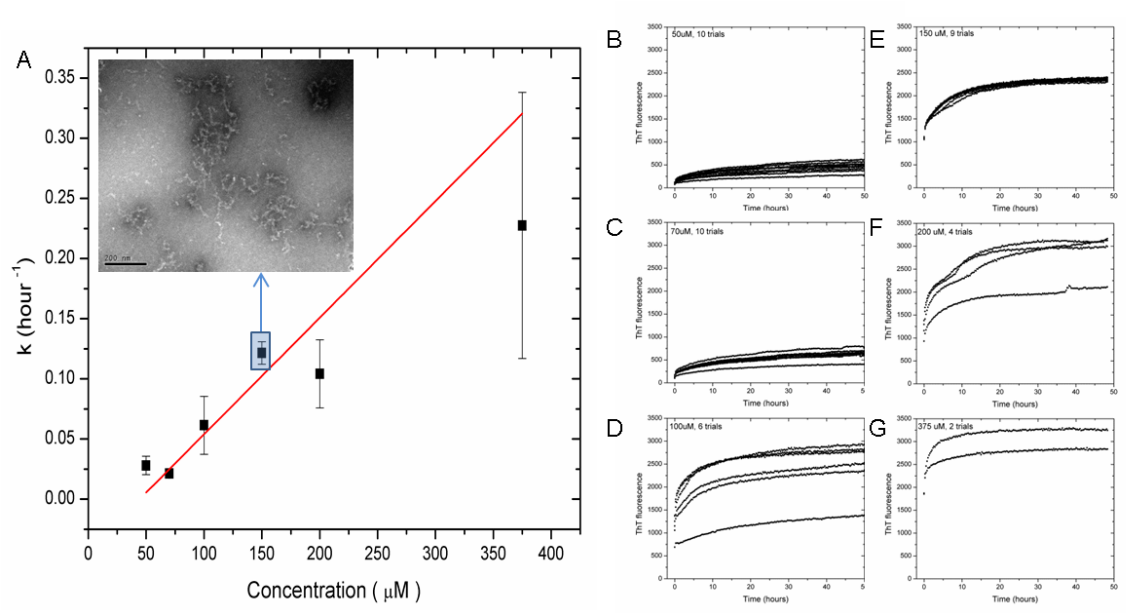

Figure 5.1 αsyn aggregation in 10 % TFE. A. Linear correlation of αsyn concentration and aggregation rate k. Inset is the final fibril morphology of 150 μM αsyn; The aggregation kinetics of different concentration of αsyn: 50 μM (B), 70 μM (C), 100 μM (D), 150 μM (E), 200 μM (F), 375 μM (G).

5.3.2 Backbone assignments of αsyn at 10% TFE.

Backbone assignments of 150 μM αsyn with 10% TFE were performed with a series of triple resonance experiments, including HNCA, HNCOCA and CBCACONH (Figure 5.2). All the experiments are finished within 80 hours before the monomer peak diminishes. During acquisition peak broadening is observed, however after 60 hours the peak become sharp again although with weak intensity. This phenomenon may associate

with aggregation process and broadening could be fast exchange between monomer and higher order oligomer. Albeit broadening, all the peaks are centered at the same position which enables further secondary structure propensity analysis using ^{13}C chemical shift.

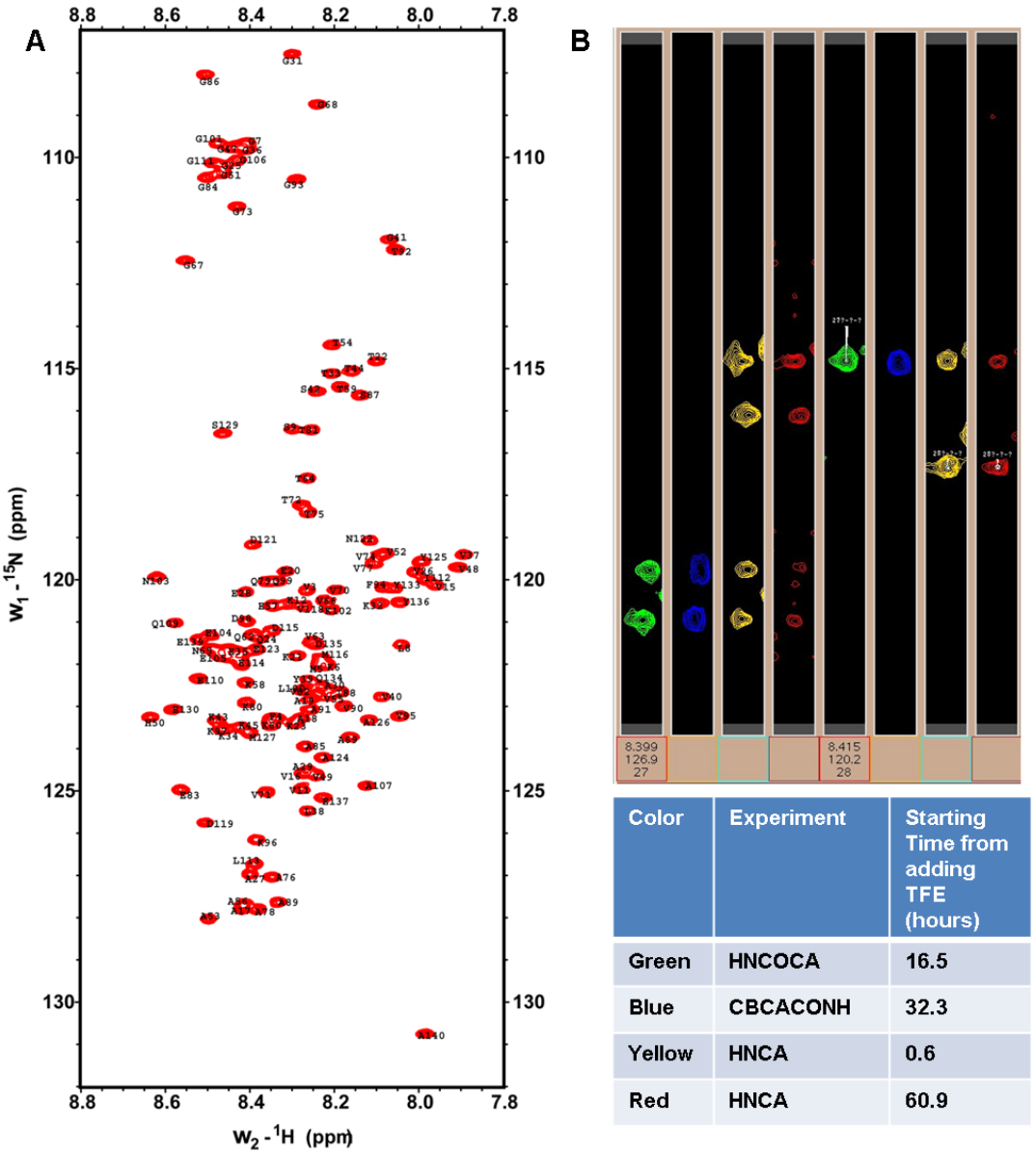

Color	Experiment	Starting Time from adding TFE (hours)
Green	HNCOCA	16.5
Blue	CBCACONH	32.3
Yellow	HNCA	0.6
Red	HNCA	60.9

Figure 5.2 ^{1}H-^{15}N HSQC and triple resonance strips for αsyn in 10 % TFE. A. ^{1}H-^{15}N HSQC of 150 µM αsyn in 10% TFE. B. Triple resonance trips with HNCOCA (green) acquired 16.5 hours after adding TFE, CBCACONH (blue) acquired 32.3 hours

after adding TFE, HNCA (yellow) acquired 0.6 hours after adding TFE and HNCA (red) acquired 60.9 hours after adding TFE.

NMR chemical shifts are sensitive indicators of secondary structure propensities of IDPs and have been analyzed to determine the differences in the conformational propensities of αsyn with and without TFE conditions. We used secondary structure propensity scores (SSP) developed by Marsh, et. al. (Marsh, Singh et al. 2006) with $^{13}C^{\alpha}$ chemical shifts as input and a 5-residue sliding window to define a residue-specific secondary structure propensity. The $^{13}C^{\alpha}$ chemical shifts were determined by HNCA and HNCOCA within 32 hours from adding TFE. The results show that αsyn with TFE has increased SSP in the first 30 residues and around residue 55 to 65. Other than those regions the rest of the SSP along the sequence including NAC and C-terminal region are quite similar to αsyn without TFE. It is interesting to note that Anderson et. al. also implicates TFE-induced structural transitions involving the N-terminus of the protein by revealing that αsyn and αsyn 1-102 have a similar conformational change (Anderson, Ramlall et al. 2010). Our NMR SSP study shows residue specific TFE-induced αsyn conformational changes.

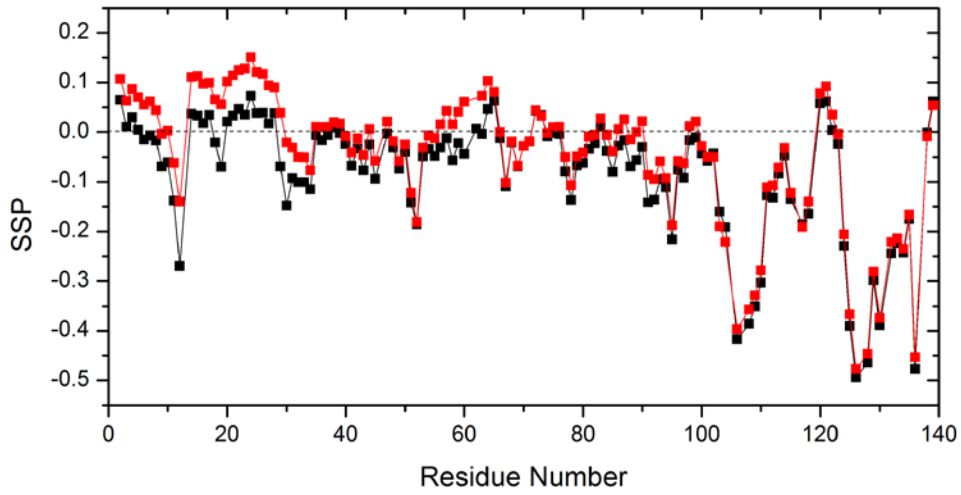

Figure 5.3 SSP of αsyn with (red) and without (black) 10% TFE.

5.3.3 Time-dependent HSQC and backbone dynamics R_2 of TFE-induced αsyn monomer.

As soon as TFE is added, the aggregation starts with loss of the lag phase. The ^{1}H-^{15}N HSQC experiment is performed to monitor the monomer conformational changes. Time dependent ^{1}H-^{15}N HSQC were acquired over a period of 228.5 hours with 25 hours intervals. Major peaks stayed the same over the examined time, however, extra peaks started to appear at 96.2 hours. A sharp decrease of about 16% of original peak intensity occurred in the first 25 hours which covered the whole exponential growth phase determined by ThT fluorescence (Figure 5.1E). After 25 hours, the aggregation reached a mature phase and the peak intensity decreased with almost no changes in peak intensity after 150 hours (Figure 5.4A). However, the peak intensity decrease is strongly dependent on where residues reside. Peak intensity for residues in the N-terminal region has a sharp decrease without reaching a plateau while the C-terminal residues almost stay the same after the sharp decrease in first 25 hours (Figure 5.4B). The NAC region has

some residues behaving like the N-terminal residues and some behaving like C-terminal residues. The results suggest different interaction N-terminal, NAC and C-terminal region possess during aggregation and after mature phase.

^{15}N relaxation experiments were performed to explore the backbone dynamics of αsyn with 10% TFE. The elevated R_2 values are observed throughout the sequence compared to that without TFE. The experiment was conducted within 25 hours after adding TFE. The result shows that TFE-induced αsyn monomer exhibits elevated $R_{2,}$ especially in the N-terminal region, bigger increase around 3 Hz are detected (Figure 5.4C). Time-dependent R_2 experiments show that after 80.2 hours the R_2 values decrease in the N-terminal first 30 residues and from 80.2 hours to 253.7 hours all the R_2 data acquired stays almost the same (Figure 5.4D). The decrease of R_2 values happened at the same time as when extra peaks appeared at ^{1}H-^{15}N spectrum. Both the backbone dynamic probe and the monomer conformation spectrum indicate a process other than aggregation, possibly degradation (MALDI-TOF and SDS-PAGE of final product shows the existence of smaller fractions), has started after the mature phase.

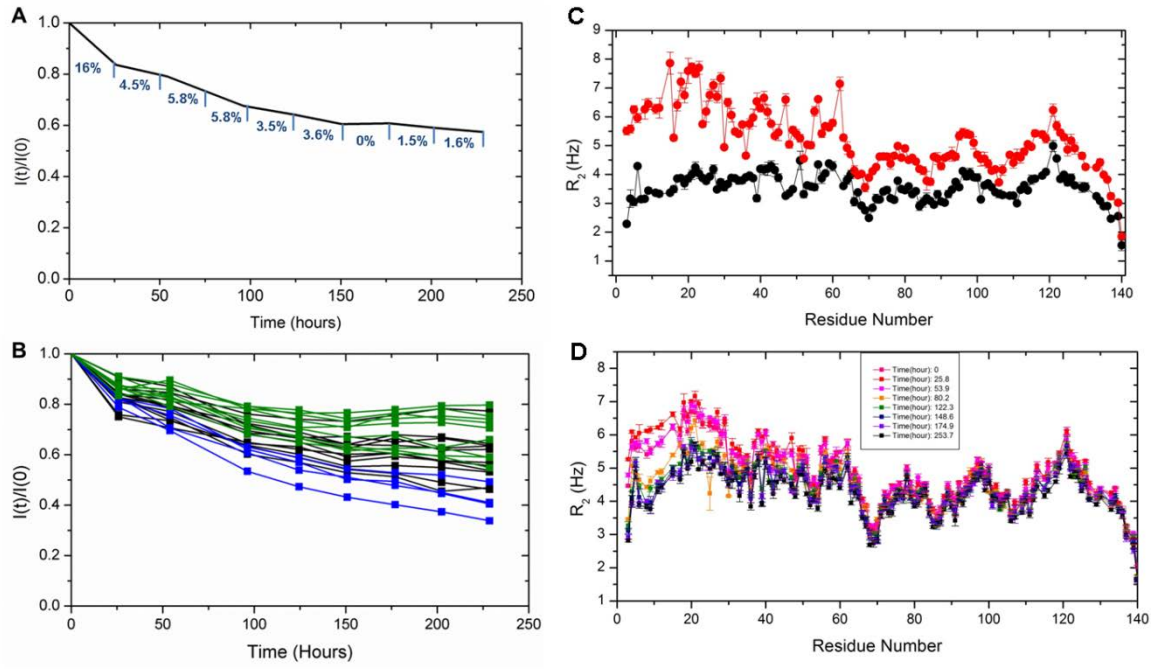

Figure 5.4 Time-dependent HSQC and R_2 of αsyn with 10% TFE. A. The normalized peak intensity at different time point. The decrease of peak intensity in 25 hours is shown as percentage labeled at the according time period. B. A collection of residues from N-terminal (blue), NAC (black) and C-terminal (green) regions. C. R_2 of αsyn in 10% TFE (red) and without 10% TFE (black). D. Time-dependent R_2 value of αsyn in 10% TFE, color code shows in the graph.

As elevated R_2 could come from the restricted motion from transient secondary structure, local clustering effects, or conformation exchange in micro- to millisecond timescale, experiments determining chemical exchange rate (R_{ex}) were performed (Wu, Kim et al. 2008). One experiment, the η_{xy} (CSA/dipolar cross-correlation rate) experiment(Tjandra, Szabo et al. 1996; Kroenke, Loria et al. 1998), is designed to quantify the intrinsic R_2 (R_2^0), under conditions where chemical exchange is totally suppressed and the second

experiment, the in-phase Hahn echo experiment (R_2^{HE})(Wang, Grey et al. 2001), is designed to measure R_2 under conditions where the full exchange contribution to relaxation is obtained. R_{ex} values derived from the difference in these two experiments shows that for αsyn in 10% TFE , R_{ex} is primarily -1 ~1.5 Hz, suggesting minimal or no chemical exchange across the protein sequence (Figure 5.5). Ser, Thr, Gly residues tend to have slightly higher R_{ex} values, closer to 2.5 Hz, which is observed previously and is believed that it may relate to solvent water exchange and a manuscript by Seho Kim et. al. investigating the phenomon is under review. Hydrodynamic radius of αsyn with 10% TFE (24.4±0.22 Å) is much smaller than αsyn without 10% TFE (26.4±0.22 Å). Elevated R_2 of αsyn with 10% TFE may come from restricted motion from transient secondary structure, local clustering effects and inter-molecular interactions.

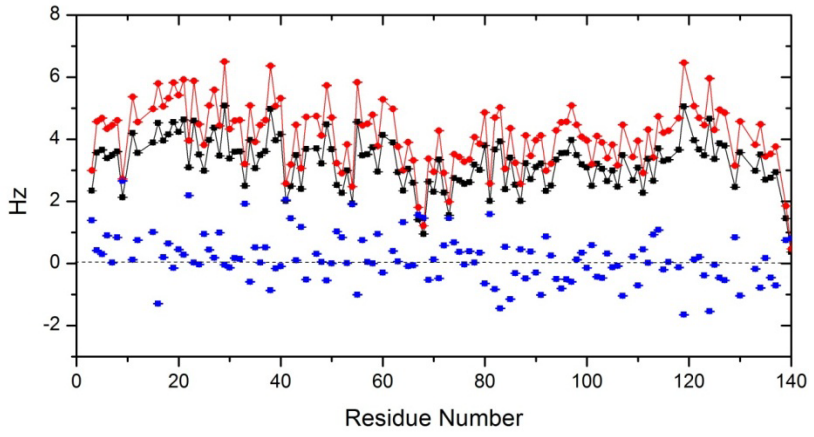

Figure 5.5 R_{ex} (blue), R_2^0 (black), R_2^{HE} (red) of αsyn in 10% TFE.

5.3.4 Inter-molecular interactions correlate with N-terminal helical propensity induced by TFE.

Previously our lab have used NMR paramagnetic relaxation enhancement (PRE) experiments to detect the transient inter-molecular contacts of αsyn in pH6 in MES buffer

with 100 mM NaCl (Wu and Baum 2010). The PRE effect is observable only when αsyn concentration reaches 1100 μM. The detected transient interaction is in head-to-tail arrangement with non-interacting NAC regions. The weak contact between N- and C-terminal may be due to the fact that the highly charged molecule favors solvation rather than interacting with another molecule. Further study on the salt free condition revealed this head-to-tail arrangement is an aggregation-protective inter-molecular off-pathway interaction. Low concentration of TFE enhances αsyn aggregation (Munishkina, Phelan et al. 2003), which provides a condition to detect the transient interaction that is on-pathway of aggregation. By using the inter-molecular PRE experiment on 150 μM αsyn with 10% TFE, the experimental data was acquired within 12 hours from adding TFE and with HSQC intensity changes during experiment less than a few percent. The condition compared with the previous study has almost 7 times lower protein concentration but with the addition of 10% TFE. The inter-chain PRE profiles of αsyn in 10% TFE with spin label at A19C, A90C and G132C separately are shown in Figure 5.6. The inter-chain interactions are only observed between the A19C spin label and residue 1 to 8, residue 16 to 26 and residue 58 to 64. However, the NAC and C-terminal spin labels display no inter-molecular contacts. The results suggest that the transient inter-molecular interactions exist in αsyn with 10% TFE is in head-to-head arrangement and with relatively strong contact as compared to without TFE.

Good correlation between the increased helical propensity and the increased HR_2 value representing inter-molecular interactions suggests transient helix-helix inter-molecular interactions in the TFE-induced αsyn aggregation (Figure 5.6A). The regions have inter-molecular interactions at residue 1 to 8, residue 16 to 26 and residue 58 to 64 also

populating increased helical propensity. The detected inter-molecular interactions and increased secondary structural propensity may suggest the transient helical intermediate is on-pathway of TFE induced aggregation as described by Anderson, et. al. (Anderson, Ramlall et al. 2010).

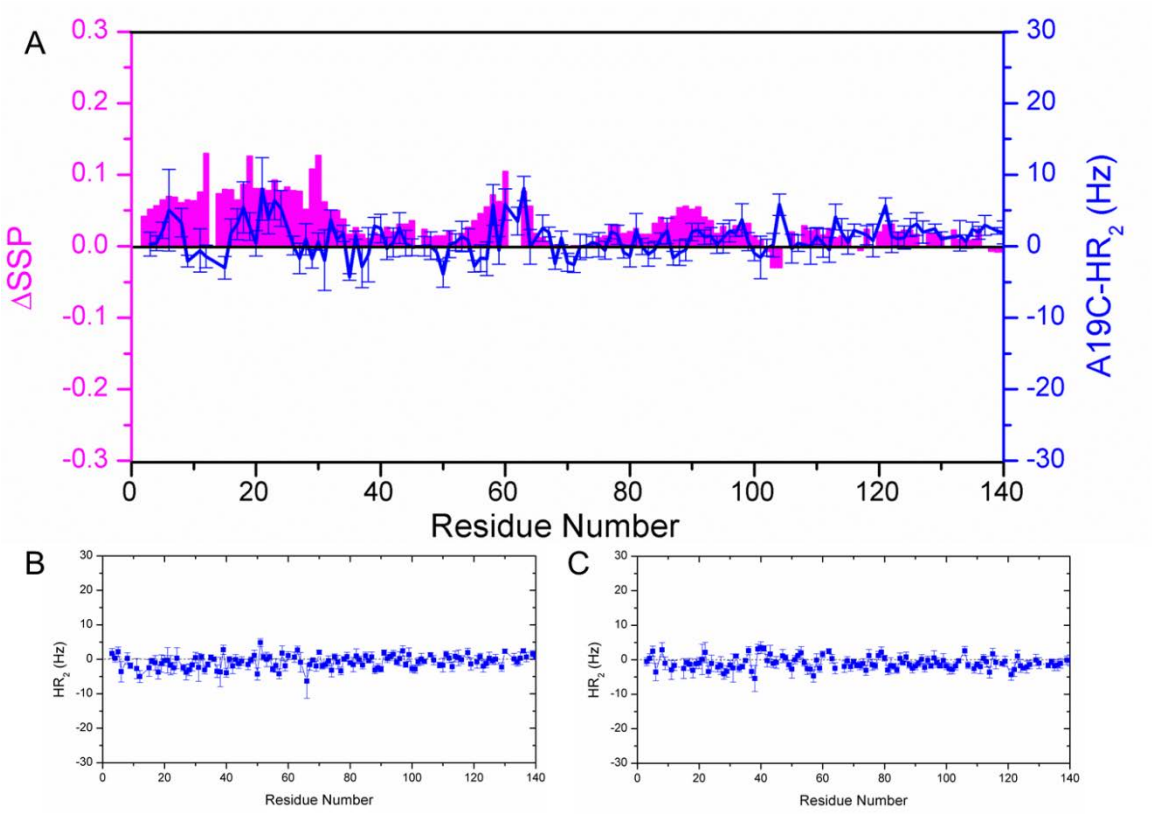

Figure 5.6 Correlation between ΔSSP and HR2 of αsyn in 10% TFE. A. Correlation between SSP (magenta bar) and A19C inter-molecular HR_2 (blue line); B. A90C inter-molecular HR_2; C. G132C inter-molecular HR_2.

5.4 Conclusion.

In this study, we are the first to show the residue-specific conformation and head-to-head inter-molecular interactions of transient helical intermediate in TFE-induced αsyn aggregation. Our results further support previous view on increased helical propensity in

first 30 residues and around 55–65 regions are critical for increased aggregation rate. The N-terminal transient helix-to-helix interactions observed in elongation phase directly show how those intermediate transform into dimer and big aggregates as well as fibrils. The characterization of this intermediate may imply the relevant pathway for αsyn associate with membranes.

Chapter 6. N-terminal acetylation in α-synuclein and familial A53T

6.1 Introduction.

Alpha synuclein (αsyn) is a small primarily neuronal protein that is known to make a structural transition to amyloid fibrils in several neurodegenerative diseases. It is a major component of Lewy Bodies in patients with Parkinson's, a disease resulting from a loss of dopaminergic neurons (Baba, Nakajo et al. 1998; Spillantini, Crowther et al. 1998). While a large body of evidence over many years has supported the characterization of αsyn as an intrinsically disordered monomer, a recent study by Bartels, et. al. in which αsyn was isolated from red blood cells, as well as neuronal and non-neuronal cell lines, reported that in its physiological form αsyn exists as a helical tetramer that is resistant to amyloid formation and has a mass corresponding to the sole modification of the monomer by an acetyl group (Bartels, Choi et al. 2011). Shortly thereafter, a GST recombinant αsyn protein purified from the micellar reagent ß-octyl glucoside (BOG) similarly showed the existence of a dynamic αsyn tetramer (Wang, Perovic et al. 2011). In response to these papers, Lashuel and an assemblage of groups went on to demonstrate that αsyn isolated from rodent and human nervous system tissues, and erythrocytes presents as an intrinsically disordered monomer. In this work, Lashuel was the first to address the role of the acetyl group, referred to in the Bartels paper, and showed the acetylated and non-acetylated proteins migrate similarly on non-denaturing gels(Fauvet, Mbefo et al. 2012). A follow up report by Rhoades has indicated that recombinant acetylated αsyn (Ac-αsyn) is monomeric under physiological conditions, but that it may

display a greater preference for helical structure and higher-order oligomerization states when purified in the presence of BOG(Trexler and Rhoades 2012).

It has been demonstrated that soluble and insoluble fractions of brain tissues from patients suffering from Parkinson's and from dementia with Lewy bodies universally contain N-terminal Ac-αsyn.(Anderson, Walker et al. 2006; Ohrfelt, Zetterberg et al. 2011) While an uncommon modification to prokaryotic proteins, the N-termini of eukaryotes are often processed at the initiating amino acid with the addition of an acetyl group by N-acetyltransferase complexes (Polevoda and Sherman 2003). The role of N-terminal acetylation, however, is poorly understood, but has been suggested to affect the kinetic or thermal stability of proteins (Polevoda and Sherman 2000; Arnesen 2011). Because N-terminal Ac-αsyn is now believed to be the physiologically relevant species in the brain, it is critically important to characterize the conformational properties and fibrillation kinetics of this protein in order to understand how acetylation impacts on the mechanism of fibril formation and disease.

Here we present the first direct experimental evidence that N-terminal acetylation affects the secondary structure propensities and kinetics of fibril assembly of Ac-αsyn relative to the non acetylated protein. Using NMR, non-covalent electrospray ionization mass spectrometry (ESI-MS), ion mobility spectrometry combined with ESI-MS (ESI-IMS-MS), Thioflavin T (ThT) fluorescence and electron microscopy (EM) we demonstrate that the 100% N-terminal acetylated recombinant αsyn protein purified under mild physiological conditions presents primarily as a disordered monomer. Our results highlight that N-terminal acetylation impacts on secondary structure propensity in important functional regions including the N-terminal and His-50 metal binding

regions(Bisaglia, Tessari et al. 2009) and the regions of the three familial mutations A30P, E46K and A53T (Polymeropoulos, Lavedan et al. 1997; Kruger, Kuhn et al. 1998; Zarranz, Alegre et al. 2004). The removal of the positive charge at the N-terminus arising from acetylation thus has short and long-range conformational effects that impact on the distribution of states sampled by the intrinsically disordered αsyn monomer and on the rate of fibril assembly. The acetylation of on familial mutation A53T is also examined. The result shows that with acetyl group A53T lost long range effect which induce helical propensity to residue 6~32. The apparent growth rate of acetylated A53T (Ac-A53T) is faster than that of Ac-αsyn but slower than A53T, which further confirmed helical propensity in regions 6~32 and around 53 are aggregation prone while helical propensity induced by acetyl group in first 12 residues is aggregation protective. This result confirmed previous finding that secondary structure play a key role in fibril assembly kinetics and helical propensity in regions 6~32 and 53 correlates to faster apparent growth rate.

6.2 Material and Methods.

6.2.1 Co-expression of acetylated αsyn.

Ac-αsyn was produced by co-expressing the αsyn plasmid and NatB plasmid in E. coli. The NatB plasmid was a kind gift from Dr. Daniel Mulvihill. The αsyn and NatB plasmids were first co-transformed into E. coli DE3 cells as follows:

1. Transfer 3ul of αsyn with 3ul of NatB plasmid into 100uL DE3 competent cell.
2. Leave it on ice for 2 mins
3. Heat at 42 °C for 60s.
4. Leave it on ice for 2mins.

5. Add 1mL LB into the tube and incubate in 37 °C shaking 220 rpm for 45 mins.

6. Centrifuge at 4000 rpm and get rid of 900mL solution.

7. Resuspend the cell and transfer 200ul to the plate (with ampicillin and chloramphenicol)

8. Incubate at 37 °C overnight.

E. coli cells were cultured in LB medium (Sigma) with 25 μg/L chloramphenicol (Sigma) and 50 μg/L ampicillin (Fisher) and grown in Erlenmeyer flasks at 37 °C with vigorous shaking. Expression was induced by addition of 1 mM isopropyl-β-D-1-galactopyranoside (Fisher) once the cell culture had reached an OD_{600} of 0.4-0.6 and incubation was then allowed to proceed at 20 °C overnight. Cells were harvested the next morning. Uniform isotope labeling of acetylated αsyn was performed in standard minimal M9 medium containing $^{15}NH_4Cl$ (CIL, Inc.) as the sole nitrogen source and ^{13}C-glucose (CIL, Inc.) was substituted for ^{12}C-glucose (Sigma) when $^{13}C/^{15}N$ doubly labeled samples were expressed.

The induction step was also experimented at 37 °C for 4 hours as for non-acetylated αsyn (Chapter 2.2). The expression yield for induction at 37 °C is more than that of induction at 20 °C, however, at the same time other unwanted proteins are more too (Figure 6.1). Gina M. Moriarty purified Ac-αsyn from induction at 37 °C batch using salting-out protocol and the protein migrate at the same place as proteins expressed in 20 °C.

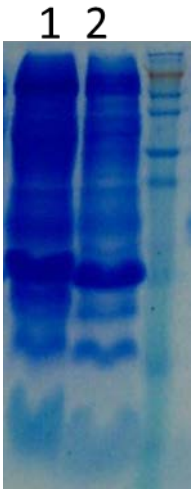

Figure 6.1 Expression result for Ac-αsyn induced in 37 °C (Lane 1) and 20 °C (Lane 2).

6.2.2 Protein purification.

Ac-αsyn and Ac-A53T were purified under "mild" and "salting-out" conditions; αsyn protein was purified under both "mild" and "harsh" conditions. Comparison of αsyn purified under harsh or mild purification protocols by ^{1}H-^{15}N HSQC, ESI-MS, CD, native gel and SEC indicate that they are essentially indistinguishable (Figure 6.2), consistent with other comparisons made by Lashuel(Fauvet, Mbefo et al. 2012).

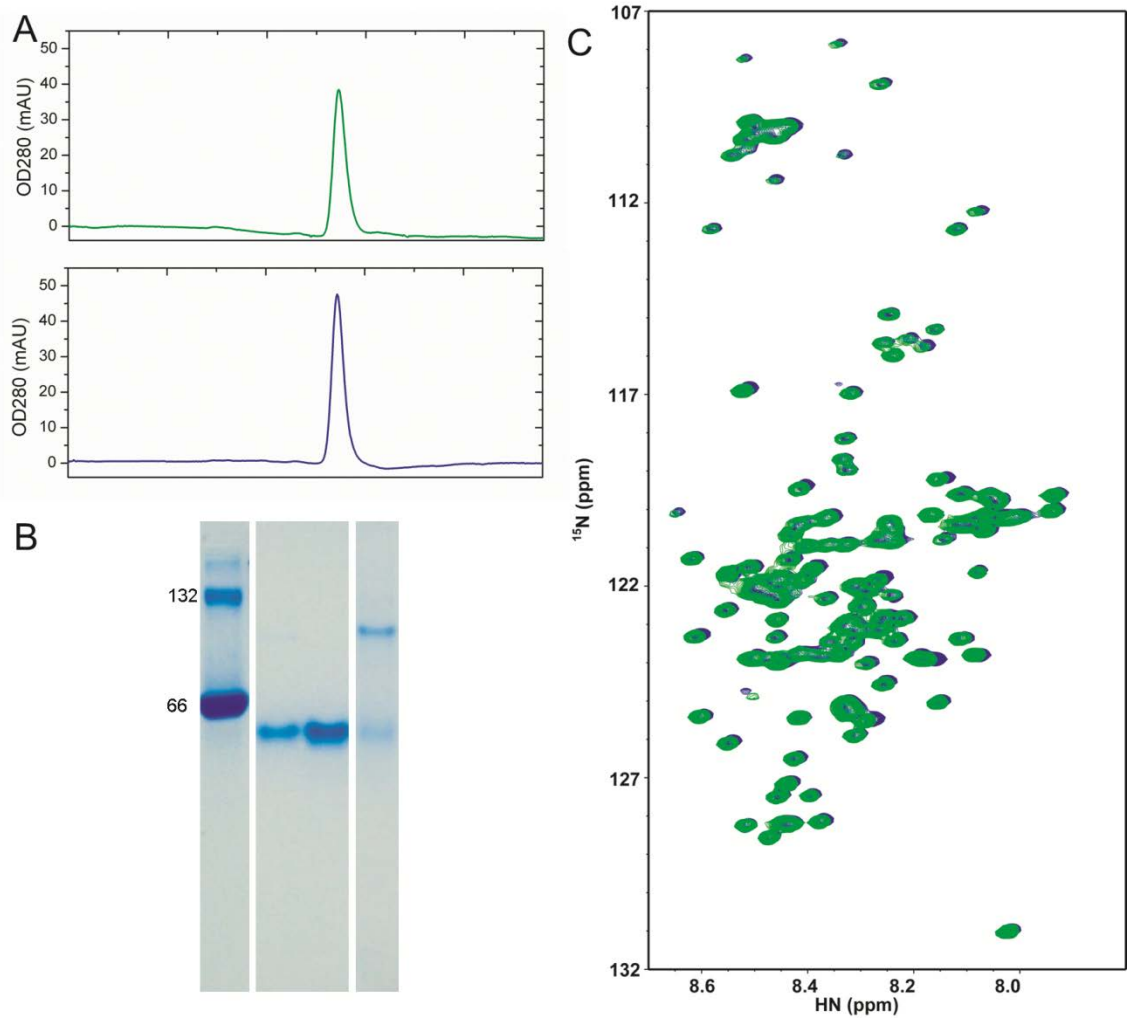

Figure 6.2 αsyn purified using mild (blue) and harsh conditions (green) are biochemically and structurally indistinguishable. A. Analytical SEC (conditions described in 6.2.3); B. Native gel electrophoresis (conditions described in 6.2.4). Lane 1: BSA, Lane 2: mildly purified αsyn; Lane 3: harshly purified αsyn; Lane 4: harshly purified G132C αsyn. C. ^{1}H-^{15}N HSQC NMR spectra obtained by Lashuel also showed that αsyn purified under harsh and mild conditions exists as a disordered monomer that gives rise to similar ^{1}H -^{15}N HSQC spectra(Fauvet, Mbefo et al. 2012).

6.2.2.1 Mild protocol.

Pelleted cells were retrieved from storage at -80°C and suspended in 25 mM Tris HCl buffer, pH 7.7. The cell pellet was then homogenized three times at 10,000–15,000 psi. The cell lysates were centrifuged for 30 minutes at 13,000 rpm. The supernatants were then passed through a 0.22 µm filter before being loaded onto a HiTrap Q 5 mL column on an AKTA FPLC system (GE Healthcare LifeSciences). The column was equilibrated with 25 mM Tris HCl, pH 7.7 and synuclein protein was eluted by applying increasing concentrations of up to 500 mM NaCl. αSyn usually eluted at ~250 mM NaCl. αsyn enriched fractions were concentrated to 2–3 mL using an Amicon 10k MWCO centrifugal filter (Millipore) before injection onto a Superdex 75 HiLoad 26/600 prep grade size exclusion column (GE Healthcare LifeSciences). The column was equilibrated with 25 mM Tris HCl and 250 mM NaCl or phosphate buffered saline (PBS) before sample injection. The flow rate ranged from 1~2.5 ml/min and synuclein usually elutes around 160 mL. Pure protein fractions were detected by SDS-PAGE. Fractions containing αsyn were then collected and flash-frozen in liquid nitrogen before storage at –80 °C.

6.2.2.2 Salting-out protocol.

Pelleted cells were retrieved from storage at –80°C and suspended in PBS pH 7.4. The cell pellet was then homogenized three times at 10,000-15,000 psi. The cell lysates were centrifuged for 30 minutes at 13,000 rpm. Two different ways of salting-out were studied: (1) Streptomycin sulfate (Fisher) (10 mg/ml) was added to the supernatant and the mixture was stirred at 4 °C for at least 15 minutes followed by centrifugation at 13,000 rpm for 30 minutes. Ammonium sulfate (Sigma) (0.361 g/ml) was added to the supernatant and the mixture was stirred at 4 °C for 30 minutes after fully dissolution of

ammonium sulfate, followed by centrifugation at 13,000 rpm for 30 minutes. (2) Ammonium sulfate (Sigma) (0.166 g/ml) was added to the supernatant and the mixture was stirred at 4 °C for at least 15 minutes followed by centrifugation at 13,000 rpm for 30 minutes. Ammonium sulfate (Sigma) (0.244 g/ml) was added to the supernatant and the mixture was stirred at 4 °C for 30 minutes after fully dissolution of ammonium sulfate, followed by centrifugation at 13,000 rpm for 30 minutes. The pellet was re-suspended in 25 mM Tris HCl, pH 7.7 and dialyzed against 25 mM Tris HCl buffer overnight. The supernatants were then passed through a 0.22 μm filter before being loaded onto a Hitrap Q column on an AKTA FPLC system (GE Healthcare LifeSciences). The column was equilibrated with 25 mM Tris HCl, pH 7.7 and αsyn was eluted by applying increasing concentrations of up to 500 mM NaCl. αsyn usually eluted at ~250 mM NaCl. αsyn enriched fractions were concentrated to 2-3 mL using an Amicon 10k MWCO centrifugal filter (Millipore) before injection onto a Superdex 75 HiLoad 26/600 prep grade size exclusion column (GE Healthcare LifeSciences). The column was equilibrated with 25 mM Tris HCl and 250 mM NaCl or phosphate buffered saline (PBS) before sample injection. The flow rate ranged from 1~2.5 ml/min and synuclein usually elutes around 160 mL. Pure protein fractions were detected by SDS-PAGE.

6.2.2.3 Harsh protocol.

Purification of αsyn was as previously described in Chapter 2.3.

6.2.3 Analytical SEC.

All αsyn samples were thawed from storage at –80 °C or from lyophilized powder stored at –20°C or –80 °C. The samples were prepared by dissolving them in PBS if needed, and passing them through an Amicon 100k MWCO filter to remove large aggregates.

Samples were concentrated to 100 μM if needed with an Amicon 10k MWCO centrifugal filter (Millipore). 100 μL was loaded onto the column. Samples were eluted at 0.5 mL/min on a Superdex 200 10/300 (GE Healthcare Lifesciences) column in PBS, pH 7.4. The work is done by Gina M. Moriarty.

6.2.4 Native gel electrophoresis.

Ac-αsyn and αsyn samples purified from mild conditions, BSA (Sigma), and lyophilized G132C αsyn purified from harsh conditions were loaded onto gels with Native Sample buffer (Bio-Rad). Gels were run at 140V for 3 hours and stained with SimplyBlue SafeStain (Life Technologies Corporation). Native gel electrophoresis was performed on 13% acrylamide home-made gels which were prepared according to standard protocol in the absence of sodium dodecyl sulfate.

6.2.5 NMR assignment.

^{13}C assignments for Ac-αsyn and Ac-A53T were obtained from a 350 μM doubly labeled protein in PBS buffer at 15 °C and ^{13}C assignments for αsyn were used as described in Chapter 2.4.

6.2.6 Thioflavin T fluorescence assay for fibril formation.

The methods for fibril assembly and analysis are described in chapter 2.x.x. In brief, protein was thawed and exchanged to PBS buffer pH 7.4, NaCl 137 mM (dissolved from Sigma PBS tablet) using Amicon 10k MWCO centrifugal filter (Millipore) for three times. Then the solution was filtered through Amicon 100k MWCO centrifugal filter

(Millipore) to remove the big aggregates and the final protein concentration was around 150 μM (ε_{280}=5120 M^{-1} cm^{-1}) with 20 μM ThioflavinT for fluorescence measurements. 100 μL of the mixture was then pipetted onto plate for Thioflavin T fluorescence assay.

To test whether fibril assembly kinetics is dependent on sample preparation method, a comparison of samples purified using three different purifying protocols on αsyn was performed. Salting-out protocol was using the chapter 6.2.2.2 (2) protocol with two ammonium sulfate cut off. All the data sets were fit to Boltzmann function directly. One filter, adjusted R^2 bigger than 0.99, was set up to get rid of bad fittings. For samples purified using salting-out protocol big noise came after the mature phase, data points with time longer than 250 hours was not used. The brief summary of fibril assembly kinetics and data sets is shown in Table 6.1. Samples purified using different protocols give different lag times and k_{app}. Samples purified using salting-out protocols give the slowest aggregation kinetics with the longest lag time and shortest k_{app}. Sample purified by harsh protocol show around two times faster rates and shorter lag time than that of sample purified using salting-out protocol. Samples purified using mild protocol show similar lag times to that of samples purified from salting-out protocol but the fastest k_{app} rate among samples purified by all three protocols (Figure 6.3.A). Also relatively large error was observed for sample purified by mild condition. It seems that there are two sets of distributions one with lag time centered around 50 hours while the other with lag time centered around 100 hours. Based on this analysis, it is important to conduct ThT fluorescence with samples purified using same protocol.

Table 6.1 Fibril assembly kinetics for αsyn using different purification protocols

	Lag Time	Lag (error)	k_{app}	k_{app} (error)	Used data set	Total data sets
Mild	79.89	40.27	0.40	0.13	7	7
Salting-out	83.73	7.45	0.10	0.03	7	24
Harsh	53.48	15.79	0.22	0.07	12	12

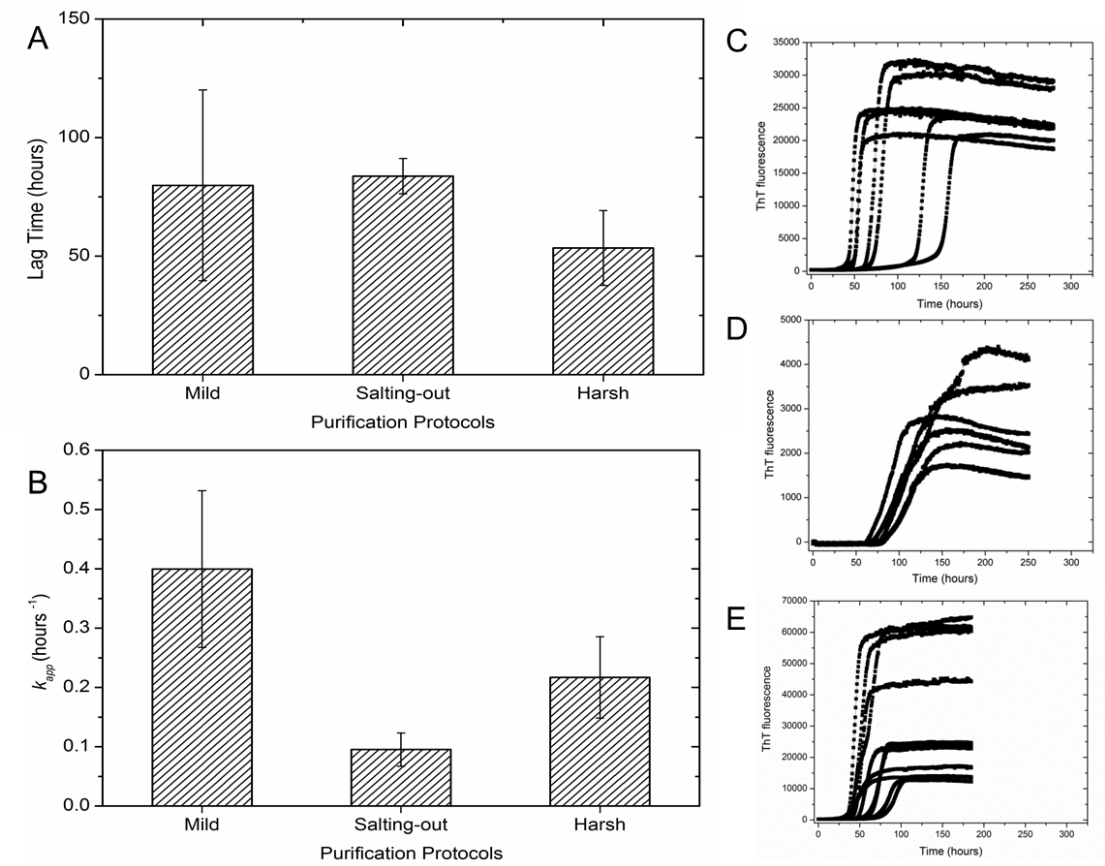

Figure 6.3 Fibril assembly kinetics for αsyn purified using three different protocols. A. Lag time of αsyn purified using mild, salting-out, harsh protocols; B. k_{app} of αsyn purified using mild, salting-out, harsh protocols. C. raw data of ThT fluorescence assay for sample purified using mild protocol, 7 data sets; D. raw data of ThT fluorescence assay for sample purified using salting-out with two ammonium sulfate cut off protocol, 7

data sets; E. raw data of ThT fluorescence assay for sample purified using harsh protocol, 12 data sets.

6.2.7 Fibril morphology examination.

The fibril morphology is examined by TEM. The detailed method is described in Chapter 2.5.2.

6.2.8 ESI-IMS-MS.

Electron spray ionization-ion mobility spectroscopy-mass spectroscopy (ESI-IMS-MS) experiments were in collaboration of Dr. Sheena Radford lab and performed by Lucy A. Woods using similar procedures to Smith et. al.(Smith, Radford et al. 2010) αsyn proteins (35 μM) were dissolved or buffer exchanged into 165 mM ammonium acetate, pH 7.4 and the sampling cone voltage was varied from native conditions (30 V) to conditions that allow for the detection of large non-covalent species (170 V).

6.3 Results and Discussion.

6.3.1 Ac-αsyn is unfolded monomer with 100% acetylation.

In order to determine the oligomeric status and the conformational properties of Ac-αsyn and to compare this with αsyn, Ac-αsyn was generated from an *E. coli* co-expression system containing the yeast N-terminal acetyltransferase (NatB)(Johnson, Coulton et al. 2010; Trexler and Rhoades 2012)and purified using mild physiological purification conditions (herein described as “mild” purification) that avoid steps involving the application of heat or salting out (herein described as ‘harsh’ conditions) (see “material

and method" for detailed protocols of "mild" and "harsh" purification). Taking into account recent suggestions that harsh purification steps such as boiling can destroy tetramer formation(Bartels, Choi et al. 2011; Wang, Perovic et al. 2011) or that purification under non-physiological conditions(Trexler and Rhoades 2012) can promote higher order oligomerization states of αsyn, a mild physiological purification protocol that applies only homogenization and liquid chromatography was adopted for Ac-αsyn in this work. ESI-MS confirms that purified Ac-αsyn co-expressed with this eukaryotic modification system exists as 100% acetylated protein (observed mass 14502.5 Da, expected mass 14502.1 Da) (Figure 6.4A, B).

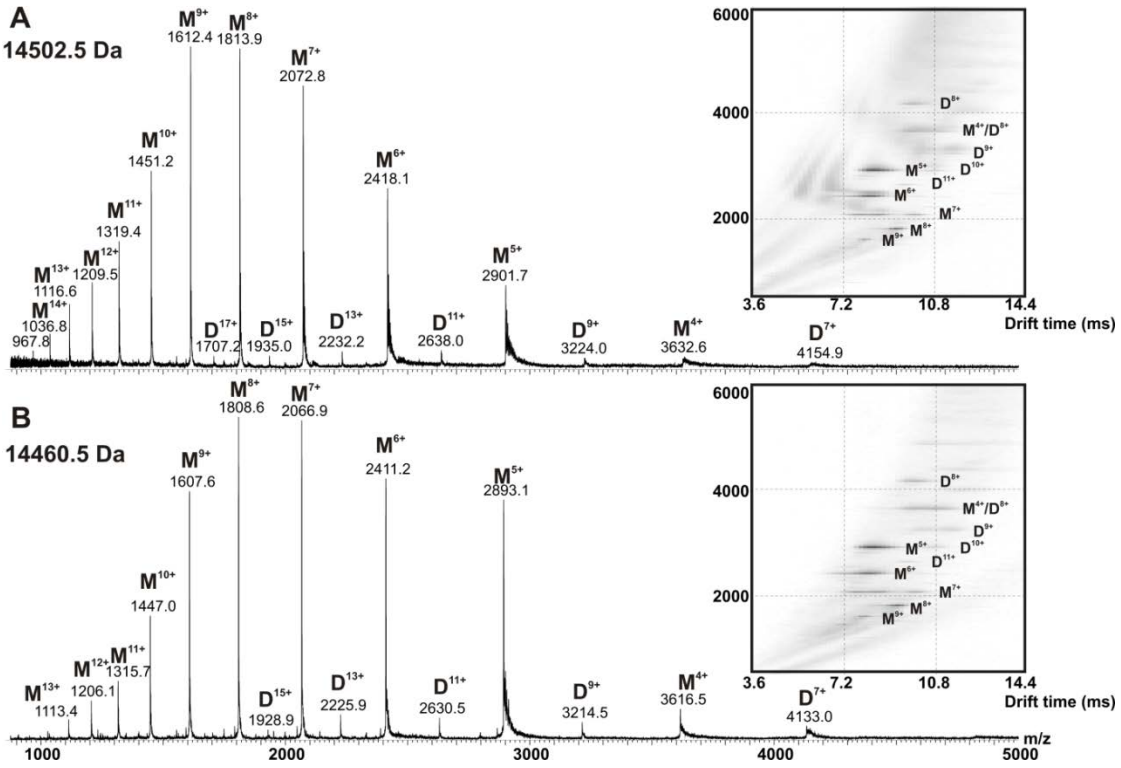

Figure 6.4 Native ESI-IMS-MS analysis of (A) Ac-αsyn and (B) αsyn.

Native ESI-IMS-MS analysis of Ac-αsyn and αsyn shows both samples to be predominantly monomeric. Ac-αsyn or αsyn (35 μM) were dissolved or buffer exchanged

into 165 mM ammonium acetate, pH 7.4. Inset shows the driftscope plot of each sample acquired under conditions optimized for the detection of large non-covalent species (cone voltage 170V). ESI mass spectra of αsyn purified under “harsh” and “mild” conditions indicate that the purification procedure does not affect the results obtained (not shown).

Investigation of the existence of higher-order oligomeric states in the Ac-αsyn was performed using ESI-MS and ESI-IMS-MS (Figure 6.4A), along with solution methods including analytical size-exclusion chromatography (SEC) and migration on a native gel (Figure 6.5). The latter two methods show that both proteins elute at the same volume as a single peak using SEC and migrate at the same position on the native gel. These data show that the acetylated protein exhibits indistinguishable hydrodynamic dimensions from the non-acetylated protein purified under mild conditions.

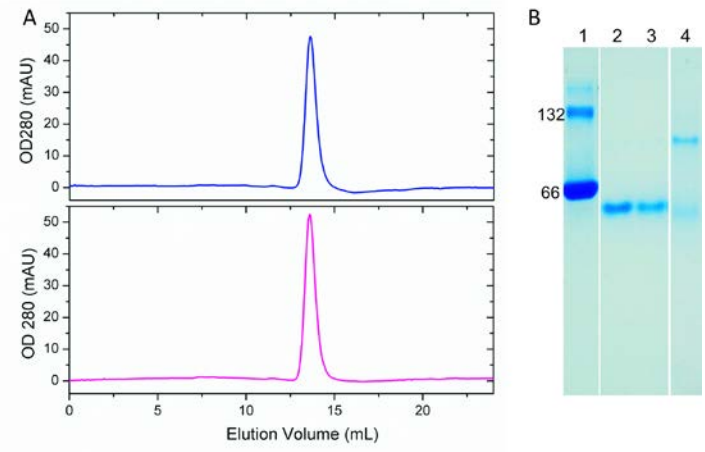

Figure 6.5 Ac-αsyn and αsyn both purified under mild conditions elute at the same position in analytical SEC and migrate similarly by native gel electrophoresis. Additionally they migrate as previously observed for unfolded monomers(Fauvet, Mbefo et al. 2012; Trexler and Rhoades 2012). A. Analytical SEC profiles of purified Ac-αsyn (lower panel) and αsyn (upper panel). B. Native gel electrophoresis Lane 1: BSA (66

kDa); Lane 2: Ac-αsyn (14.502 kDa); Lane 3: αsyn (14.460 kDa) ; Lane 4: αsyn G132C (14.506 kDa and 29 kDa). BSA marks the migration position of a 66 kDa globular protein. G132C αsyn, which also migrates as monomer and covalently linked dimer on SDS-PAGE marks the migration of a unfolded monomer of 14.5 kDa and dimer on the native gel.

ESI-IMS-MS experiments add further information about the oligomerization status of Ac-αsyn, as the population distributions can be obtained quantitatively from these experiments by the ability of ESI-IMS-MS to separate peaks of identical m/z and to quantify their population and conformational properties(Smith, Radford et al. 2010). Comparison of the ESI-IMS-MS spectra of Ac-αsyn and αsyn indicate that acetylation does not perturb the oligomerization status of αsyn, as both αsyn and Ac-αsyn appear predominantly monomeric (~90-95%), with the presence of a small population of dimeric species (~5-10%), where the former appears in both more compact and extended forms at physiological pH (Figure. 6.4 A, B). These data are consistent with previous analyses using ESI-MS(Bernstein, Liu et al. 2004; Frimpong, Abzalimov et al. 2010; Natalello, Benetti et al. 2011), and inter-chain NMR PRE experiments that have shown weak dimer N- to C-terminal inter-chain interactions in αsyn under physiological conditions(Wu and Baum 2010). Because of the suggestion in the recent literature that Ac-αsyn purified under micellar BOG conditions can shift the monomer populations towards oligomeric species(Trexler and Rhoades 2012), the possibility of higher order transient oligomeric species purified under physiological conditions was further probed using a higher cone voltage (170V) in ESI-IMS-MS which favors detection of large non-covalent aggregates.

These experiments revealed no difference between the oligomeric distribution of acetylated and non-acetylated samples and no evidence for the population of higher-order species, consistent with results obtained by Rhoades when purification was performed under physiological conditions. While the biochemical techniques inform about the hydrodynamic radii, ESI-IMS-MS provides definite evidence that both proteins are predominantly monomeric in aqueous solution at pH 7.4.

6.3.2 Acetylation induced helical propensity in first 12 residues.

Residue-specific analysis of Ac-αsyn by NMR was next pursued to enable the secondary structure propensities of Ac-αsyn and αsyn monomers to be compared (Figure 6.6, 6.7). Backbone assignments by triple resonance experiments confirmed that Ac-αsyn is acetylated on the N-terminal residue Met-1 (Figure 6.6B). An overlay of the ^{1}H-^{15}N spectrum of Ac-αsyn and αsyn at pH 7.4, shows that the two proteins share a high degree of similarity, except at the first nine N-terminal residues (Figure 6.6A). Both Ac-αsyn and αsyn display narrow chemical shift dispersion, characteristic of a predominantly unfolded protein, consistent with analyses using far UV CD. Acetylation of the N-terminus results in the appearance of the Met-1 and Asp-2 resonances in the Ac-αsyn ^{1}H-^{15}N HSQC spectrum possibly because of changes in hydrogen exchange rates arising from the modification at Met-1. Additionally, acetylation results in up-field shifting of residues observable in both spectra in the region of the first nine N-terminal residues, (inset Figure 6.6A.) further supporting the site of acetylation as Met-1 and demonstrating the extent to which N-terminal acetylation alters the conformational properties of the polypeptide chain.

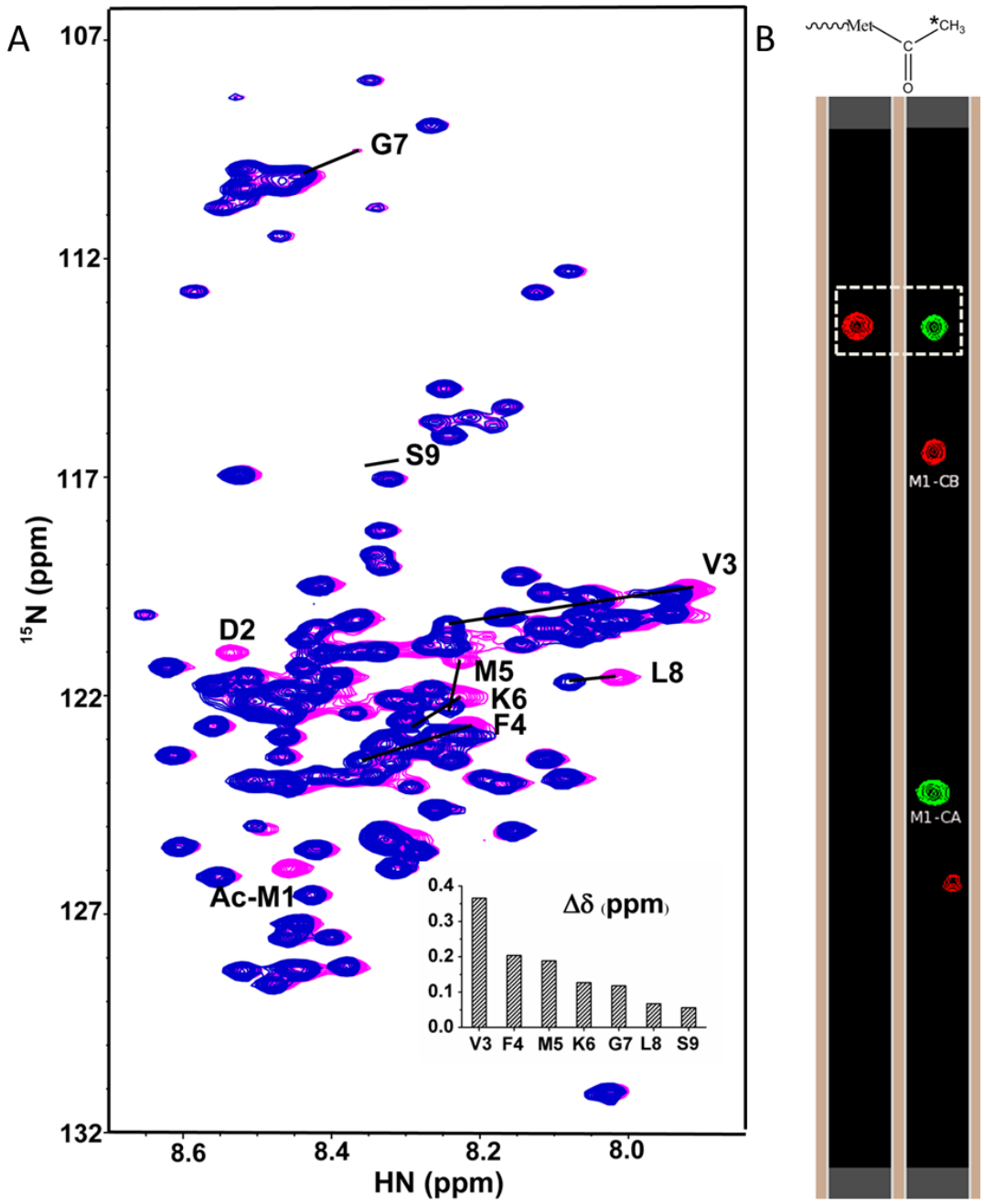

Figure 6.6 A. 1H-15N HSQC spectra of Ac-αsyn (magenta) vs. αsyn (blue) at 15ºC. The changes in the first 9 residues of Ac-αsyn are indicated in the spectrum. The Δδ(ppm) for the inset is calculated by the expression $((\Delta H)^2+(0.159*\Delta^{15}N)^2)^{½}$ (Liokatis, Dose et al. 2010)(inset). B. The CBCA(CO)NH (left) and HNCACB (right) spectrum of Ac-αsyn. Met-1 is labeled as M1. The rectangular box designates the ^{13}C methyl carbon of the

acetyl group that is shown by a star on the schematic representation of Ac-αsyn at the top of the graph.

The secondary structure propensity of Ac-αsyn was next examined by analysing NMR chemical shift perturbations and was compared with that of αsyn (Figure 6.6A). A number of methods have been developed to determine the secondary structural propensities of unfolded proteins (Wang and Jardetzky 2002; Marsh, Singh et al. 2006; Camilloni, De Simone et al. 2012). Here we use secondary structure propensity scores (SSP)(Marsh, Singh et al. 2006) which represent ensemble-averaged values over a distribution of states to obtain the secondary structure propensities of both Ac-αsyn and αsyn. Paralleling the amide chemical shift deviations observed in ^{1}H-^{15}N HSQC spectra (Figure 6.6A), increased SSP values up to 0.3 are observed for the first twelve residues in the N-terminal region of Ac-αsyn. These values are significantly larger than those observed previously for αsyn and mutants of this protein (Bussell and Eliezer 2001; Sung and Eliezer 2007; Rospigliosi, McClendon et al. 2009; Kang, Wu et al. 2011) and represent a significant stabilization of transient helix and hence a redistribution of the structural ensemble sampled by the monomeric protein within the N-terminal region (Figure 6.7A). Longer-range perturbations, although small, are observed, in other regions of the N-terminus in the regions between residues 28-31, 43-46, 50-66 and are marked by a decrease in β-sheet propensity in Ac-αsyn (Figure 6.7B). By contrast, the NAC and C-terminal regions remain relatively unperturbed by acetylation. The change of secondary structure propensities arising from acetylation may relate to important structural and functional properties of the protein. Specifically, changes are observed at Met-1, Asp-2

and His-50, the high affinity copper binding regions(Rasia, Bertoncini et al. 2005; Binolfi, Rasia et al. 2006; Sung and Eliezer 2007; Bisaglia, Tessari et al. 2009), and at the three familial mutants A30P, E46K and A53T associated with Parkinson's disease that affect the rate of fibril formation (Conway, Harper et al. 1998; Greenbaum, Graves et al. 2005). Together, the results reveal that N-terminal acetylation of αsyn does not by itself cause the intrinsically disordered protein (IDP) to self-assemble into tetrameric or other higher oligomeric forms, however, marked short range and subtle long-range effects of N-terminal acetylation are observed on the disordered monomer.

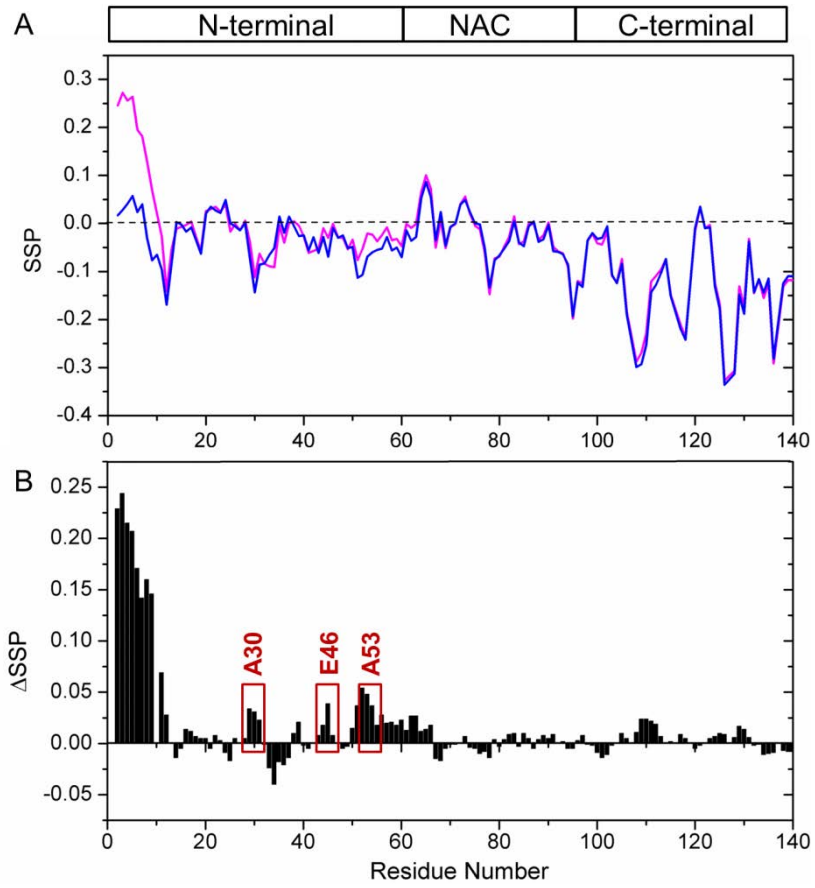

Figure 6.7 SSP analysis of Ac-αsyn and αsyn. A: SSP analysis of Ac-αsyn (magenta) and αsyn (blue) using $^{13}C^{\alpha}$ and $^{13}C^{\beta}$ chemical shifts as input and a 5 residue sliding

window with Zhang et. al. random coil references(Zhang, Neal et al. 2003) . B: Differences of SSP (ΔSSP= SSP(Ac-αsyn) – SSP(αsyn)) between Ac-αsyn and αsyn with boxes shown at positions of familial mutations. ^{1}H-^{15}N HSQC comparison of αsyn purified under mild and harsh conditions indicate that they are very similar (Figure 6.2).

While N-terminal acetylation has been shown to increase helicity in peptides(Chakrabartty, Doig et al. 1993), the data presented here represent the first investigation of the acetylation at the N-terminus of a full-length IDP. The increased helicity in Ac-αsyn can be rationalized by stabilization of the helix macrodipole(Fairman, Shoemaker et al. 1989), where removal of the α-amino positive charge upon acetylation is favorable to the overall dipole moment of the helix that this IDP transiently samples. The acetyl group is also known to form a highly favorable helix N-cap, in which the acetyl-carbonyl group interacts favorably with unsatisfied hydrogen bond donors in the N-terminal turn of the helix (Doig, Chakrabartty et al. 1994; Aurora and Rose 1998).

6.3.4 The effect of acetylation on fibril assembly process.

The fibrillation properties of Ac-αsyn and αsyn were also examined using ThT fluorescence assay to provide macroscopic information about the role of N-terminal acetylation in modifying the efficiency of fibril nucleation and elongation. The ThT fluorescence of Ac-αsyn and αsyn at pH 7.4 exhibits sigmoidal curves for fibril assembly. Comparison of Ac-αsyn and αsyn fibril assembly was shown with protein purified by mild and salting-out protocols. Proteins purified by both protocols show that Ac-αsyn aggregates slower than αsyn with slower apparent growth rate and longer lag times. For

protein purified by salting-out protocol, the lag time of Ac-αsyn is around 2.7 times longer than that of αsyn and the apparent growth rate k_{app} of Ac-αsyn is around 1.9 times slower than that of αsyn (Figure 6.8 A, C).

The change in fibrillation rate may result from stabilization of the N-terminal region of the protein by acetylation, or changes in secondary structure propensities at residues 50-66 which have been shown previously to have significant effects upon the kinetics of fibril formation, (Bussell and Eliezer 2001; Uversky and Eliezer 2009; Kang, Wu et al. 2011) or both. Physicochemical changes resulting from acetylation may affect electrostatic and hydrophobic interactions, resulting in alterations in transient long-range contacts between the highly charged C-terminal region and the helix stabilized N-terminal region. This redistribution of states may have effects upon fibril formation.

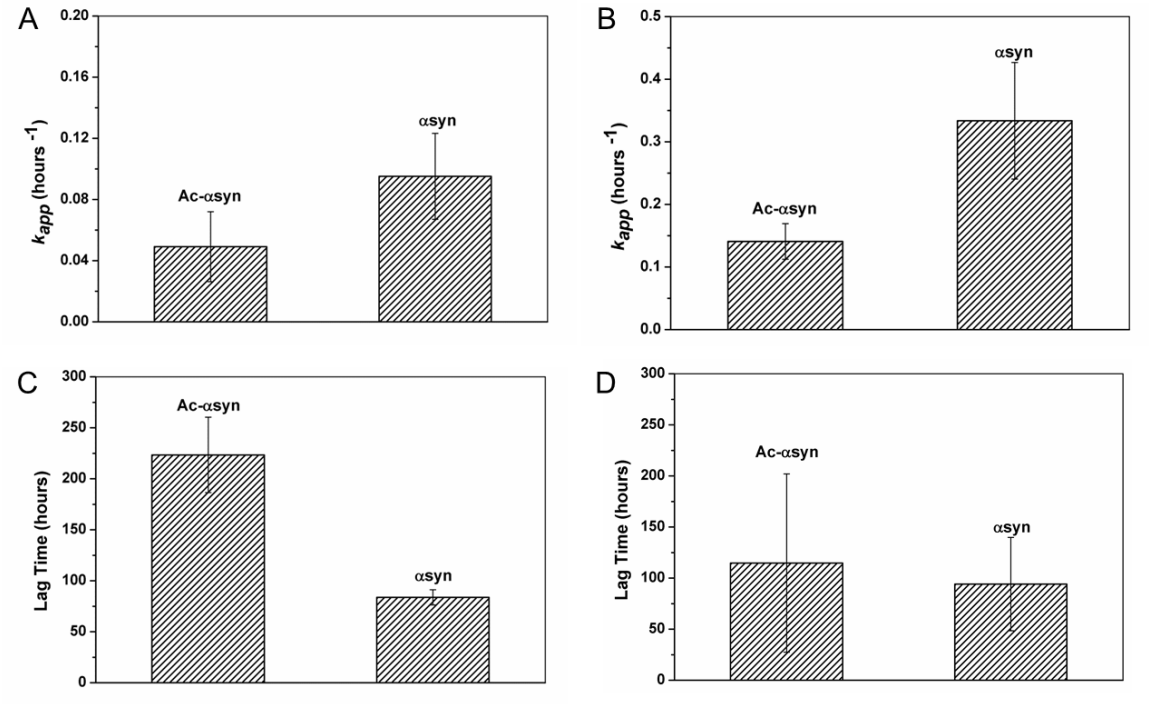

Figure 6.8 Fibril assembly kinetics of Ac-αsyn and αsyn. A. The apparent growth rate of fibril elongation of Ac-αsyn and αsyn purified using salting-out protocol with two

ammonium salt cut off, where 12 data sets were used for Ac-αsyn and 7 data sets were used for αsyn; B. The apparent growth rate of fibril elongation of Ac-αsyn and αsyn purified by mild protocol; C. Lag time of Ac-αsyn and αsyn purified by salting-out protocol with two ammonium salt cut off; D. Lag time of Ac-αsyn and αsyn purified by mild protocol. In total, 12 data sets were used for Ac-αsyn purified by salting-out protocol, 7 data sets were used for αsyn purified by salting-out protocol, 10 data sets were used for Ac-αsyn purified by mild protocol and 12 data sets were used for αsyn purified by mild protocol.

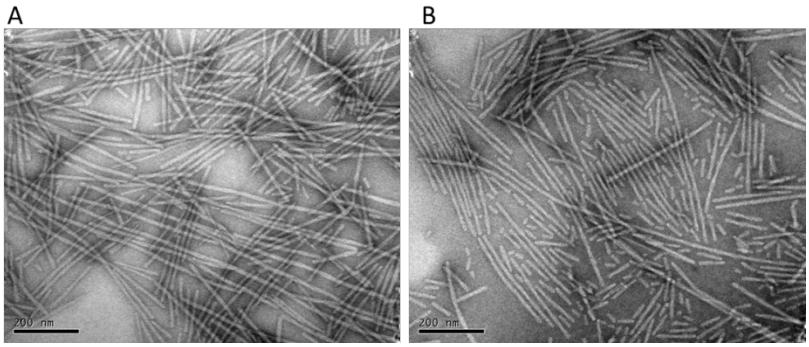

Figure 6.9 Fibril morphology of Ac-αsyn (A) and αsyn (B).

6.3.5 A53T mutation induces helical propensity locally and increased fibril assembly kinetics in acetylated αsyn.

Familial mutations (A30P, E46K and A53T) which cause early on-set PD are widely studied in non-acetylated form (Bussell and Eliezer 2001; Rasia, Bertoncini et al. 2005; Rospigliosi, McClendon et al. 2009) and secondary structure propensities are determined as a key factor in controlling aggregation kinetics. With the determination of Ac-αsyn, a more physiological form existing in human neuron system it is in a great demand to

investigate and characterize the acetylated familial mutations. Here we continued to investigate the biophysical properties of Ac-A53T mutation.

6.3.5.1 A53T induced helical propensity in regions 6~32 is suppressed by N-terminal acetylation.

Residue-specific analysis of Ac-A53T by NMR was performed and an overlay of the ^{1}H-^{15}N spectrum of Ac-A53T and Ac-αsyn at pH 7.4 shows that the two proteins share a high degree of similarity, except residues around residue 53 (Figure 6.10). Similar to Ac-αsyn, Ac-A53T displays narrow chemical shift dispersion which is the characteristic of a predominantly unfolded protein. The secondary structure propensity of Ac-A53T was next examined by analysing NMR chemical shift perturbations and was compared with that of Ac-αsyn (Figure 6.11A). SSP were used to obtain the secondary structure propensities of both Ac-A53T and Ac-αsyn. Paralleling the amide chemical shift deviations observed in ^{1}H-^{15}N HSQC spectra (Figure 6.10), increased SSP values up to 0.1 are observed for the residues around 53. These values are similar to those observed previously for αsyn and A53T (Figure 3.9). Longer-range perturbations, although small, were observed between residues 6-12. Ac-A53T reduced helical propensity at the region where increased helical propensity is induced by acetylation (Figure 6.7B). The NAC and C-terminal regions remain relatively unperturbed by A53T mutation.

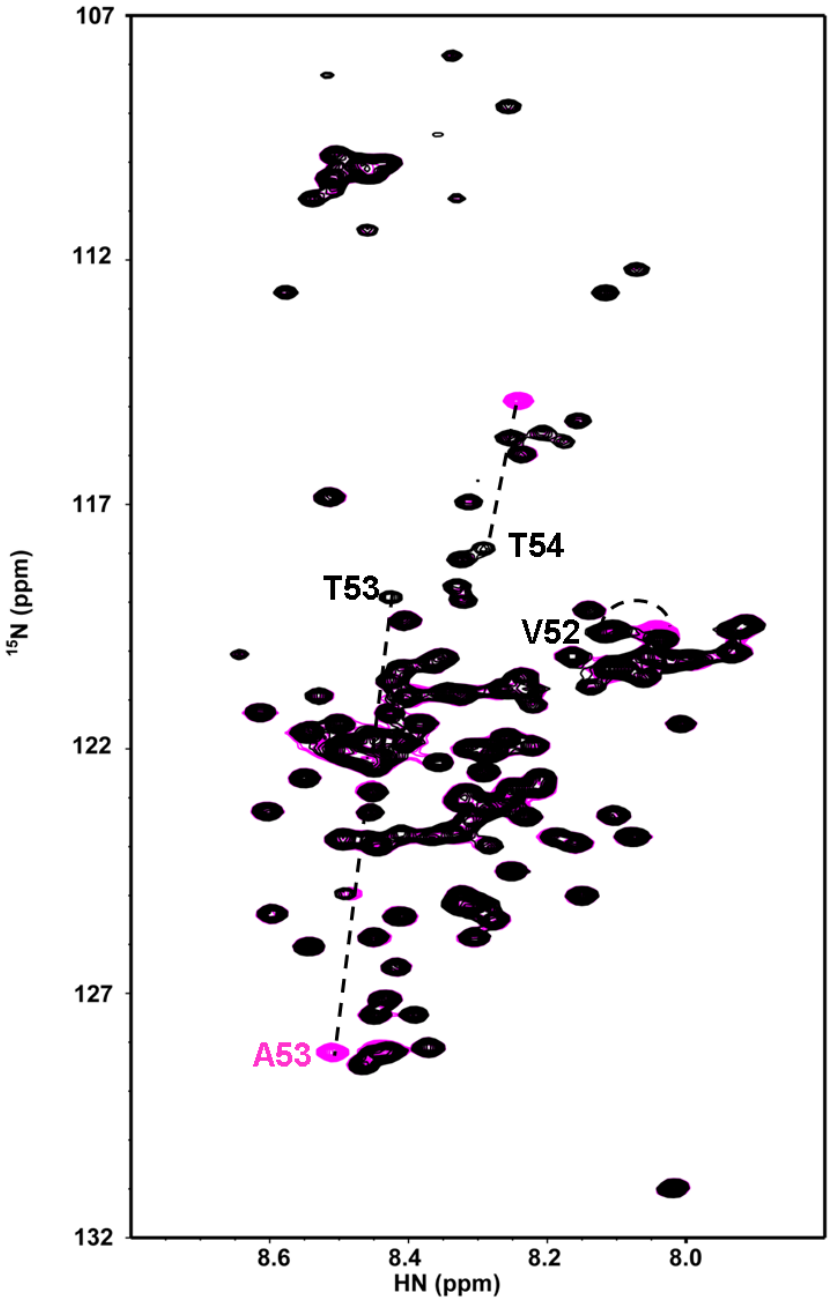

Figure 6.10 1H-15N HSQC spectra of Ac-A53T (black) vs. Ac-αsyn (magenta) at 15ºC. The changes in residues around 53 are indicated in the spectrum.

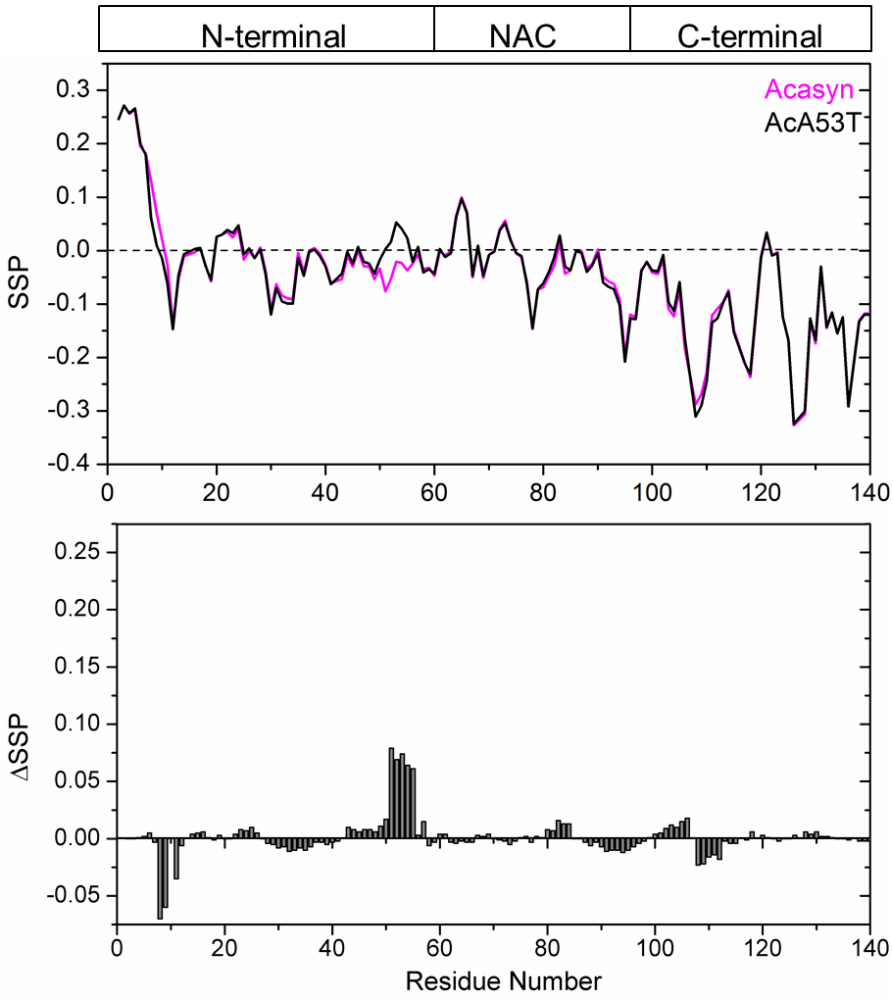

Figure 6.11 SSP analysis of Ac-A53T and Ac-αsyn. A: SSP analysis of Ac-A53T (black) and Ac-αsyn (magenta) using $^{13}C^{\alpha}$ and $^{13}C^{\beta}$ chemical shifts as input and a 5 residue sliding window with Zhang et. al. random coil references(Zhang, Neal et al. 2003) . B: Differences of SSP (ΔSSP= SSP(Ac-A53T) – SSP(Ac-αsyn)) between Ac-A53T and Ac-αsyn with boxes shown at positions of familial mutations.

6.3.5.2 Fibril assembly kinetics for Ac-A53T.

The fibrillation properties of Ac-A53T and Ac-αsyn were also examined using ThT fluorescence to provide macroscopic information about the role of A53T mutation on Ac-

αsyn in modifying the efficiency of fibril nucleation and elongation. The proteins were purified by salting-out protocols (6.2.2.2 (1)). The result shows that Ac-A53T aggregates faster than Ac-αsyn with lag time around 5 times shorter than that of Ac-αsyn and apparent growth rate k_{app} around 2 times faster than that of Ac-αsyn (Figure 6.12A,B). Ac-A53T also formed fibril with indistinguishable morphology from Ac-αsyn (Figure 6.12C). The result shows that Ac-A53T, which causes early on-set PD aggregates faster than Ac-αsyn.

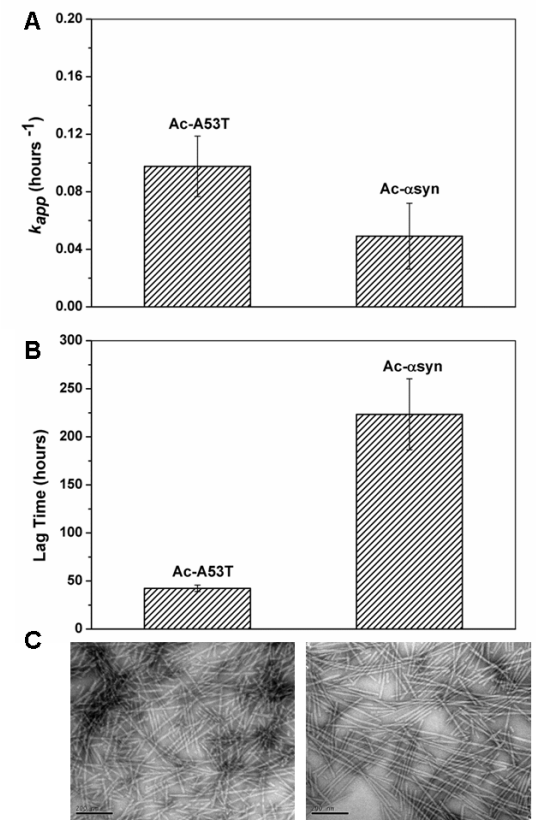

Figure 6.12 Fibril assembly kinetics and fibril morphology of Ac-A53T and Ac-αsyn. A. Apparent growth rate k_{app} of Ac-A53T and Ac-αsyn; B. Lag time of Ac-A53T and Ac-αsyn; C. Fibril morphology of Ac-A53T (left) and Ac-αsyn (right). Both samples are purified using salting-out protocols (Chapter 6.2.2.2(1)).

6.3.6 Aggregation-prone and aggregation-protective secondary structure propensities.

By investigating a systematic designed human-mouse chimera set, we revealed A53T play an important role in determining aggregation kinetics described in Chapter 3 (Kang, Wu et al. 2011). Successive study revealed that increased helical propensity around 6~32 and 53 induced by A53T is the key factor in controlling k_{app}. It is exciting to reveal that in A53T, Ac-αsyn, αsyn and A53T set, this relationship is verified: A53T with the helical propensity around residue 53 and residue 6–31 is the fastest; Ac-A53T with helical propensity around residue 53 and N-terminal stabilization transient helix is the next; αsyn without N-terminal stabilization transient helix and aggregation prone helical propensity is similar to Ac-A53T; Ac-αsyn with N-terminal stabilization transient helix is the slowest (Figure 6.13). It is interesting to note that A53T mutation has long region perturbation to the beginning of N-terminal without N-terminal acetyl group. With the presence of acetyl group which induced up to 30% helical propensity in N-terminal first 12 residues, A53T failed to induce helical propensity around residue 6–31, but instead it disturbed transient N-terminal helix by decreasing helical propensity in residue 6–12 (Figure 6.14). With this result, it is reasonable to predict that the unwinding of N-terminal transient aggregation-protective helical propensity may be a necessary step for Ac-αsyn to aggregate.

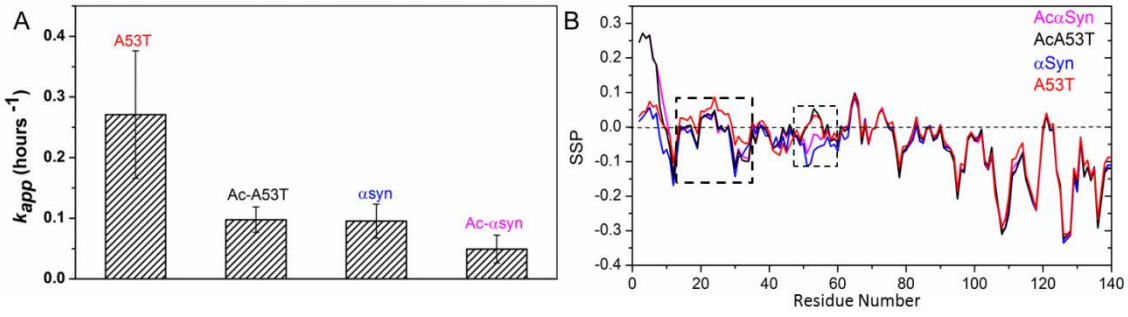

Figuer 6.13 kapp (A) and SSP (B) for A53T, Ac-A53T, αsyn and Ac-αsyn. The k_{app} of A53T was normalized to samples purified by salting-out protocol.

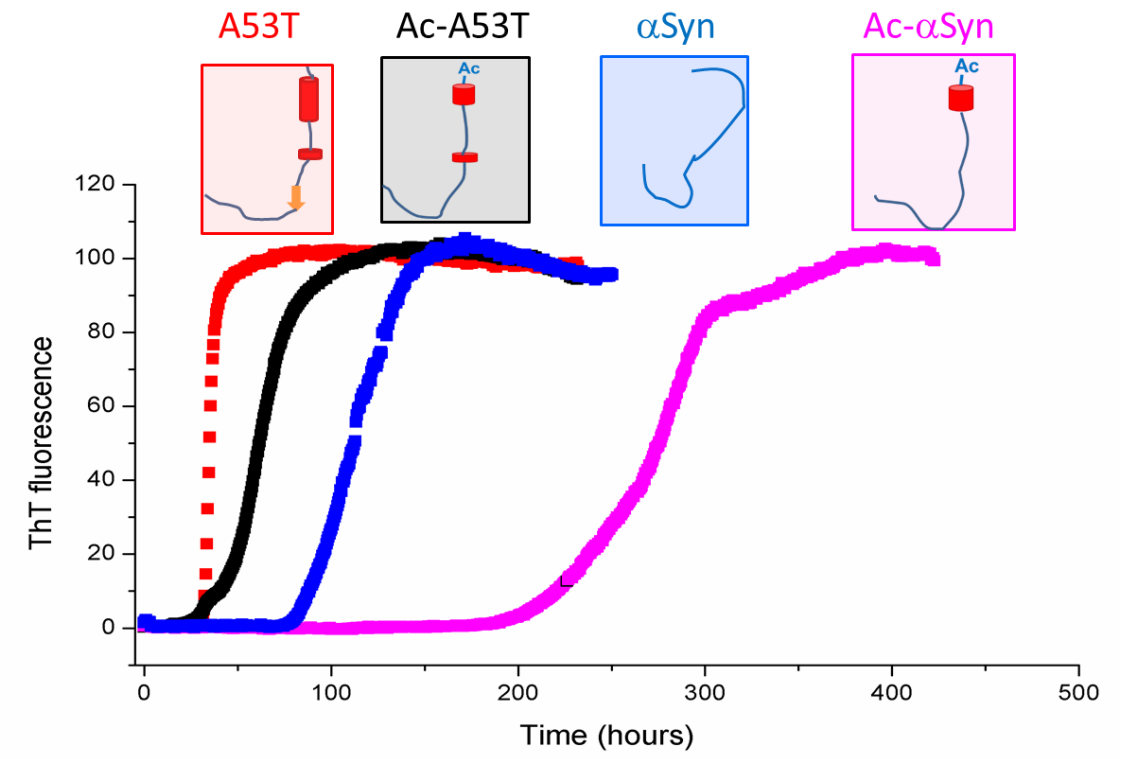

Figure 6.14 Schematic representation of critical conformations (Top) and ThT fluorescence (Bottom) for A53T (red), Ac-A53T (black), αsyn (blue) and Ac-αsyn (magenta) aggregation.

6.4 Conclusion.

This work presents the first NMR structural characterization of N-terminal Ac-αsyn, Ac-A53T and illustrates the effect of N-terminal acetylation on the fibrillation rates of the protein. We demonstrate conclusively using ESI-IMS-MS that the equilibrium states that are sampled in the Ac-αsyn are primarily monomer and a small population of dimer.

NMR data support the view that both Ac-αsyn and αsyn exist at pH 7.4 as intrinsically disordered monomers, and further shows that N-terminal acetylation results in significant stabilization of transient helical propensity in the first twelve residues of the protein along with longer range changes in secondary structure between residues 50–66 and around the three familial mutants A30P, E46K and A53T. These regions represent important functional regions associated with metal ion binding and with familial mutants that affect aggregation rates. We show that N-terminal acetylation not only changes the distribution of the intrinsically disordered monomeric conformers within the structural ensemble of αsyn, but that this co-translational modification disfavors fibril formation presumably caused by the conformational redistribution of the monomeric protein.

Chapter 7 Conclusions

This dissertation focuses on mutations and environmental effects on the aggregation of α-synuclein (αsyn). Conformations with critical secondary structure propensity in several regions in the N-terminal and NAC region are determined to be important to αsyn aggregation. Selective molecular recognition is proposed as a possible mechanism for αsyn aggregation based on the study on the partially folded intermediate, which is in equilibrium with unfolded structures. The helical propensity in residues 6–31, containing the first two six-residue repeats, is determined to be the key to increasing aggregation rates. The helical propensity in this region is a shared aggregation-prone factor determined by the investigation of human-mouse αsyn variants, TFE-induced αsyn aggregation and acetylation of αsyn and A53T. The perturbation in this region will greatly affect the behavior of αsyn aggregation. This discovery provides insights into the molecular mechanism for Parkinson's diseases (PD) and may shed light on pharmaceutical candidate for PD.

PD is a complex disease. It is important to understand the key molecular events that provoke neurodegeneration. Current *in vitro* work mainly focused on the structural and aggregation behavior of αsyn. There are three additional important aspects worthy for future consideration. First, the more physiological form of αsyn should be investigated to better translate *in vitro* results to *in vivo* phenomenon. As αsyn is undergoing numerous cellular processes in the human body, it is critical for *in vitro* studies to resemble the *in vivo* forms of αsyn. Acetylated αsyn is different in terms of the secondary structure propensity and the aggregation behavior from non-acetylated αsyn. Many cellular processes and factors are found to contribute to the pathogenesis of PD such as oxidative

modification, phosphorylation, C-terminal truncation, etc. The elucidation of the potential effects from the cellular processes would provide molecular insights into αsyn inclusion and neuron cell death. Second, it is important to investigate the cytotoxic species formed during αsyn aggregation. It has been shown that oligomers or protofibrils, instead of fibrils, are neurotoxic. αSyn aggregation is a heterogeneous process. The initial and final states of the process have been well characterized; however, the species populated between those two states remains elusive. Recent investigations revealed that oligomers formed in the early aggregation events could lead to cell death. Valid methods need to be developed to study this process and the important cytotoxic intermediates. Third, studies on the interactions between the small molecule aggregation inhibitors and αsyn will bring new perspectives on the molecular mechanism of αsyn aggregation and PD. It has shown that catecholamines (Li, Zhu et al. 2004), flavonoids (Meng, Munishkina et al. 2009) and rifampicin (Li, Zhu et al. 2004) inhibit fibril formation and disaggregate existing fibrils *in vitro*, leading to the formation of soluble oligomers. Among them, Levodopa, the immediate precursor of dopamine, is currently used to treat PD by increasing dopamine levels in the brain. This observation ties αsyn aggregation and dopamine together, which also reveals the potential link between the formation of Lewy body and dopaminergic cell death. The elucidation of these interactions and the characterization of disaggregated oligomers will provide clues for the mechanism of αsyn aggregation and possible therapeutic agent to cure PD.

Reference

Abedini, A. and D. P. Raleigh (2009). "A critical assessment of the role of helical intermediates in amyloid formation by natively unfolded proteins and polypeptides." Protein Eng Des Sel **22**(8): 453-459.

Abedini, A. and D. P. Raleigh (2009). "A role for helical intermediates in amyloid formation by natively unfolded polypeptides?" Physical Biology **6**(1): -.

Anderson, J. P., D. E. Walker, et al. (2006). "Phosphorylation of Ser-129 is the dominant pathological modification of alpha-synuclein in familial and sporadic Lewy body disease." J Biol Chem **281**(40): 29739-29752.

Anderson, V. L., T. F. Ramlall, et al. (2010). "Identification of a helical intermediate in trifluoroethanol-induced alpha-synuclein aggregation." Proc Natl Acad Sci U S A.

Arnesen, T. (2011). "Towards a functional understanding of protein N-terminal acetylation." PLoS Biol **9**(5): e1001074.

Aurora, R. and G. D. Rose (1998). "Helix capping." Protein Sci **7**(1): 21-38.

Baba, M., S. Nakajo, et al. (1998). "Aggregation of alpha-synuclein in Lewy bodies of sporadic Parkinson's disease and dementia with Lewy bodies." Am J Pathol **152**(4): 879-884.

Bai, Y., J. S. Milne, et al. (1993). "Primary structure effects on peptide group hydrogen exchange." Proteins **17**(1): 75-86.

Bartels, T., J. G. Choi, et al. (2011). "alpha-Synuclein occurs physiologically as a helically folded tetramer that resists aggregation." Nature **477**(7362): 107-110.

Beal, M. F. (1998). "Excitotoxicity and nitric oxide in Parkinson's disease pathogenesis." Ann Neurol **44**(3 Suppl 1): S110-114.

Bernado, P., C. W. Bertoncini, et al. (2005). "Defining long-range order and local disorder in native alpha-synuclein using residual dipolar couplings." J Am Chem Soc **127**(51): 17968-17969.

Bernstein, S. L., D. Liu, et al. (2004). "Alpha-synuclein: stable compact and extended monomeric structures and pH dependence of dimer formation." J Am Soc Mass Spectrom **15**(10): 1435-1443.

Bertoncini, C. W., C. O. Fernandez, et al. (2005). "Familial mutants of alpha-synuclein with increased neurotoxicity have a destabilized conformation." J Biol Chem **280**(35): 30649-30652.

Bertoncini, C. W., Y. S. Jung, et al. (2005). "Release of long-range tertiary interactions potentiates aggregation of natively unstructured alpha-synuclein." Proc. Natl. Acad. Sci. U. S. A. **102**(5): 1430-1435.

Bertoncini, C. W., R. M. Rasia, et al. (2007). "Structural Characterization of the Intrinsically Unfolded Protein beta-Synuclein, a Natural Negative Regulator of alpha-Synuclein Aggregation." J Mol Biol **372**(3): 708-722.

Bi, W., G. Zhang, et al. (2011). "Serine 129 Phosphorylation of alpha-Synuclein Cross-Links with Tissue Transglutaminase to Form Lewy Body-Like Inclusion Bodies." ISRN Neurol **2011**: 732879.

Binolfi, A., R. M. Rasia, et al. (2006). "Interaction of alpha-synuclein with divalent metal ions reveals key differences: a link between structure, binding specificity and fibrillation enhancement." J Am Chem Soc **128**(30): 9893-9901.

Bisaglia, M., I. Tessari, et al. (2009). "Interaction between alpha-synuclein and metal ions, still looking for a role in the pathogenesis of Parkinson's disease." Neuromolecular Med **11**(4): 239-251.

Brorsson, A. C., B. Bolognesi, et al. (2010). "Intrinsic determinants of neurotoxic aggregate formation by the amyloid beta peptide." Biophys J **98**(8): 1677-1684.

Bruening, W., B. I. Giasson, et al. (2000). "Synucleins are expressed in the majority of breast and ovarian carcinomas and in preneoplastic lesions of the ovary." Cancer **88**(9): 2154-2163.

Buck, M. (1998). "Trifluoroethanol and colleagues: cosolvents come of age. Recent studies with peptides and proteins." Q Rev Biophys **31**(3): 297-355.

Burre, J., M. Sharma, et al. (2010). "Alpha-synuclein promotes SNARE-complex assembly in vivo and in vitro." Science **329**(5999): 1663-1667.

Bussel Jr., R., T. F. Ramlall, et al. (2005). "Helix periodicity, topology, and dynamics of membrane-assoicated α-Synuclein." Protein Science **14**: 862-872.

Bussell, R., Jr. and D. Eliezer (2001). "Residual structure and dynamics in Parkinson's disease-associated mutants of alpha-synuclein." J. Biol. Chem. **276**(49): 45996-46003.

Camilloni, C., A. De Simone, et al. (2012). "Determination of secondary structure populations in disordered States of proteins using nuclear magnetic resonance chemical shifts." Biochemistry **51**(11): 2224-2231.

Chabrier, P. E., C. Demerle-Pallardy, et al. (1999). "Nitric oxide synthases: targets for therapeutic strategies in neurological diseases." Cell Mol Life Sci **55**(8-9): 1029-1035.

Chakrabartty, A., A. J. Doig, et al. (1993). "Helix capping propensities in peptides parallel those in proteins." Proc Natl Acad Sci U S A **90**(23): 11332-11336.

Chandra, S., F. Fornai, et al. (2004). "Double-knockout mice for alpha- and beta-synucleins: effect on synaptic functions." Proc Natl Acad Sci U S A **101**(41): 14966-14971.

Charcot, J. M. (1878). Lectures on the diseases of the nervous system. London, The New Sydenham Society.

Chen, M., M. Margittai, et al. (2007). "Investigation of alpha-synuclein fibril structure by site-directed spin labeling." J Biol Chem **282**(34): 24970-24979.

Chiti, F., M. Stefani, et al. (2003). "Rationalization of the effects of mutations on peptide and protein aggregation rates." Nature **424**(6950): 805-808.

Chiti, F., N. Taddei, et al. (2002). "Kinetic partitioning of protein folding and aggregation." Nature Structrual Biology **9**: 137-143.

Clayton, D. F. and J. M. George (1998). "The synucleins: a family of proteins involved in synaptic function, plasticity, neurodegeneration and disease." Trends Neurosci **21**(6): 249-254.

Clayton, D. F. and J. M. George (1999). "Synucleins in synaptic plasticity and neurodegenerative disorders." J Neurosci Res **58**(1): 120-129.

Conway, K. A., J. D. Harper, et al. (1998). "Accelerated in vitro fibril formation by a mutant alpha-synuclein linked to early-onset Parkinson disease." Nat Med **4**(11): 1318-1320.

Conway, K. A., J. D. Harper, et al. (1998). "Accelerated in vitro fibril formation by a mutant alpha-synuclein linked to early-onset Parkinson disease." Nat. Med. **4**(11): 1318-1320.

Cooper, A. A., A. D. Gitler, et al. (2006). "Alpha-synuclein blocks ER-Golgi traffic and Rab1 rescues neuron loss in Parkinson's models." Science **313**(5785): 324-328.

Cowan, R. and R. G. Whittaker (1990). "Hydrophobicity indices for amino acid residues as determined by high-performance liquid chromatography." Pept Res **3**(2): 75-80.

Croke, R. L., C. O. Sallum, et al. (2008). "Hydrogen exchange of monomeric alpha-synuclein shows unfolded structure persists at physiological temperature and is independent of molecular crowding in Escherichia coli." Protein Sci **17**(8): 1434-1445.

Crowther, R. A., S. E. Daniel, et al. (2000). "Characterisation of isolated alpha-synuclein filaments from substantia nigra of Parkinson's disease brain." Neurosci Lett **292**(2): 128-130.

de Lau, L. M. and M. M. Breteler (2006). "Epidemiology of Parkinson's disease." Lancet Neurol **5**(6): 525-535.

Delaglio, F., S. Grzesiek, et al. (1995). "NMRPipe: a multidimensional spectral processing system based on UNIX pipes." J. Biomol. NMR. **6**(3): 277-293.

Doig, A. J., A. Chakrabartty, et al. (1994). "Determination of free energies of N-capping in alpha-helices by modification of the Lifson-Roig helix-coil therapy to include N- and C-capping." Biochemistry **33**(11): 3396-3403.

Donaldson, L. W., N. R. Skrynnikov, et al. (2001). "Structural characterization of proteins with an attached ATCUN motif by paramagnetic relaxation enhancement NMR spectroscopy." J Am Chem Soc **123**(40): 9843-9847.

DuBay, K. F., A. P. Pawar, et al. (2004). "Prediction of the absolute aggregation rates of amyloidogenic polypeptide chains." J Mol Biol **341**(5): 1317-1326.

Dunker, A. K., C. J. Brown, et al. (2002). "Identification and functions of usefully disordered proteins." Adv Protein Chem **62**: 25-49.

Dunker, A. K., I. Silman, et al. (2008). "Function and structure of inherently disordered proteins." Curr Opin Struct Biol **18**(6): 756-764.

Dyson, H. J. and P. E. Wright (2004). "Unfolded proteins and protein folding studied by NMR." Chem Rev **104**(8): 3607-3622.

Eliezer, D., E. Kutluay, et al. (2001). "Conformational properties of alpha-synuclein in its free and lipid-associated states." J Mol Biol **307**(4): 1061-1073.

Fairman, R., K. R. Shoemaker, et al. (1989). "Further studies of the helix dipole model: effects of a free alpha-NH3+ or alpha-COO- group on helix stability." Proteins **5**(1): 1-7.

Fandrich, M. (2007). "Absolute correlation between lag time and growth rate in the spontaneous formation of several amyloid-like aggregates and fibrils." J. Mol. Biol. **365**: 1266-1270.

Farrow, N. A., R. Muhandiram, et al. (1994). "Backbone dynamics of a free and phosphopeptide-complexed Src homology 2 domain studied by 15N NMR relaxation." Biochemistry **33**(19): 5984-6003.

Fauvet, B., M. K. Mbefo, et al. (2012). "alpha-Synuclein in central nervous system and from erythrocytes, mammalian cells, and Escherichia coli exists predominantly as disordered monomer." J Biol Chem **287**(19): 15345-15364.

Fauvet, B., M. K. Mbefo, et al. (2012). "Alpha-synuclein in the central nervous system and from erythrocytes, mammalian cells and E. coli exists predominantly as a disordered monomer." J Biol Chem.

Feany, M. B. (2000). "Studying human neurodegenerative diseases in flies and worms." J Neuropathol Exp Neurol **59**(10): 847-856.

Fink, A. L. (2006). "The aggregation and fibrillation of alpha-synuclein." Acc. Chem. Res. **39**(9): 628-634.

Frimpong, A. K., R. R. Abzalimov, et al. (2010). "Characterization of intrinsically disordered proteins with electrospray ionization mass spectrometry: conformational heterogeneity of alpha-synuclein." Proteins **78**(3): 714-722.

George, J. M. (2001). "The synucleins." Genome Biol. **3**: 3002.3001-3002.3006.

Goddard, T. D. and D. G. Kneller Sparky 3, University of California, San Francisco.

Goedert, M. (2001). "Alpha-synuclein and neurodegenerative diseases." Nature Reviews Nueroscience **2**(7): 492-501.

Goedert, M. (2001). "Alpha-Synuclein and Neurodegernative Diseases." Nature **2**: 492-501.

Gowers, W. R. (1888). Diseases of the nervous system. Philadelphia, P. Blakiston, Son and Company.

Graham, D. G. (1978). "Oxidative pathways for catecholamines in the genesis of neuromelanin and cytotoxic quinones." Mol Pharmacol **14**(4): 633-643.

Greenbaum, E. A., C. L. Graves, et al. (2005). "The E46K mutation in alpha-synuclein increases amyloid fibril formation." J Biol Chem **280**(9): 7800-7807.

Hamilton, B. A. (2004). "alpha-Synuclein A53T substitution associated with Parkinson disease also marks the divergence of old world and new world primates." Genomics **83**: 739-742.

Heise, H., W. Hoyer, et al. (2005). "Molecular-level secondary structure, polymorphism, and dynamics of full-length alpha-synuclein fibrils studied by solid-state NMR." Proc Natl Acad Sci U S A **102**(44): 15871-15876.

Hirsch, E. C., T. Breidert, et al. (2003). "The role of glial reaction and inflammation in Parkinson's disease." Ann N Y Acad Sci **991**: 214-228.

Hortschansky, P., V. Schroeckh, et al. (2005). "The aggregation kinetics of Alzheimer's beta-amyloid peptide is controlled by stochastic nucleation." Protein Sci **14**(7): 1753-1759.

Hoyer, W. G., D. Cherny, et al. (2004). "Rapid self-assembly of alpha-synuclein observed by in situ atomic force microscopy." Journal of Molecular Biology **340**(1): 127-139.

Hwang, T. L., P. C. van Zijl, et al. (1998). "Accurate quantitation of water-amide proton exchange rates using the phase-modulated CLEAN chemical EXchange (CLEANEX-PM) approach with a Fast-HSQC (FHSQC) detection scheme." J Biomol NMR **11**(2): 221-226.

Irizarry, M. C., T. W. Kim, et al. (1996). "Characterization of the precursor protein of the non-A beta component of senile plaques (NACP) in the human central nervous system." J Neuropathol Exp Neurol **55**(8): 889-895.

Iwai, A., E. Masliah, et al. (1995). "The precursor protein of non-A beta component of Alzheimer's disease amyloid is a presynaptic protein of the central nervous system." Neuron **14**(2): 467-475.

Jakes, R., M. G. Spillantini, et al. (1994). "Identification of two distinct synucleins from human brain." FEBS Lett **345**(1): 27-32.

Johnson, M., A. T. Coulton, et al. (2010). "Targeted amino-terminal acetylation of recombinant proteins in E. coli." PLoS One **5**(12): e15801.

Kang, L., K.-P. Wu, et al. (2011). "The A53T mutation is key in defining the aggregation kinetics of human and mouse α-synuclein." J. Am. Chem. Soc.: in press.

Kang, L., K. P. Wu, et al. (2011). "The A53T mutation is key in defining the differences in the aggregation kinetics of human and mouse alpha-synuclein." J Am Chem Soc **133**(34): 13465-13470.

Kessler, J. C., J. C. Rochet, et al. (2003). "The N-terminal repeat domain of alpha-synuclein inhibits beta-sheet and amyloid fibril formation." Biochemistry **42**(3): 672-678.

Khurana, R., C. Ionescu-Zanetti, et al. (2003). "A general model for amyloid fibril assembly based on morphological studies using atomic force microscopy." Biophys J **85**(2): 1135-1144.

Kim, T. D., S. R. Paik, et al. (2002). "Structural and functional implications of C-terminal regions of alpha-synuclein." Biochemistry **41**(46): 13782-13790.

Kirkitadze, M. D., M. M. Condron, et al. (2001). "Identification and characterization of key kinetic intermediates in amyloid b-protein fibrillogenesis." J. Mol. Biol. **312**: 1103-1119.

Knowles, T. P., C. A. Waudby, et al. (2009). "An analytical solution to the kinetics of breakable filament assembly." Science **326**(5959): 1533-1537.

Kroenke, C. D., J. P. Loria, et al. (1998). "Longitudinal and Transverse 1H-15N Dipolar/15N Chemical Shift Anisotropy Relaxation Interference: Unambiguous Determination of Rotational Diffusion Tensors and Chemical Exchange Effects in Biological Macromolecules." J. Am. Chem. Soc. **120**(31): 7905-7915.

Kruger, R., W. Kuhn, et al. (1998). "Ala30Pro mutation in the gene encoding alpha-synuclein in Parkinson's disease." Nat Genet **18**(2): 106-108.

Lai, B. C., S. A. Marion, et al. (2002). "Occupational and environmental risk factors for Parkinson's disease." Parkinsonism Relat Disord **8**(5): 297-309.

Langston, J. W., P. Ballard, et al. (1983). "Chronic Parkinsonism in humans due to a product of meperidine-analog synthesis." Science **219**(4587): 979-980.

Lapid, C. and Y. Gao Primer X, Bioinformatics.org.

Lashuel, H. A., B. M. Petre, et al. (2002). "Alpha-synuclein, especially the Parkinson's disease-associated mutants, forms pore-like annular and tubular protofibrils." J Mol Biol **322**(5): 1089-1102.

Lavedan, C. (1998). "The synuclein family." Genome Res **8**(9): 871-880.

Lee, H. J., C. Choi, et al. (2002). "Membrane-bound alpha-synuclein has a high aggregation propensity and the ability to seed the aggregation of the cytosolic form." J Biol Chem **277**(1): 671-678.

Lesage, S. and A. Brice (2009). "Parkinson's disease: from monogenic forms to genetic susceptibility factors." Hum Mol Genet **18**(R1): R48-59.

Li, J., M. Zhu, et al. (2004). "Dopamine and L-dopa disaggregate amyloid fibrils: implications for Parkinson's and Alzheimer's disease." FASEB J **18**(9): 962-964.

Li, J., M. Zhu, et al. (2004). "Rifampicin inhibits alpha-synuclein fibrillation and disaggregates fibrils." Chem Biol **11**(11): 1513-1521.

Li, Y., S. Kim, et al. (2005). "Identification of partially disordered peptide intermediates through residue-specific NMR diffusion measurements." J Am Chem Soc **127**(30): 10490-10491.

Liokatis, S., A. Dose, et al. (2010). "Simultaneous detection of protein phosphorylation and acetylation by high-resolution NMR spectroscopy." J Am Chem Soc **132**(42): 14704-14705.

Liu, G., A. Prabhakar, et al. (2010). "Mechanistic studies of peptide self-assembly: transient alpha-helices to stable beta-sheets." J Am Chem Soc **132**(51): 18223-18232.

Liu, S., I. Ninan, et al. (2004). "alpha-Synuclein produces a long-lasting increase in neurotransmitter release." EMBO J **23**(22): 4506-4516.

Ma, B. and R. Nussinov (2012). "Selective molecular recognition in amyloid growth and transmission and cross-species barriers." J Mol Biol **421**(2-3): 172-184.

Maroteaux, L., J. T. Campanelli, et al. (1988). "Synuclein: a neuron-specific protein localized to the nucleus and presynaptic nerve terminal." J Neurosci **8**(8): 2804-2815.

Marsh, J. A., V. K. Singh, et al. (2006). "Sensitivity of secondary structure propensities to sequence differences between alpha- and gamma-synuclein: implications for fibrillation." Protein Sci. **15**(12): 2795-2804.

Masliah, E., E. Rockenstein, et al. (2001). "beta-amyloid peptides enhance alpha-synuclein accumulation and neuronal deficits in a transgenic mouse model linking Alzheimer's disease and Parkinson's disease." Proc Natl Acad Sci U S A **98**(21): 12245-12250.

Meng, F., A. Abedini, et al. (2007). "Amyloid formation by pro-islet amyloid polypeptide processing intermediates: examination of the role of protein heparan sulfate interactions and implications for islet amyloid formation in type 2 diabetes." Biochemistry **46**(43): 12091-12099.

Meng, X., L. A. Munishkina, et al. (2009). "Molecular mechanisms underlying the flavonoid-induced inhibition of alpha-synuclein fibrillation." Biochemistry **48**(34): 8206-8224.

Mohana-Borges, R., N. K. Goto, et al. (2004). "Structural characterization of unfolded states of apomyoglobin using residual dipolar couplings." J Mol Biol **340**(5): 1131-1142.

Morar, A. S., A. Olteanu, et al. (2001). "Solvent-induced collapse of α-synuclein and acid denature cytochrom c." Protein Science **10**: 2195-2199.

Mukrasch, M. D., P. Markwick, et al. (2007). "Highly populated turn conformations in natively unfolded tau protein indentified from residual dipolar couplings and molecular simulations." J. Am. Chem. Soc. **129**: 5235-5243.

Munishkina, L. A., C. Phelan, et al. (2003). "Conformational behavior and aggregation of alpha-synuclein in organic solvents: modeling the effects of membranes." Biochemistry **42**(9): 2720-2730.

Murphy, D. D., S. M. Rueter, et al. (2000). "Synucleins are developmentally expressed, and alpha-synuclein regulates the size of the presynaptic vesicular pool in primary hippocampal neurons." J Neurosci **20**(9): 3214-3220.

Natalello, A., F. Benetti, et al. (2011). "Compact conformations of alpha-synuclein induced by alcohols and copper." Proteins **79**(2): 611-621.

Nielsen, L., S. Frokjaer, et al. (2001). "Probing the mechanism of insulin fibril formation with insulin mutants." Biochemistry **40**: 8397-8409.

Obolensky, O. I., K. Schlepckow, et al. (2007). "Theoretical framework for NMR residual dipolar couplings in unfolded proteins." J. Biomol. NMR **39**: 1-16.

Ohrfelt, A., H. Zetterberg, et al. (2011). "Identification of Novel alpha-Synuclein Isoforms in Human Brain Tissue by using an Online NanoLC-ESI-FTICR-MS Method." Neurochem Res.

Ottiger, M., F. Delaglio, et al. (1998). "Measurement of J and dipolar couplings from simplified two-dimensional NMR spectra." J Magn Reson **131**(2): 373-378.

Otzen, D. E. (2010). "Amyloid formation in surfactants and alcohols: membrane mimetics or structural switchers?" Curr Protein Pept Sci **11**(5): 355-371.

Outeiro, T. F. and S. Lindquist (2003). "Yeast cells provide insight into alpha-synuclein biology and pathobiology." Science **302**(5651): 1772-1775.

Panchal, S. C., N. S. Bhavesh, et al. (2001). "Improved 3D triple resonance experiments, HNN and HN(C)N, for HN and 15N sequential correlations in (13C, 15N) labeled proteins: application to unfolded proteins." J Biomol NMR **20**(2): 135-147.

Parkinson, J. (1817). An Essay on the Shaking Palsy. London, Whittingham and Rowland.

Petrovitch, H., G. W. Ross, et al. (2002). "Plantation work and risk of Parkinson disease in a population-based longitudinal study." Arch Neurol **59**(11): 1787-1792.

Platt, G. W., K. E. Routledge, et al. (2008). "Fibril growth kinetics reveal a region of beta2-microglobulin important for nucleation and elongation of aggregation." J. Mol. Biol. **378**(1): 251-263.

Polevoda, B. and F. Sherman (2000). "Nalpha -terminal acetylation of eukaryotic proteins." J Biol Chem **275**(47): 36479-36482.

Polevoda, B. and F. Sherman (2003). "N-terminal acetyltransferases and sequence requirements for N-terminal acetylation of eukaryotic proteins." J Mol Biol **325**(4): 595-622.

Polymeropoulos, M. H., C. Lavedan, et al. (1997). "Mutation in the alpha-synuclein gene identified in families with Parkinson's disease." Science **276**(5321): 2045-2047.

Prestegard, J. H., C. M. Bougault, et al. (2004). "Residual dipolar couplings in structure determination of biomolelcules." Chem. Rev. **104**: 3519-3540.

Pronchik, J., X. He, et al. (2010). "In vitro formation of amyloid from alpha-synuclein is dominated by reactions at hydrophobic interfaces." J Am Chem Soc **132**(28): 9797-9803.

Rasia, R. M., C. W. Bertoncini, et al. (2005). "Structural characterization of copper(II) binding to alpha-synuclein: Insights into the bioinorganic chemistry of Parkinson's disease." Proc Natl Acad Sci U S A **102**(12): 4294-4299.

Rauscher, S. and R. Pomes (2010). "Molecular simulations of protein disorder." Biochem Cell Biol **88**(2): 269-290.

Rezaei-Ghaleh, N., M. Blackledge, et al. (2012). "Intrinsically disordered proteins: from sequence and conformational properties toward drug discovery." Chembiochem **13**(7): 930-950.

Rivers, R. C., J. R. Kumita, et al. (2008). "Molecular determinants of the aggregation behavior of alpha- and beta-synuclein." Protein Sci **17**(5): 887-898.

Rochet, J. C., K. A. Conway, et al. (2000). "Inhibition of fibrillization and accumulation of prefibrillar oligomers in mixtures of human and mouse alpha-synuclein." Biochemistry **39**(35): 10619-10626.

Rospigliosi, C. C., S. McClendon, et al. (2009). "E46K Parkinson's-linked mutation enhances C-terminal-to-N-terminal contacts in alpha-synuclein." J. Mol. Biol. **388**(5): 1022-1032.

Routledge, K. E., G. G. Tartaglia, et al. (2009). "Competition between Intramolecular and Intermolecular Interactions in Amyloid-Forming Protein." J.Mol. Biol. **389**: 776-786.

Ruckert, M. and G. Otting (2000). "Alignment of Biological Macromolecules in Novel Nonionic Liquid Crystalline Media for NMR Experiments." J Am Chem Soc **122**(32): 7793-7797.

Ryan, T. M., C. L. Teoh, et al. (2010). "Phospholipids enhance nucleation but not elongation of apolipoprotein C-II amyloid fibrils." J. Mol. Biol. **399**(5): 731-740.

Salmon, L., M. R. Jensen, et al. (2012). "Measurement and analysis of NMR residual dipolar couplings for the study of intrinsically disordered proteins." Methods Mol Biol **895**: 115-125.

Samii, A., J. G. Nutt, et al. (2004). "Parkinson's disease." Lancet **363**(9423): 1783-1793.

Schulz, J. B. and M. F. Beal (1994). "Mitochondrial dysfunction in movement disorders." Curr Opin Neurol **7**(4): 333-339.

Schwieters, C. D., J. J. Kuszewski, et al. (2003). "The Xplor-NIH NMR molecular structure determination package." J Magn Reson **160**(1): 65-73.

Serpell, L. C., J. Berriman, et al. (2000). "Fiber diffraction of synthetic alpha-synuclein filaments shows amyloid-like cross-beta conformation." Proc. Natl. Acad. Sci. U. S. A. **97**(9): 4897-4902.

Singleton, A. B., M. Farrer, et al. (2003). "alpha-Synuclein locus triplication causes Parkinson's disease." Science **302**(5646): 841.

Sivanandam, V. N., M. Jayaraman, et al. (2011). "The aggregation-enhancing huntingtin N-terminus is helical in amyloid fibrils." J Am Chem Soc **133**(12): 4558-4566.

Smith, D. P., S. E. Radford, et al. (2010). "Elongated oligomers in beta2-microglobulin amyloid assembly revealed by ion mobility spectrometry-mass spectrometry." Proc Natl Acad Sci U S A **107**(15): 6794-6798.

Smith, W. W., R. L. Margolis, et al. (2005). "Alpha-synuclein phosphorylation enhances eosinophilic cytoplasmic inclusion formation in SH-SY5Y cells." J Neurosci **25**(23): 5544-5552.

Spillantini, M. G., R. A. Crowther, et al. (1998). "alpha-Synuclein in filamentous inclusions of Lewy bodies from Parkinson's disease and dementia with lewy bodies." Proc Natl Acad Sci U S A **95**(11): 6469-6473.

Spillantini, M. G., M. L. Schmidt, et al. (1997). "α-Synuclein in Lewy Bodies." Nature **388**: 839-840.

Spillantini, M. G., M. L. Schmidt, et al. (1997). "Alpha-synuclein in Lewy bodies." Nature **388**(6645): 839-840.

Sung, Y. H. and D. Eliezer (2007). "Residual Structure, Backbone Dynamics, and Interactions within the Synuclein Family." J Mol Biol **372**(3): 689-707.

Tanner, C. M., F. Kamel, et al. (2011). "Rotenone, paraquat, and Parkinson's disease." Environ Health Perspect **119**(6): 866-872.

Tjandra, N., A. Szabo, et al. (1996). "Protein Backbone Dynamics and 15N Chemical Shift Anisotropy from Quantitative Measurement of Relaxation Interference Effects." J. Am. Chem. Soc. **118**(29): 6986-6991.

Trexler, A. J. and E. Rhoades (2012). "N-terminal acetylation is critical for forming alpha-helical oligomer of alpha-Synuclein." Protein Sci.

Trexler, A. J. and E. Rhoades (2012). "N-Terminal acetylation is critical for forming alpha-helical oligomer of alpha-synuclein." Protein Sci **21**(5): 601-605.

Trojanowski, J. Q. and V. M. Lee (2003). "Parkinson's disease and related alpha-synucleinopathies are brain amyloidoses." Ann N Y Acad Sci **991**: 107-110.

Ueda, K., H. Fukushima, et al. (1993). "Molecular cloning of cDNA encoding an unrecognized component of amyloid in Alzheimer disease." Proc Natl Acad Sci U S A **90**(23): 11282-11286.

Ulrih, N. P., C. H. Barry, et al. (2008). "Impact of Tyr to Ala mutations on alpha-synuclein fibrillation and structural properties." Biochim Biophys Acta **1782**(10): 581-585.

Uversky, V. N. (2003). "A Protein-Chameleon: Conformational Plasticity of α-Synclein, a Disordered Protein Involved in Neurodegenerative Disorders." Journal of Biomolecular Structure & Dynamics **21**(2): 211-234.

Uversky, V. N. (2007). "Neuropathology, biochemistry, and biophysics of alpha-synuclein aggregation." J Neurochem **103**(1): 17-37.

Uversky, V. N. and D. Eliezer (2009). "Biophysics of Parkinson's disease: structure and aggregation of alpha-synuclein." Curr Protein Pept Sci **10**(5): 483-499.

Uversky, V. N., J. Li, et al. (2001). "Evidence for a partially folded intermediate in alpha-synuclein fibril formation." J Biol Chem **276**(14): 10737-10744.

Vilar, M., H. T. Chou, et al. (2008). "The fold of alpha-synuclein fibrils." Proc Natl Acad Sci U S A **105**(25): 8637-8642.

Volles, M. J. and P. T. Lansbury, Jr. (2007). "Relationships between the sequence of alpha-synuclein and its membrane affinity, fibrillization propensity, and yeast toxicity." J Mol Biol **366**(5): 1510-1522.

Wang, C., M. J. Grey, et al. (2001). "CPMG sequences with enhanced sensitivity to chemical exchange." J Biomol NMR **21**(4): 361-366.

Wang, W., I. Perovic, et al. (2011). "A soluble alpha-synuclein construct forms a dynamic tetramer." Proc Natl Acad Sci U S A **108**(43): 17797-17802.

Wang, Y. and O. Jardetzky (2002). "Probability-based protein secondary structure identification using combined NMR chemical-shift data." Protein Sci **11**(4): 852-861.

Waudby, C. (2009). Structural and biophysical studies of a-synuclein and protein aggregation, St John's College, University of Cambridge. **Doctor of Philosophy**.

Weinreb, P. H., W. Zhen, et al. (1996). "NACP, a protein implicated in Alzheimer's disease and learning, is natively unfolded." Biochemistry **35**(43): 13709-13715.

Wersinger, C. and A. Sidhu (2006). "An inflammatory pathomechanism for Parkinson's disease?" Curr Med Chem **13**(5): 591-602.

Williamson, J. A., J. P. Loria, et al. (2009). "Helix stabilization precedes aqueous and bilayer-catalyzed fiber formation in islet amyloid polypeptide." J. Mol. Biol. **393**(2): 383-396.

Winner, B., R. Jappelli, et al. (2011). "In vivo demonstration that alpha-synuclein oligomers are toxic." Proc Natl Acad Sci U S A **108**(10): 4194-4199.

Wu, K.-P. (2010). NMR Characterization of Intrinsically Disordered a-synuclein: implication for aggregation in Parkinson's Disease. Department of Chemistry and Chemical Biology, Rutgers, the State University of New Jersey. **Doctor of Philosophy**.

Wu, K.-P., D. S. Weinstock, et al. (2009). "Structural Reorganization of alpha-Synuclein at Low pH Observed by NMR and REMD Simulations." J. Mol. Biol. **391**(4): 784-796.

Wu, K. P. and J. Baum (2010). "Detection of transient interchain interactions in the intrinsically disordered protein alpha-synuclein by NMR paramagnetic relaxation enhancement." J Am Chem Soc **132**(16): 5546-5547.

Wu, K. P., S. Kim, et al. (2008). "Characterization of conformational and dynamic properties of natively unfolded human and mouse alpha-synuclein ensembles by NMR: implication for aggregation." J. Mol. Biol. **378**(5): 1104-1115.

Zarranz, J. J., J. Alegre, et al. (2004). "The new mutation, E46K, of alpha-synuclein causes Parkinson and Lewy body dementia." Ann Neurol **55**(2): 164-173.

Zarranz, J. J., J. Alegre, et al. (2004). "The new mutation, E46K, of alpha-synuclein causes Parkinson and Lewy body dementia." Ann. Neurol. **55**(2): 164-173.

Zhang, H., S. Neal, et al. (2003). "RefDB: a database of uniformly referenced protein chemical shifts." J Biomol NMR **25**(3): 173-195.

Appendix

A.1 Backbone assignment of human α-synuclein at 15 °C and pH 7.4.

Res		Number	CA	CB	CO	^{15}N	HN
Met	M	1					
Asp	D	2	54.34	41.55	176.00		
Val	V	3	62.46	32.80	175.95	120.37	8.26
Phe	F	4	58.10	39.46	175.88	123.51	8.36
Met	M	5	55.34	32.67	175.99	122.29	8.24
Lys	K	6	56.89	32.72	177.14	122.63	8.30
Gly	G	7	45.22		174.21		
Leu	L	8	55.08	42.55	177.66	121.60	8.08
Ser	S	9	58.30	63.79	174.58	116.75	8.35
Lys	K	10	56.70	32.78	176.46		
Ala	A	11	52.64	19.19	177.91	125.38	8.32
Lys	K	12	56.48	32.97	176.70	120.92	8.36
Glu	E	13				122.23	8.46
Gly	G	14	45.30		174.04	110.12	8.49
Val	V	15	62.55	32.88	176.47	120.16	8.00
Val	V	16	62.50	32.76	176.00	125.32	8.33
Ala	A	17	52.53	19.26	177.67	128.53	8.47
Ala	A	18	52.67	19.18	177.91	123.76	8.34
Ala	A	19	52.75	19.12	178.20	123.14	8.31
Glu	E	20	56.83	30.28	176.95	120.15	8.36
Lys	K	21	56.73	32.84	177.15	122.33	8.37
Thr	T	22	62.21	69.75	174.70	115.31	8.16
Lys	K	23	56.67	32.79	176.70	123.81	8.38
Gln	Q	24	56.16	29.45	176.60	121.85	8.45
Gly	G	25	45.32		174.26	110.59	8.51
Val	V	26	62.66	32.80	176.38	119.80	8.04
Ala	A	27	52.78	19.03	178.13	127.47	8.46
Glu	E	28	56.73	30.20	176.67	120.64	8.43
Ala	A	29	52.64	19.22	177.73	125.02	8.32
Ala	A	30	52.82	19.08	178.47	123.13	8.27
Gly	G	31	45.24		174.22	107.84	8.34
Lys	K	32	56.23	33.19	177.01	120.77	8.15
Thr	T	33	61.92	69.93	174.66	115.65	8.26
Lys	K	34	56.57	32.97	176.50	123.87	8.50
Glu	E	35	56.97	30.23	176.97	122.07	8.47
Gly	G	36	45.40		174.03	110.00	8.44

Res		Number	CA	CB	CO	^{15}N	HN
Val	V	37	62.28	32.80	175.93	119.60	7.93
Leu	L	38	54.92	42.50	176.66	125.88	8.31
Tyr	Y	39	57.96	38.80	175.59	122.48	8.30
Val	V	40	62.16	32.97	176.16	123.37	8.11
Gly	G	41	45.16		173.96	112.21	8.08
Ser	S	42	58.33	63.84	174.74	115.69	8.28
Lys	K	43	56.43	33.05	176.87		
Thr	T	44	61.83	69.84	174.60	115.54	8.21
Lys	K	45	56.48	33.09	176.48	123.89	8.46
Glu	E	46	56.78	30.23	176.97	122.17	8.47
Gly	G	47	45.30		173.87	110.06	8.46
Val	V	48	62.48	32.88	176.00	120.00	7.94
Val	V	49	62.28	32.79	175.86	125.27	8.31
His	H	50	56.21	31.06	175.79	124.76	8.52
Gly	G	51	45.12		173.80	110.63	8.44
Val	V	52	62.00	33.01	175.94	119.62	8.06
Ala	A	53	52.49	19.35	177.84	128.23	8.52
Thr	T	54	61.93	70.01	174.55	114.90	8.25
Val	V	55	62.23	32.88	175.87	123.13	8.27
Ala	A	56	52.50	19.23	177.78	128.13	8.45
Asp	E	57	56.71	30.36	176.72	120.95	8.40
Lys	K	58	56.50	32.96	176.98	122.87	8.46
Thr	T	59	62.07	69.75	174.63	115.99	8.24
Lys	K	60	56.51	32.98	176.70	123.75	8.42
Glu	E	61	56.69	30.47	176.45		
Gln	Q	62	55.84	29.54	175.97	121.85	8.45
Val	V	63	62.51	32.82	176.35	122.00	8.32
Thr	T	64	61.82	69.94	174.06	118.15	8.33
Asn	N	65	53.08	38.93	175.25	121.89	8.55
Val	V	66	62.73	32.50	176.86	120.80	8.27
Gly	G	67	45.36		174.67	112.68	8.58
Gly	G	68	45.13		173.74	108.88	8.26
Ala	A	69	52.39	19.34	177.66	123.83	8.19
Val	V	70	62.55	32.64	176.34	120.55	8.24
Val	V	71	62.14	32.80	176.29	125.45	8.42
Thr	T	72	61.92	69.97	174.92	118.69	8.34
Gly	G	73	45.27		174.03	111.40	8.47
Val	V	74	62.39	32.87	176.56	119.56	8.11
Thr	T	75	62.10	69.80	174.09	118.98	8.33

Res		Number	CA	CB	CO	^{15}N	HN
Ala	A	76	52.50	19.31	177.58	127.46	8.40
Val	V	77	62.19	32.87	176.02	120.12	8.17
Ala	A	78	52.50	19.08	177.64	128.16	8.43
Gln	Q	79	55.79	29.58	175.95	120.35	8.42
Lys	K	80	56.30	33.24	176.69	123.33	8.46
Thr	T	81	61.85	69.97	174.45	116.97	8.32
Val	V	82	62.36	32.83	176.15	123.08	8.33
Glu	E	83	56.79	30.24	177.05	125.39	8.60
Gly	G	84	45.24		174.16	110.76	8.55
Ala	A	85	52.93	19.19	178.50	124.01	8.29
Gly	G	86	45.30		174.31	108.24	8.52
Ser	S	87	58.32	63.82	174.73	115.75	8.18
Ile	I	88	61.41	38.68	176.28	122.84	8.22
Ala	A	89	52.63	19.07	177.57	128.12	8.38
Ala	A	90	52.46	19.21	177.73	123.41	8.24
Ala	A	91	52.64	19.18	178.14	123.48	8.32
Thr	T	92	61.96	69.76	175.16	112.68	8.12
Gly	G	93	45.20		173.63	110.76	8.34
Phe	F	94	57.96	39.72	175.48	120.37	8.12
Val	V	95	62.04	32.25	175.41	123.81	8.08
Lys	K	96	56.38	33.05	176.50	126.48	8.42
Lys	K	97	56.53	33.18	176.37	123.86	8.50
Asp	D	98	54.42	41.07	176.22	121.28	8.43
Gln	Q	99	55.97	29.44	176.03	120.24	8.37
Leu	L	100	55.48	42.25	178.00	122.93	8.33
Gly	G	101	45.30		174.09	109.88	8.51
Lys	K	102	56.21	32.97	176.46	120.81	8.24
Asn	N	103	53.32	38.81	175.30	120.08	8.65
Glu	E	104	56.74	30.18	176.56	121.48	8.51
Glu	E	105	56.72	30.32	177.02	122.02	8.50
Gly	G	106	45.03		173.44	110.25	8.46
Ala	A	107	50.49	18.24	175.57	125.01	8.16
Pro	P	108	63.15	32.05	177.06		
Gln	Q	109	55.70	29.67	176.00	121.27	8.62
Glu	E	110	56.65	30.43	176.86	122.62	8.56
Gly	G	111	45.20		173.77	110.32	8.52
Ile	I	112	60.87	38.67	176.26	120.22	8.03
Lue	L	113	54.87	42.39	177.14	127.13	8.44
Glu	E	114	56.52	30.60	175.88	122.32	8.45

Res		Number	CA	CB	CO	^{15}N	HN
Asp	D	115	54.29	41.17	175.76	121.52	8.39
Met	M	116	53.23	32.49	174.06	122.09	8.29
Pro	P	117	62.90	32.13	176.72		
Val	V	118	62.01	33.09	175.76	120.92	8.33
Asp	D	119	52.11	41.13	174.71	126.06	8.55
Pro	P	120	63.53	32.21	176.93		
Asp	D	121	54.56	40.96	176.19	119.39	8.41
Asn	N	122	53.49	39.34	175.38	119.19	8.14
Glu	E	123	56.90	30.11	176.09	121.86	8.41
Ala	A	124	52.30	19.19	177.21	124.51	8.26
Tyr	Y	125	57.80	39.00	175.34	120.10	8.06
Glu	E	126	55.64	30.79	175.44	123.93	8.17
Met	M	127	53.28	32.63	174.25	123.98	8.45
Pro	P	128	63.10	32.20	176.89		
Ser	S	129	58.30	63.92	174.81	116.86	8.52
Glu	E	130	56.48	30.33	176.53	123.28	8.61
Glu	E	131	56.84	30.25	177.02		
Gly	G	132	45.18		173.84	110.07	8.47
Tyr	Y	133	58.22	38.77	175.74	120.40	8.09
Gln	Q	134	55.47	29.86	174.88	122.81	8.25
Asp	D	135	54.27	41.19	175.52	121.78	8.26
Tyr	Y	136	57.61	39.11	175.08	120.58	8.07
Glu	E	137	53.65	30.30	173.70	125.50	8.28
Pro	P	138	62.97	32.29	176.87		
Glu	E	139	56.64	30.32	175.41	121.69	8.55
Ala	A	140	53.82	20.25		131.00	8.02

A.2 Backbone assignment of human A53T at 15 °C and pH 7.4.

Res		Number	CA	CB	CO	^{15}N	HN
Met	M	1					
Asp	D	2	54.31	41.49	176.00		
Val	V	3	62.64	32.67	175.98	120.32	8.27
Phe	F	4	58.08	39.32	175.90	123.50	8.37
Met	M	5	55.39	32.68	176.01	122.25	8.26
Lys	K	6	56.89	32.81	177.19	122.67	8.32
Gly	G	7	45.38		174.22	110.03	8.46
Leu	L	8	55.25	42.55	177.68	121.60	8.09
Ser	S	9	58.41	63.80	174.59	116.70	8.36
Lys	K	10	56.42	32.76	176.48		
Ala	A	11	52.81	19.19	177.94	125.46	8.32
Lys	K	12	56.53	32.93	173.71	120.88	8.37
Glu	E	13					
Gly	G	14	45.34		174.04		
Val	V	15	62.50	32.68	176.48	120.14	8.02
Val	V	16	62.48	32.70	176.02	125.21	8.35
Ala	A	17	52.62	19.17	177.69	128.50	8.49
Ala	A	18	52.72	19.02	177.93	123.75	8.35
Ala	A	19	52.96	19.12	178.22	123.13	8.31
Glu	E	20	56.79	30.19	176.96	120.11	8.37
Lys	K	21	56.75	32.91	177.18	122.28	8.38
Thr	T	22	62.39	69.85	174.72	115.24	8.17
Lys	K	23	56.68	32.86	176.70	123.80	8.39
Gln	Q	24	56.62	29.56	176.88	121.78	8.47
Gly	G	25	45.41		174.27	110.57	8.53
Val	V	26	62.65	32.71	176.40	119.75	8.05
Ala	A	27	52.90	19.02	178.15	127.45	8.47
Glu	E	28	56.90	30.25	176.69	120.62	8.45
Ala	A	29	52.80	19.04	177.77	125.05	8.34
Ala	A	30	52.93	19.13	178.50	123.12	8.28
Gly	G	31	45.41		174.24	107.82	8.36
Lys	K	32	56.33	33.16	177.03	120.74	8.15
Thr	T	33	62.09	70.04	174.69	115.60	8.27
Lys	K	34	56.60	32.95	176.52	123.95	8.48
Glu	E	35	56.89	30.22	177.04	122.02	8.47
Gly	G	36	45.41		174.04	109.97	8.45

Res		Number	CA	CB	CO	^{15}N	HN
Val	V	37	62.37	32.77	175.95	119.57	7.95
Leu	L	38	55.05	42.48	176.68	125.83	8.32
Tyr	Y	39	57.92	38.90	175.61	122.47	8.31
Val	V	40	62.26	32.81	176.18	123.30	8.12
Gly	G	41	45.21		173.98	112.18	8.09
Ser	S	42				115.61	8.29
Lys	K	43	56.46	33.00	176.89		
Thr	T	44	61.96	69.94	174.62	115.48	8.22
Lys	K	45	56.48	33.06		123.90	8.52
Glu	E	46				122.18	8.48
Gly	G	47	45.27		173.87		
Val	V	48	62.36	32.84	176.04	119.97	7.95
Val	V	49	62.23	32.70	175.89	125.22	8.33
His	H	50	56.38	30.91	175.77	124.74	8.53
Gly	G	51	45.21		173.85	110.68	8.45
Val	V	52	62.27	32.93	176.56	119.62	8.14
Thr	T	53	61.91	69.87	174.57	118.86	8.45
Thr	T	54	61.85	69.96	174.39	117.86	8.31
Val	V	55	62.32	32.79	175.90	123.11	8.27
Ala	A	56	52.58	19.17	177.81	128.20	8.47
Asp	E	57	56.69	30.37	176.71	120.94	8.42
Lys	K	58	56.47	33.05	177.00	122.84	8.47
Thr	T	59	62.22	69.85	174.67	115.92	8.25
Lys	K	60	56.67	32.95	176.71	123.74	8.43
Glu	E	61				122.34	8.47
Gln	Q	62	55.90	29.57	176.00		
Val	V	63	62.51	32.79	176.37	121.95	8.33
Thr	T	64	61.90	69.97	174.07	118.09	8.34
Asn	N	65	53.11	38.90	175.27	121.84	8.56
Val	V	66	62.72	32.50	176.89	120.73	8.28
Gly	G	67	45.38		174.69	112.64	8.59
Gly	G	68	45.11		173.76	108.87	8.28
Ala	A	69	52.41	19.37	177.68	123.83	8.20
Val	V	70	62.48	32.69	176.36	120.50	8.25
Val	V	71	62.31	32.79	176.31	125.37	8.43
Thr	T	72	61.89	69.98	174.93	118.62	8.35
Gly	G	73	45.22		174.05	111.37	8.48
Val	V	74	62.37	32.77	176.57	119.54	8.12
Thr	T	75	61.98	69.82	174.10	118.90	8.34

Res		Number	CA	CB	CO	^{15}N	HN
Ala	A	76	52.54	19.33	177.60	127.41	8.41
Val	V	77	62.33	32.80	176.04	120.05	8.17
Ala	A	78	52.66	19.09	177.66	128.20	8.45
Gln	Q	79	55.74	29.71	175.97	120.33	8.43
Lys	K	80	56.43	33.15	176.71	123.28	8.47
Thr	T	81	61.98	69.94	174.46	116.91	8.33
Val	V	82	62.36	32.79	176.18	123.07	8.34
Glu	E	83	56.86	30.21	177.06	125.34	8.61
Gly	G	84	45.33		174.18	110.73	8.55
Ala	A	85	52.94	19.21	178.53	124.01	8.30
Gly	G	86	45.34		174.33	108.22	8.53
Ser	S	87	58.38	63.97	174.75	115.73	8.19
Ile	I	88	61.32	38.66	176.30	122.79	8.23
Ala	A	89	52.70	19.10	177.59	128.07	8.39
Ala	A	90	52.61	19.18	177.75	123.37	8.25
Ala	A	91	52.73	19.14	178.16	123.47	8.33
Thr	T	92	62.04	69.89	175.18	112.63	8.13
Gly	G	93	45.23		173.64	110.73	8.35
Phe	F	94	57.84	39.73	175.49	120.41	8.14
Val	V	95	62.02	33.09	175.43	123.73	8.09
Lys	K	96	56.41	33.03	176.50	126.44	8.44
Lys	K	97	56.49	33.15	176.40	123.80	8.50
Asp	D	98	54.58	41.03	176.24	121.25	8.45
Gln	Q	99	55.91	29.44	176.05	120.20	8.39
Leu	L	100	55.43	42.27	178.03	122.91	8.34
Gly	G	101	45.35		174.11	109.84	8.52
Lys	K	102	56.30	33.14	176.49	120.79	8.25
Asn	N	103	53.36	38.81	175.31	120.07	8.66
Glu	E	104	56.71	30.30	176.55	121.48	8.52
Glu	E	105	56.83	30.24	177.01	122.02	8.51
Gly	G	106	45.07		173.46	110.25	8.47
Ala	A	107	50.53	18.13	175.59	125.00	8.16
Pro	P	108	63.11	32.06	177.08		
Gln	Q	109	55.80	29.65	176.01	121.23	8.62
Glu	E	110	56.73	30.52	176.87	122.58	8.56
Gly	G	111	45.33		173.78	110.29	8.52
Ile	I	112	61.00	38.64	176.27	120.19	8.04
Lue	L	113	55.08	42.40	177.17	127.09	8.45
Glu	E	114	56.49	30.62	175.91	122.29	8.47

Res		Number	CA	CB	CO	^{15}N	HN
Asp	D	115	54.34	41.12	175.81	121.49	8.40
Met	M	116	53.20	32.57	174.09	122.06	8.30
Pro	P	117	62.92	32.16	176.74		
Val	V	118	61.96	33.01	175.78	120.86	8.34
Asp	D	119	52.13	41.08	174.74	126.02	8.55
Pro	P	120	63.54	32.23	176.94		
Asp	D	121	54.62	40.96	176.21	119.39	8.43
Asn	N	122	53.53	39.34	175.41	119.17	8.16
Glu	E	123	56.87	30.14	176.10	121.83	8.43
Ala	A	124	52.51	19.18	177.22	124.50	8.27
Tyr	Y	125	57.81	39.01	175.36	120.07	8.07
Glu	E	126	55.74	30.78	175.46	123.88	8.19
Met	M	127	53.36	32.54	174.27	123.96	8.46
Pro	P	128	63.08	32.24	176.91		
Ser	S	129	58.25	63.99	174.82	116.83	8.53
Glu	E	130	56.59	30.28	176.55	123.27	8.62
Glu	E	131	56.97	30.29	176.99		
Gly	G	132	45.19		173.86	110.05	8.49
Tyr	Y	133	58.16	38.82	175.77	120.35	8.11
Gln	Q	134	55.48	29.85	174.88	122.78	8.27
Asp	D	135	54.31	41.19	175.54	121.77	8.28
Tyr	Y	136	57.63	39.12	175.10	120.54	8.08
Glu	E	137	53.66	30.21	173.74	125.47	8.30
Pro	P	138	63.00	32.26	176.90		
Glu	E	139	56.61	30.34	175.43	121.65	8.56
Ala	A	140	53.87	20.16		130.97	8.03

A.3 Backbone assignment of human S87N at 15 °C and pH 7.4.

Res		Number	CA	CB	CO	^{15}N	HN
Met	M	1					
Asp	D	2	54.30	41.55	176.02		
Val	V	3	62.56	32.64	175.98	120.35	8.25
Phe	F	4	58.09	39.42	175.90	123.49	8.36
Met	M	5	55.34	32.75	175.99	122.28	8.24
Lys	K	6	56.97	32.72	177.17	122.67	8.30
Gly	G	7	45.22		174.21		
Leu	L	8	55.08	42.55	177.66	121.60	8.08
Ser	S	9	58.30	63.79	174.58	116.74	8.35
Lys	K	10	56.28	32.81	176.47		
Ala	A	11	52.55	19.19	177.91	125.27	8.32
Lys	K	12	56.48	32.97	176.69	120.92	8.37
Glu	E	13	56.76	30.48		122.20	8.45
Gly	G	14	45.30		174.05	110.15	8.49
Val	V	15	62.55	32.88	176.46	120.19	8.01
Val	V	16	62.50	32.76	176.00	125.26	8.33
Ala	A	17	52.53	19.26	177.66	128.53	8.47
Ala	A	18	52.67	19.18	177.91	123.77	8.34
Ala	A	19	52.69	19.18	178.20	123.16	8.31
Glu	E	20	56.82	30.25	176.94	120.15	8.36
Lys	K	21	56.74	32.88	177.15	122.32	8.37
Thr	T	22	62.21	69.71	174.69	115.30	8.16
Lys	K	23	56.54	32.88	176.69	123.82	8.38
Gln	Q	24	56.36	29.59	176.60	121.82	8.45
Gly	G	25	45.32		174.25	110.59	8.51
Val	V	26	62.66	32.80	176.38	119.80	8.04
Ala	A	27	52.82	19.07	178.13	127.47	8.46
Glu	E	28	56.85	30.24	176.66	120.64	8.43
Ala	A	29	52.63	19.22	177.75	125.06	8.33
Ala	A	30	52.82	19.08	178.47	123.17	8.27
Gly	G	31	45.24		174.22	107.84	8.35
Lys	K	32	56.23	33.19	177.02	120.76	8.14
Thr	T	33	61.92	69.93	174.67	115.65	8.26
Lys	K	34	56.69	33.02	176.49	123.90	8.50
Glu	E	35	56.97	30.23	176.96	122.09	8.48
Gly	G	36	45.44		174.03	110.01	8.45

Res		Number	CA	CB	CO	^{15}N	HN
Val	V	37	62.28	32.80	175.93	119.60	7.93
Leu	L	38	54.92	42.50	176.66	125.87	8.31
Tyr	Y	39	57.96	38.80	175.59	122.51	8.30
Val	V	40	62.16	32.97	176.17	123.37	8.11
Gly	G	41	45.16		173.95	112.21	8.08
Ser	S	42	58.41	63.89	174.73	115.67	8.29
Lys	K	43	56.47	33.05	176.88	123.50	8.51
Thr	T	44	61.83	69.84	174.60	115.53	8.21
Lys	K	45	56.47	33.09	176.50	123.89	8.46
Glu	E	46	56.78	30.23	176.96		
Gly	G	47	45.30		173.87	110.06	8.46
Val	V	48	62.23	32.82	176.01	120.01	7.94
Val	V	49	62.25	32.73	175.86	125.19	8.32
His	H	50	56.21	31.06	175.83	124.80	8.52
Gly	G	51	45.12		173.80	110.63	8.44
Val	V	52	62.00	33.01	175.94	119.61	8.06
Ala	A	53	52.43	19.35	177.84	128.23	8.52
Thr	T	54	61.85	70.01	174.54	114.90	8.25
Val	V	55	62.15	32.88	175.86	123.11	8.27
Ala	A	56	52.50	19.23	177.78	128.15	8.45
Asp	E	57	56.67	30.46	176.70	120.95	8.40
Lys	K	58	56.45	33.15	176.97	122.87	8.46
Thr	T	59	62.05	69.75	174.65	115.99	8.24
Lys	K	60	56.61	32.94	176.69	123.75	8.41
Glu	E	61	56.69	30.47	176.44		
Gln	Q	62	55.84	29.54	175.97	121.82	8.45
Val	V	63	62.51	32.82	176.36	122.00	8.32
Thr	T	64	61.82	69.94	174.05	118.14	8.33
Asn	N	65	53.08	38.91	175.25	121.90	8.55
Val	V	66	62.73	32.50	176.86	120.78	8.27
Gly	G	67	45.36		174.67	112.68	8.58
Gly	G	68	45.13		173.74	108.88	8.26
Ala	A	69	52.30	19.34	177.65	123.83	8.19
Val	V	70	62.57	32.64	176.33	120.55	8.24
Val	V	71	62.14	32.80	176.30	125.45	8.42
Thr	T	72	61.92	69.97	174.92	118.69	8.34
Gly	G	73	45.27		174.02	111.40	8.47
Val	V	74	62.39	32.87	176.56	119.57	8.11
Thr	T	75	62.05	69.86	174.08	118.98	8.33

Res		Number	CA	CB	CO	^{15}N	HN
Ala	A	76	52.50	19.31	177.57	127.46	8.40
Val	V	77	62.19	32.87	176.01	120.12	8.17
Ala	A	78	52.79	19.08	177.64	128.20	8.44
Gln	Q	79	55.79	29.58	175.96	120.38	8.42
Lys	K	80	56.38	33.11	176.70	123.32	8.46
Thr	T	81	61.85	69.97	174.45	116.96	8.32
Val	V	82	62.37	32.83	176.17	123.11	8.33
Glu	E	83	56.82	30.24	177.07	125.41	8.61
Gly	G	84	45.24		174.09	110.87	8.54
Ala	A	85	53.00	19.37	178.40	123.83	8.26
Gly	G	86	45.30		173.99	107.77	8.48
Asn	N	87	53.18	38.86	175.35	118.81	8.30
Ile	I	88	61.30	38.74	176.17	121.65	8.16
Ala	A	89	52.54	19.05	177.54	128.11	8.40
Ala	A	90	52.45	19.08	177.72	123.36	8.21
Ala	A	91	52.68	19.14	178.12	123.49	8.32
Thr	T	92	61.95	69.76	175.16	112.71	8.13
Gly	G	93	45.25		173.62	110.77	8.34
Phe	F	94	57.86	39.72	175.47	120.40	8.12
Val	V	95	62.04	33.25	175.41	123.82	8.08
Lys	K	96	56.38	33.09	176.48	126.49	8.42
Lys	K	97	56.53	33.18	176.38	123.87	8.50
Asp	D	98	54.42	41.07	176.22	121.28	8.43
Gln	Q	99	55.97	29.44	176.03	120.27	8.37
Leu	L	100	55.52	42.25	178.00	122.92	8.32
Gly	G	101	45.30		174.09	109.88	8.51
Lys	K	102	56.21	32.97	176.46	120.81	8.24
Asn	N	103	53.32	38.81	175.30	120.08	8.65
Glu	E	104	56.70	30.18	176.56	121.49	8.51
Glu	E	105	56.78	30.32	176.99	122.04	8.50
Gly	G	106	45.03		173.44	110.27	8.46
Ala	A	107	50.49	18.24	175.57	125.01	8.16
Pro	P	108	63.15	32.05	177.07		
Gln	Q	109	55.70	29.67	176.00	121.27	8.62
Glu	E	110	56.65	30.43	176.85	122.62	8.56
Gly	G	111	45.17		173.76	110.32	8.52
Ile	I	112	60.88	38.67	176.25	120.23	8.03
Leu	L	113	54.98	42.39	177.14	127.13	8.44
Glu	E	114	56.52	30.60	175.87	122.30	8.46

Res		Number	CA	CB	CO	^{15}N	HN
Asp	D	115	54.29	41.17	175.79	121.52	8.39
Met	M	116	53.23	32.53	174.07	122.08	8.29
Pro	P	117	62.90	32.13	176.72		
Val	V	118	62.01	33.09	175.76	120.92	8.33
Asp	D	119	52.11	41.13	174.71	126.06	8.55
Pro	P	120	63.53	32.21	176.93		
Asp	D	121	54.56	40.96	176.19	119.40	8.41
Asn	N	122	53.49	39.34	175.39	119.19	8.15
Glu	E	123	56.90	30.11	176.09	121.86	8.41
Ala	A	124	52.30	19.19	177.20	124.51	8.26
Tyr	Y	125	57.80	39.00	175.34	120.11	8.06
Glu	E	126	55.64	30.79	175.44	123.94	8.17
Met	M	127	53.28	32.63	174.25	123.99	8.45
Pro	P	128	63.10	32.20	176.89		
Ser	S	129	58.30	63.92	174.80	116.86	8.52
Glu	E	130	56.48	30.33	176.52	123.29	8.61
Glu	E	131	56.84	30.25	176.97		
Gly	G	132	45.18		173.84	110.09	8.47
Tyr	Y	133	58.22	38.77	175.74	120.37	8.10
Gln	Q	134	55.47	29.86	174.87	122.82	8.25
Asp	D	135	54.27	41.19	175.52	121.78	8.26
Tyr	Y	136	57.61	39.11	175.07	120.56	8.07
Glu	E	137	53.65	30.30	173.71	125.51	8.28
Pro	P	138	63.01	32.29	176.87		
Glu	E	139	56.64	30.32	175.41	121.67	8.55
Ala	A	140	53.82	20.25		131.00	8.02

A.4 Backbone assignment of human A53T-S87N at 15 °C and pH 7.4.

Res		Number	CA	CB	CO	^{15}N	HN
Met	M	1					
Asp	D	2	54.32	41.58	176.02		
Val	V	3	62.58	32.67	175.99	120.37	8.25
Phe	F	4	58.06	39.29	175.91	123.50	8.36
Met	M	5	55.52	32.65	176.02	122.29	8.24
Lys	K	6	56.87	32.88	177.18	122.67	8.29
Gly	G	7	45.43		174.23		
Leu	L	8	55.27	42.51	177.67	121.60	8.08
Ser	S	9	58.46	63.80	174.59	116.75	8.35
Lys	K	10	56.35	32.92	176.49		
Ala	A	11	52.76	19.25	177.93	125.32	8.32
Lys	K	12	56.59	32.92	176.71	120.92	8.36
Glu	E	13					
Gly	G	14	45.31		174.06	110.15	8.49
Val	V	15	62.59	32.69	176.49	120.17	8.00
Val	V	16	62.45	32.73	176.02	125.26	8.33
Ala	A	17	52.62	19.17	177.69	128.53	8.47
Ala	A	18	52.81	18.94	177.93	123.76	8.34
Ala	A	19	52.86	19.14	178.23	123.14	8.30
Glu	E	20	56.83	30.25	176.96	120.15	8.36
Lys	K	21	56.77	32.96	177.17	122.33	8.36
Thr	T	22	62.39	69.82	174.72	115.31	8.16
Lys	K	23	56.75	32.80	176.71	123.81	8.37
Gln	Q	24	56.57	29.45	176.62	121.85	8.45
Gly	G	25	45.37		174.27	110.59	8.51
Val	V	26	62.64	32.72	176.41	119.80	8.04
Ala	A	27	52.86	18.94	178.15	127.46	8.45
Glu	E	28	56.96	30.29	176.70	120.64	8.43
Ala	A	29	52.77	18.98	177.76	125.02	8.32
Ala	A	30	52.86	19.13	178.50	123.13	8.27
Gly	G	31	45.35		174.23	107.84	8.34
Lys	K	32	56.29	33.13	177.03	120.76	8.14
Thr	T	33	62.20	69.90	174.69	115.66	8.25
Lys	K	34	56.59	33.00	176.51		
Glu	E	35	56.91	30.17	177.10	122.21	8.47
Gly	G	36	45.34		174.04	110.01	8.44

Res		Number	CA	CB	CO	^{15}N	HN
Val	V	37	62.42	32.73	175.95	119.60	7.93
Leu	L	38	54.99	42.45	176.67	125.88	8.31
Tyr	Y	39	57.91	38.86	175.61	122.51	8.29
Val	V	40	62.27	32.83	176.17	123.37	8.10
Gly	G	41	45.15		173.97	112.21	8.07
Ser	S	42				115.69	8.28
Lys	K	43	56.39	33.04	176.89		
Thr	T	44	61.93	69.97	174.62	115.54	8.21
Lys	K	45	56.56	33.00	176.51	123.92	8.51
Glu	E	46			176.98		
Gly	G	47	45.33		173.89		
Val	V	48	62.36	32.76	176.04	120.01	7.94
Val	V	49	62.23	32.73	175.90	125.28	8.31
His	H	50	56.43	30.98	175.81	124.80	8.52
Gly	G	51	45.24		173.86	110.73	8.44
Val	V	52	62.36	32.96	176.57	119.65	8.13
Thr	T	53	61.90	69.90	174.57	118.93	8.43
Thr	T	54	61.81	70.01	174.37	117.92	8.30
Val	V	55	62.45	32.64	175.90	123.13	8.26
Ala	A	56	52.63	19.09	177.80	128.29	8.46
Asp	E	57	56.67	30.33	176.73	120.96	8.41
Lys	K	58	56.41	32.96	176.99	122.89	8.46
Thr	T	59	62.25	69.86	174.67	115.99	8.24
Lys	K	60	56.67	32.80	176.71	123.75	8.41
Glu	E	61			176.47		
Gln	Q	62	55.87	29.57	175.99	121.85	8.45
Val	V	63	62.45	32.76	176.38	122.00	8.31
Thr	T	64	62.10	69.90	174.08	118.15	8.33
Asn	N	65	53.16	38.98	175.27	121.90	8.55
Val	V	66	62.71	32.52	176.89	120.80	8.26
Gly	G	67	45.36		174.69	112.68	8.58
Gly	G	68	45.07		173.75	108.88	8.26
Ala	A	69	52.43	19.45	177.68	123.84	8.19
Val	V	70	62.52	32.72	176.36	120.55	8.24
Val	V	71	62.36	32.80	176.32	125.45	8.42
Thr	T	72	61.91	69.97	174.93	118.69	8.34
Gly	G	73	45.30		174.04	111.40	8.47
Val	V	74	62.38	32.76	176.59	119.55	8.11
Thr	T	75	62.01	69.82	174.11	118.98	8.33

Res		Number	CA	CB	CO	^{15}N	HN
Ala	A	76	52.56	19.29	177.59	127.45	8.40
Val	V	77	62.29	32.80	176.04	120.12	8.16
Ala	A	78	52.62	19.05	177.67	128.16	8.43
Gln	Q	79	55.81	29.65	175.98	120.35	8.41
Lys	K	80	56.44	33.16	176.72	123.32	8.46
Thr	T	81	62.05	69.94	174.47	116.96	8.32
Val	V	82	62.37	32.83	176.19	123.08	8.33
Glu	E	83	56.85	30.33	177.09	125.41	8.60
Gly	G	84	45.32		174.10	110.87	8.54
Ala	A	85	52.72	19.14	178.41	123.83	8.25
Gly	G	86	45.31		174.00	107.77	8.48
Asn	N	87	53.25	38.90	175.38	118.81	8.29
Ile	I	88	61.40	38.58	176.18	121.65	8.15
Ala	A	89	52.68	19.14	177.56	128.10	8.40
Ala	A	90	52.71	19.17	177.73	123.36	8.21
Ala	A	91	52.72	19.19	178.15	123.49	8.31
Thr	T	92	62.05	69.90	175.17	112.71	8.12
Gly	G	93	45.27		173.64	110.76	8.34
Phe	F	94	57.84	39.79	175.49	120.37	8.12
Val	V	95	62.11	33.04	175.43	123.82	8.08
Lys	K	96	56.42	33.08	176.49	126.49	8.42
Lys	K	97	56.51	33.16	176.39	123.81	8.49
Asp	D	98	54.56	41.13	176.24	121.28	8.43
Gln	Q	99	55.87	29.49	176.05	120.24	8.37
Leu	L	100	55.50	42.32	178.02	122.93	8.32
Gly	G	101	45.38		174.05	109.88	8.51
Lys	K	102	56.31	33.17	176.49	120.81	8.23
Asn	N	103	53.36	38.86	175.32	120.08	8.64
Glu	E	104	56.87	30.13	176.57	121.51	8.51
Glu	E	105			177.00	122.02	8.50
Gly	G	106	45.07		173.46		
Ala	A	107	50.57	18.14	175.59	125.01	8.15
Pro	P	108	63.11	32.08	177.09		
Gln	Q	109	55.82	29.61	176.01	121.27	8.61
Glu	E	110	56.59	30.53	176.87	122.62	8.55
Gly	G	111	45.31		173.78	110.32	8.51
Ile	I	112	60.96	38.62	176.28	120.23	8.02
Leu	L	113	55.05	42.33	177.16	127.14	8.44
Glu	E	114	56.47	30.72	175.89	122.35	8.45

Res		Number	CA	CB	CO	^{15}N	HN
Asp	D	115	54.38	41.15	175.81	121.52	8.39
Met	M	116	53.24	32.54	174.09	122.09	8.28
Pro	P	117	63.00	32.16	176.75		
Val	V	118	61.97	33.07	175.80	120.92	8.33
Asp	D	119	52.26	41.08	174.73	126.07	8.54
Pro	P	120	63.56	32.24	176.95		
Asp	D	121	54.60	40.90	176.21	119.40	8.41
Asn	N	122	53.52	39.26	175.40	119.20	8.14
Glu	E	123	56.87	30.09	176.09	121.87	8.41
Ala	A	124	52.48	18.98	177.22	124.52	8.25
Tyr	Y	125	57.82	39.04	175.36	120.10	8.06
Glu	E	126	55.73	30.80	175.46	123.92	8.17
Met	M	127	53.30	32.44	174.27	123.98	8.45
Pro	P	128	63.08	32.24	176.92		
Ser	S	129	58.31	63.99	174.82	116.86	8.52
Glu	E	130	56.64	30.17	176.55	123.29	8.60
Glu	E	131	56.85	30.21	177.03		
Gly	G	132	45.19		173.86	110.09	8.46
Tyr	Y	133	58.14	38.85	175.77	120.40	8.09
Gln	Q	134	55.45	29.85	174.89	122.82	8.25
Asp	D	135	54.27	41.22	175.54	121.78	8.26
Tyr	Y	136	57.67	39.10	175.11	120.56	8.06
Glu	E	137	53.64	30.17	173.74	125.51	8.28
Pro	P	138	62.96	32.32	176.90		
Glu	E	139	56.61	30.34	175.43	121.69	8.55
Ala	A	140	53.89	20.17		131.00	8.02

A.5 Backbone assignment of mouse α-synuclein at 15 °C and pH 7.4.

Res		Number	CA	CB	CO	^{15}N	HN
Met	M	1					
Asp	D	2	54.22	41.57	176.05		
Val	V	3	62.67	32.62	175.99	120.34	8.25
Phe	F	4	58.16	39.44	175.90	123.41	8.36
Met	M	5	55.29	32.63	176.00	122.28	8.24
Lys	K	6	56.67	32.81	177.17	122.62	8.30
Gly	G	7	45.38		174.21		
Leu	L	8	55.16	42.52	177.66	121.60	8.08
Ser	S	9	58.39	63.69	174.59	116.73	8.35
Lys	K	10	56.29	32.96			
Ala	A	11	52.68	19.15	177.91	125.38	8.32
Lys	K	12	56.41	33.07	176.69	120.93	8.37
Glu	E	13				122.30	8.46
Gly	G	14	45.30		174.04		
Val	V	15	62.51	32.72	176.46	120.18	8.00
Val	V	16	62.49	32.80	176.00	125.35	8.33
Ala	A	17	52.53	19.27	177.66	128.53	8.48
Ala	A	18	52.63	19.14	177.91	123.74	8.34
Ala	A	19	52.75	19.22	178.20	123.20	8.30
Glu	E	20	56.82	30.28	176.95	120.14	8.36
Lys	K	21	56.67	32.90	177.16	122.32	8.37
Thr	T	22	62.33	69.73	174.70	115.30	8.16
Lys	K	23	56.86	32.91	176.68	123.82	8.38
Gln	Q	24	56.34	29.59	176.60	121.82	8.45
Gly	G	25	45.18		174.26	110.58	8.52
Val	V	26	62.60	32.80	176.38	119.86	8.04
Ala	A	27	52.80	19.04	178.13	127.46	8.46
Glu	E	28	56.85	30.19	176.67	120.63	8.44
Ala	A	29	52.67	19.31	177.75	125.02	8.33
Ala	A	30	52.87	19.08	178.47	123.10	8.26
Gly	G	31	45.34		174.22	107.83	8.34
Lys	K	32	56.28	33.17	177.01	120.76	8.14
Thr	T	33	61.81	69.91	174.61	115.65	8.26
Lys	K	34	56.54	33.33	176.48	123.88	8.46
Glu	E	35	56.94	30.21	176.97	122.20	8.47
Gly	G	36	45.26		174.03	110.06	8.46

Res		Number	CA	CB	CO	^{15}N	HN
Val	V	37	62.33	32.81	175.92	119.60	7.93
Leu	L	38	54.96	42.56	176.66	125.87	8.31
Tyr	Y	39	57.80	38.84	175.59	122.52	8.30
Val	V	40	62.18	32.84	176.16	123.37	8.11
Gly	G	41	45.18		173.96	112.20	8.08
Ser	S	42	58.39	63.83	174.75	115.64	8.28
Lys	K	43	56.60	33.05	176.87	123.49	8.51
Thr	T	44	61.85	69.91	174.68	115.54	8.21
Lys	K	45	56.41	33.16	176.49	123.88	8.49
Glu	E	46			176.97		
Gly	G	47	45.27		173.86	110.15	8.47
Val	V	48	62.24	32.98	176.01	120.02	7.94
Val	V	49	62.25	32.73	175.86	125.27	8.32
His	H	50	56.37	31.11	175.87	124.89	8.51
Gly	G	51	45.25		173.85	110.68	8.43
Val	V	52	62.32	32.96	176.54	119.63	8.13
Thr	T	53	61.92	69.72	174.55	118.92	8.43
Thr	T	54	61.72	69.91	174.37	117.91	8.30
Val	V	55	62.24	32.86	175.88	123.24	8.29
Ala	A	56	52.59	19.15	177.77	128.26	8.45
Asp	E	57	56.56	30.45	176.70	120.93	8.41
Lys	K	58	56.50	33.07	176.98	122.89	8.46
Thr	T	59	62.09	69.77	174.65	115.99	8.24
Lys	K	60	56.62	32.98	176.69	123.75	8.41
Glu	E	61			176.43		
Gln	Q	62	55.84	29.52	175.97	121.82	8.45
Val	V	63	62.33	32.90	176.36	121.98	8.31
Thr	T	64	61.88	69.82	174.05	118.15	8.33
Asn	N	65	53.13	38.93	175.25	121.88	8.55
Val	V	66	62.71	32.52	176.87	120.78	8.27
Gly	G	67	45.35		174.67	112.68	8.58
Gly	G	68	45.09		173.74	108.88	8.26
Ala	A	69	52.32	19.40	177.66	123.84	8.19
Val	V	70	62.45	32.70	176.34	120.54	8.24
Val	V	71	62.20	32.78	176.29	125.45	8.42
Thr	T	72	61.90	69.91	174.92	118.68	8.33
Gly	G	73	45.27		174.03	111.40	8.46
Val	V	74	62.42	32.88	176.56	119.58	8.11
Thr	T	75	61.90	69.91	174.09	118.97	8.33

Res		Number	CA	CB	CO	^{15}N	HN
Ala	A	76	52.47	19.32	177.58	127.45	8.40
Val	V	77	62.20	32.80	176.02	120.12	8.17
Ala	A	78	52.59	19.15	177.64	128.20	8.43
Gln	Q	79	55.73	29.69	175.96	120.38	8.42
Lys	K	80	56.24	33.16	176.70	123.31	8.46
Thr	T	81	61.90	69.82	174.45	116.96	8.32
Val	V	82	62.33	32.81	176.16	123.10	8.33
Glu	E	83	56.76	30.37	177.07	125.40	8.61
Gly	G	84	45.35		174.09	110.88	8.54
Ala	A	85	52.75	19.31	178.40	123.83	8.26
Gly	G	86	45.18		173.99	107.77	8.48
Asn	N	87	53.22	38.84	175.35	118.81	8.29
Ile	I	88	61.31	38.71	176.17	121.65	8.16
Ala	A	89	52.49	19.08	177.54	128.11	8.40
Ala	A	90	52.37	19.23	177.71	123.37	8.21
Ala	A	91	52.66	19.13	178.12	123.45	8.32
Thr	T	92	61.95	69.77	175.16	112.70	8.12
Gly	G	93	45.18		173.62	110.76	8.34
Phe	F	94	57.79	39.73	175.48	120.37	8.11
Val	V	95	61.97	33.11	175.41	123.77	8.09
Lys	K	96	56.35	33.07	176.50	126.41	8.42
Lys	K	97	56.41	33.16	176.40	123.89	8.49
Asp	D	98	54.59	41.09	176.27	121.24	8.44
Gln	Q	99	56.07	29.45	176.11	120.17	8.37
Met	M	100	55.80	32.90	176.82	120.97	8.44
Gly	G	101	45.31		174.10	110.26	8.52
Lys	K	102	56.32	32.98	177.30	120.91	8.30
Gly	G	103	45.33		174.33	110.65	8.57
Glu	E	104	56.32	30.33	176.70	120.67	8.35
Glu	E	105	57.04	30.12	176.91	121.80	8.62
Gly	G	106	44.87		173.45	109.62	8.40
Thr	Y	107	55.80	38.10	174.06	121.31	8.05
Pro	P	108	63.30	32.07	176.88		
Gln	Q	109	55.88	29.67	176.04	121.32	8.57
Glu	E	110	56.67	30.63	176.87	122.29	8.56
Gly	G	111	45.18		173.74	110.27	8.51
Ile	I	112	60.98	38.65	176.25	120.16	8.01
Leu	L	113	55.05	42.35	177.16	127.08	8.43
Glu	E	114	56.47	30.56	175.88	122.30	8.45

Res		Number	CA	CB	CO	^{15}N	HN
Asp	D	115	54.32	41.16	175.78	121.46	8.39
Met	M	116	53.36	32.55	174.07	122.06	8.28
Pro	P	117	62.88	32.13	176.75		
Val	V	118	62.02	32.98	175.80	120.97	8.33
Asp	D	119	51.98	41.29	174.85	126.17	8.58
Pro	P	120	63.70	32.14	177.64		
Gly	G	121	45.32		174.57	108.99	8.57
Ser	S	122	58.55	63.88	174.80	115.70	8.13
Glu	E	123	56.71	30.01	176.15	122.98	8.55
Ala	A	124	52.29	19.23	177.15	124.43	8.23
Tyr	Y	125	57.70	38.96	175.33	119.95	8.04
Glu	E	126	55.65	30.76	175.46	123.81	8.17
Met	M	127	53.20	32.46	174.24	123.89	8.44
Pro	P	128	63.07	32.20	176.90		
Ser	S	129	58.29	63.87	174.81	116.84	8.52
Glu	E	130	56.54	30.32	176.53	123.27	8.61
Glu	E	131	57.03	30.21	176.99	122.05	8.50
Gly	G	132	45.10		173.85	110.02	8.44
Tyr	Y	133	58.30	38.78	175.75	120.38	8.10
Gln	Q	134	55.41	29.84	174.86	122.81	8.26
Asp	D	135	54.33	41.19	175.52	121.77	8.27
Tyr	Y	136	57.53	39.07	175.08	120.58	8.06
Glu	E	137	53.57	30.29	173.72	125.50	8.28
Pro	P	138	63.04	32.30	176.88		
Glu	E	139	56.63	30.32	175.41	121.67	8.55
Ala	A	140	53.80	20.23		131.00	8.02

A.6 Backbone assignment of mouse T53A at 15 °C and pH 7.4.

Res		Number	CA	CB	CO	^{15}N	HN
Met	M	1					
Asp	D	2	54.18	41.53	176.00		
Val	V	3	62.65	32.60	175.97	120.37	8.26
Phe	F	4	57.96	39.37	175.89	123.50	8.36
Met	M	5	55.29	32.63	175.99	122.28	8.24
Lys	K	6	56.67	32.81	177.17	122.63	8.30
Gly	G	7	45.35		174.21		
Leu	L	8	55.16	42.52	177.66	121.60	8.08
Ser	S	9	58.39	63.69	174.58	116.74	8.35
Lys	K	10	56.25	33.00	176.46		
Ala	A	11	52.68	19.15	177.91	125.38	8.32
Lys	K	12	56.41	33.07	176.69	120.93	8.37
Glu	E	13				122.30	8.47
Gly	G	14	45.30		174.04		
Val	V	15	62.51	32.72	176.47	120.18	8.00
Val	V	16	62.38	32.90	176.00	125.35	8.33
Ala	A	17	52.49	19.08	177.66	128.53	8.47
Ala	A	18	52.67	19.14	177.90	123.74	8.34
Ala	A	19	52.80	19.08	178.20	123.12	8.30
Glu	E	20	56.82	30.25	176.95	120.14	8.36
Lys	K	21	56.67	32.90	177.15	122.32	8.37
Thr	T	22	62.33	69.73	174.69	115.30	8.17
Lys	K	23	56.50	32.98	176.69	123.81	8.38
Gln	Q	24	56.34	29.60	176.61	121.81	8.46
Gly	G	25	45.18		174.26	110.58	8.52
Val	V	26	62.60	32.80	176.38	119.86	8.04
Ala	A	27	52.80	19.04	178.13	127.47	8.46
Glu	E	28	56.85	30.19	176.66	120.63	8.43
Ala	A	29	52.67	19.31	177.75	125.09	8.33
Ala	A	30	52.87	19.08	178.47	123.11	8.27
Gly	G	31	45.34		174.22	107.84	8.34
Lys	K	32	56.24	33.20	177.01	120.77	8.14
Thr	T	33	62.09	69.77	174.66	115.64	8.26
Lys	K	34	56.58	33.16	176.50	123.87	8.49
Glu	E	35	56.94	30.21	176.96	122.18	8.48
Gly	G	36	45.26		174.02	110.06	8.46

Res		Number	CA	CB	CO	^{15}N	HN
Val	V	37	62.33	32.81	175.91	119.60	7.93
Leu	L	38	54.96	42.51	176.66	125.87	8.31
Tyr	Y	39	57.90	38.74	175.58	122.51	8.30
Val	V	40	62.18	32.84	176.16	123.37	8.11
Gly	G	41	45.18		173.95	112.18	8.08
Ser	S	42	58.39	63.83	174.73	115.66	8.27
Lys	K	43	56.28	33.17	176.87		
Thr	T	44	61.85	69.91	174.60	115.51	8.21
Lys	K	45	56.41	33.16	176.48	123.86	8.46
Glu	E	46			176.95	122.23	8.49
Gly	G	47	45.27		173.87		
Val	V	48	62.24	32.98	176.01	120.00	7.94
Val	V	49	62.17	32.83	175.86	125.27	8.32
His	H	50	56.31	31.02	175.81	124.76	8.52
Gly	G	51	45.00		173.79	110.64	8.44
Val	V	52	62.07	32.90	175.94	119.60	8.06
Ala	A	53	52.44	19.32	177.84	128.23	8.52
Thr	T	54	61.85	69.90	174.55	114.90	8.25
Val	V	55	62.24	32.90	175.84	123.11	8.28
Ala	A	56	52.40	19.31	177.77	128.18	8.45
Asp	E	57	56.66	30.41	176.71	120.99	8.40
Lys	K	58	56.58	33.07	176.98	122.88	8.46
Thr	T	59	62.09	69.77	174.65	115.98	8.24
Lys	K	60	56.67	32.98	176.68	123.76	8.42
Glu	E	61			176.45		
Gln	Q	62	55.83	29.52	175.97	121.81	8.46
Val	V	63	62.33	32.90	176.35	122.04	8.32
Thr	T	64	61.88	69.82	174.06	118.14	8.33
Asn	N	65	53.13	38.93	175.25	121.81	8.55
Val	V	66	62.71	32.52	176.86	120.77	8.27
Gly	G	67	45.35		174.67	112.68	8.59
Gly	G	68	45.09		173.74	108.88	8.26
Ala	A	69	52.32	19.40	177.66	123.83	8.19
Val	V	70	62.45	32.70	176.34	120.54	8.24
Val	V	71	62.20	32.78	176.29	125.44	8.42
Thr	T	72	61.90	69.91	174.92	118.65	8.34
Gly	G	73	45.27		174.03	111.40	8.47
Val	V	74	62.33	32.81	176.56	119.57	8.11
Thr	T	75	62.10	69.80	174.09	118.98	8.33

Res		Number	CA	CB	CO	^{15}N	HN
Ala	A	76	52.47	19.32	177.58	127.45	8.40
Val	V	77	62.20	32.80	176.02	120.11	8.17
Ala	A	78	52.59	19.15	177.63	128.19	8.44
Gln	Q	79	55.73	29.69	175.96	120.38	8.42
Lys	K	80	56.24	33.16	176.70	123.31	8.46
Thr	T	81	61.90	69.82	174.45	116.95	8.32
Val	V	82	62.33	32.81	176.17	123.11	8.33
Glu	E	83	56.82	30.24	177.07	125.40	8.61
Gly	G	84	45.35		174.09	110.87	8.54
Ala	A	85	52.75	19.31	178.40	123.82	8.26
Gly	G	86	45.18		173.99	107.77	8.48
Asn	N	87	53.19	38.82	175.35	118.80	8.30
Ile	I	88	61.37	38.62	176.16	121.64	8.16
Ala	A	89	52.49	19.05	177.54	128.10	8.40
Ala	A	90	52.45	19.19	177.70	123.36	8.21
Ala	A	91	52.66	19.13	178.12	123.48	8.32
Thr	T	92	61.95	69.77	175.16	112.70	8.12
Gly	G	93	45.18		173.62	110.76	8.34
Phe	F	94	57.79	39.73	175.47	120.37	8.11
Val	V	95	61.97	33.11	175.42	123.77	8.09
Lys	K	96	56.35	33.07	176.50	126.41	8.42
Lys	K	97	56.41	33.16	176.41	123.89	8.50
Asp	D	98	54.59	41.09	176.27	121.24	8.44
Gln	Q	99	56.07	29.45	176.11	120.16	8.37
Met	M	100	55.80	32.90	176.82	120.97	8.43
Gly	G	101	45.31		174.10		
Lys	K	102	56.32	32.98	177.30	120.91	8.30
Gly	G	103	45.33		174.32	110.65	8.57
Glu	E	104	56.32	30.33	176.75	120.67	8.35
Glu	E	105	57.04	30.12	176.91	121.80	8.62
Gly	G	106	45.01		173.44	109.62	8.40
Tyr	Y	107	55.80	38.10	174.06	121.30	8.06
Pro	P	108	63.30	32.07	176.88		
Gln	Q	109	55.88	29.67	176.05	121.32	8.57
Glu	E	110	56.67	30.63	176.87	122.29	8.56
Gly	G	111	45.18		173.73	110.27	8.51
Ile	I	112	60.98	38.65	176.24	120.16	8.01
Lue	L	113	55.05	42.35	177.15	127.06	8.43
Glu	E	114	56.47	30.56	175.88	122.30	8.45

Res		Number	CA	CB	CO	^{15}N	HN
Asp	D	115	54.32	41.16	175.77	121.45	8.39
Met	M	116	53.36	32.55	174.07	122.06	8.28
Pro	P	117	62.88	32.13	176.75		
Val	V	118	62.02	32.98	175.80	120.97	8.33
Asp	D	119	51.98	41.29	174.85	126.16	8.58
Pro	P	120	63.70	32.14	177.64		
Gly	G	121	45.32		174.57	108.99	8.58
Ser	S	122	58.55	63.88	174.80	115.71	8.13
Glu	E	123	56.71	30.01	176.14	122.97	8.55
Ala	A	124	52.29	19.23	177.15	124.43	8.23
Tyr	Y	125	57.70	38.96	175.33	119.95	8.04
Glu	E	126	55.65	30.76	175.46	123.81	8.17
Met	M	127	53.23	32.46	174.24	123.89	8.44
Pro	P	128	63.07	32.20	176.90		
Ser	S	129	58.29	63.87	174.81	116.83	8.52
Glu	E	130	56.54	30.32	176.53	123.26	8.61
Glu	E	131	57.03	30.21	176.97	122.05	8.50
Gly	G	132	45.10		173.85	110.02	8.44
Tyr	Y	133	58.34	38.78	175.75	120.38	8.10
Gln	Q	134	55.41	29.84	174.86	122.81	8.25
Asp	D	135	54.33	41.19	175.52	121.77	8.26
Tyr	Y	136	57.61	39.14	175.08	120.57	8.07
Glu	E	137	53.57	30.29	173.71	125.50	8.28
Pro	P	138	63.04	32.21	176.88		
Glu	E	139	56.63	30.32	175.41	121.67	8.55
Ala	A	140	53.80	20.23		130.99	8.02

A.7 Backbone assignment of mouse N87S at 15 °C and pH 7.4.

Res		Number	CA	CB	CO	^{15}N	HN
Met	M	1					
Asp	D	2	54.19	41.53	176.03		
Val	V	3	62.47	32.60	175.98	120.35	8.25
Phe	F	4	57.90	39.37	175.90	123.50	8.37
Met	M	5	55.29	32.63	176.01	122.27	8.24
Lys	K	6	56.90	32.84	177.16	122.63	8.30
Gly	G	7	45.35		174.21		
Leu	L	8	55.16	42.52	177.65	121.60	8.08
Ser	S	9	58.40	63.70	174.59	116.74	8.35
Lys	K	10	56.17	33.00	176.69		
Ala	A	11	52.68	19.15	177.92	125.38	8.32
Lys	K	12	56.41	33.07	176.69	120.93	8.37
Glu	E	13				122.31	8.46
Gly	G	14	45.31		174.03		
Val	V	15	62.51	32.72	176.46	120.18	8.00
Val	V	16	62.48	32.79	176.00	125.35	8.34
Ala	A	17	52.53	19.27	177.67	128.53	8.48
Ala	A	18	52.67	19.14	177.91	123.74	8.34
Ala	A	19	52.80	19.09	178.20	123.20	8.30
Glu	E	20	56.82	30.26	176.94	120.14	8.36
Lys	K	21	56.67	32.90	177.15	122.32	8.37
Thr	T	22	62.33	69.74	174.70	115.30	8.16
Lys	K	23	56.86	32.91	176.69	123.83	8.38
Gln	Q	24	56.34	29.60	176.61	121.82	8.45
Gly	G	25	45.18		174.26	110.58	8.52
Val	V	26	62.60	32.80	176.38	119.86	8.05
Ala	A	27	52.80	19.04	178.13	127.47	8.46
Glu	E	28	56.85	30.19	176.67	120.63	8.44
Ala	A	29	52.63	19.23	177.75	125.01	8.33
Ala	A	30	52.87	19.08	178.47	123.10	8.26
Gly	G	31	45.34		174.22	107.84	8.35
Lys	K	32	56.28	33.18	177.02	120.76	8.14
Thr	T	33	61.81	69.91	174.67	115.63	8.26
Lys	K	34	56.59	33.16	176.49	123.88	8.49
Glu	E	35	56.95	30.21	176.95	122.20	8.47
Gly	G	36	45.26		174.03	110.06	8.47

Res		Number	CA	CB	CO	^{15}N	HN
Val	V	37	62.33	32.81	175.92	119.60	7.94
Leu	L	38	54.96	42.57	176.66	125.88	8.31
Tyr	Y	39	57.81	38.84	175.59	122.52	8.30
Val	V	40	62.18	32.84	176.16	123.37	8.11
Gly	G	41	45.18		173.95	112.21	8.08
Ser	S	42	58.39	63.83	174.78		
Lys	K	43	56.60	33.05	176.87	123.49	8.51
Thr	T	44	61.85	69.91	174.60	115.53	8.21
Lys	K	45	56.41	33.16	176.49	123.87	8.46
Glu	E	46			176.92	122.22	8.49
Gly	G	47	45.27		173.86	110.23	8.50
Val	V	48	62.25	32.99	176.01	120.00	7.94
Val	V	49	62.17	32.82	175.86	125.27	8.32
His	H	50	56.32	31.15	175.84	124.85	8.51
Gly	G	51	45.00		173.84	110.70	8.44
Val	V	52	62.32	32.96	176.54	119.63	8.13
Thr	T	53	61.93	69.73	174.55	118.92	8.43
Thr	T	54	61.85	69.91	174.37	117.90	8.30
Val	V	55	62.25	32.90	175.88	123.24	8.29
Ala	A	56	52.59	19.15	177.78	128.26	8.45
Asp	E	57	56.65	30.46	176.71	120.93	8.41
Lys	K	58	56.59	33.07	176.97	122.89	8.46
Thr	T	59	62.09	69.77	174.65	115.98	8.24
Lys	K	60	56.50	32.99	176.68	123.75	8.42
Glu	E	61			176.43		
Gln	Q	62	55.90	29.51	175.97	121.82	8.45
Val	V	63	62.33	32.90	176.34	122.00	8.32
Thr	T	64	61.88	69.82	174.06	118.14	8.33
Asn	N	65	53.13	38.94	175.25	121.88	8.55
Val	V	66	62.72	32.52	176.86	120.78	8.27
Gly	G	67	45.35		174.67	112.68	8.59
Gly	G	68	45.09		173.74	108.88	8.26
Ala	A	69	52.32	19.40	177.66	123.84	8.19
Val	V	70	62.45	32.70	176.34	120.54	8.25
Val	V	71	62.20	32.78	176.28	125.45	8.42
Thr	T	72	61.90	69.91	174.92	118.68	8.34
Gly	G	73	45.28		174.03	111.40	8.47
Val	V	74	62.42	32.88	176.56	119.58	8.11
Thr	T	75	61.90	69.91	174.08	118.97	8.33

Res		Number	CA	CB	CO	^{15}N	HN
Ala	A	76	52.47	19.32	177.58	127.45	8.40
Val	V	77	62.21	32.80	176.02	120.12	8.17
Ala	A	78	52.592	19.15	177.637	128.202	8.435
Gln	Q	79	55.73	29.69	175.95	120.38	8.42
Lys	K	80	56.24	33.16	176.69	123.32	8.46
Thr	T	81	61.90	69.82	174.45	116.96	8.32
Val	V	82	62.33	32.82	176.16	123.10	8.33
Glu	E	83	56.76	30.37	177.04	125.40	8.61
Gly	G	84	45.35		174.16	110.77	8.54
Ala	A	85	52.75	19.31	178.50	123.99	8.29
Gly	G	86	45.18		174.31	108.24	8.52
Ser	S	87	58.33	63.90	174.73	115.74	8.18
Ile	I	88	61.37	38.62	176.28	122.82	8.22
Ala	A	89	52.58	19.14	177.57	128.12	8.37
Ala	A	90	52.45	19.19	177.72	123.42	8.24
Ala	A	91	52.66	19.13	178.14	123.46	8.32
Thr	T	92	61.95	69.77	175.16	112.67	8.12
Gly	G	93	45.18		173.62	110.74	8.33
Phe	F	94	57.79	39.73	175.48	120.37	8.11
Val	V	95	61.97	33.12	175.42	123.78	8.09
Lys	K	96	56.35	33.07	176.50	126.41	8.42
Lys	K	97	56.41	33.16	176.40	123.89	8.49
Asp	D	98	54.60	41.10	176.27	121.24	8.44
Gln	Q	99	56.06	29.76	176.11	120.17	8.37
Met	M	100	55.80	32.90	176.86	120.97	8.44
Gly	G	101	45.31		174.10	110.28	8.52
Lys	K	102	56.32	32.99	177.30	120.91	8.30
Gly	G	103	45.33		174.31	110.65	8.58
Glu	E	104	56.32	30.33	176.76	120.67	8.35
Glu	E	105	57.04	30.12	176.91	121.80	8.62
Gly	G	106	44.84		173.45	109.62	8.40
Tyr	Y	107	55.80	38.11	174.06	121.31	8.05
Pro	P	108	63.30	32.07	176.88		
Gln	Q	109	55.89	29.67	176.06	121.32	8.57
Glu	E	110	56.67	30.63	176.85	122.29	8.57
Gly	G	111	45.18		173.74	110.27	8.51
Ile	I	112	60.98	38.65	176.24	120.16	8.01
Lue	L	113	54.99	42.36	177.16	127.07	8.43
Glu	E	114	56.59	30.46	175.88	122.30	8.45

Res		Number	CA	CB	CO	^{15}N	HN
Asp	D	115	54.32	41.16	175.78	121.46	8.39
Met	M	116	53.36	32.55	174.07	122.05	8.28
Pro	P	117	62.88	32.13	176.75		
Val	V	118	62.02	32.99	175.80	120.97	8.33
Asp	D	119	51.98	41.29	174.85	126.16	8.58
Pro	P	120	63.70	32.14	177.64		
Gly	G	121	45.33		174.57	108.99	8.58
Ser	S	122	58.55	63.88	174.81	115.71	8.13
Glu	E	123	56.71	30.01	176.15	122.98	8.55
Ala	A	124	52.29	19.23	177.16	124.43	8.23
Tyr	Y	125	57.70	38.96	175.33	119.96	8.04
Glu	E	126	55.66	30.76	175.46	123.81	8.17
Met	M	127	53.23	32.46	174.24	123.89	8.45
Pro	P	128	63.07	32.20	176.89		
Ser	S	129	58.29	63.87	174.81	116.84	8.52
Glu	E	130	56.54	30.32	176.52	123.26	8.61
Glu	E	131	57.03	30.21	176.96	122.05	8.50
Gly	G	132	45.10		173.85	110.02	8.44
Tyr	Y	133	58.34	38.78	175.75	120.38	8.10
Gln	Q	134	55.41	29.85	174.87	122.81	8.26
Asp	D	135	54.33	41.19	175.52	121.77	8.26
Tyr	Y	136	57.61	39.14	175.08	120.58	8.06
Glu	E	137	53.57	30.29	173.71	125.50	8.29
Pro	P	138	63.04	32.21	176.88		
Glu	E	139	56.63	30.32	175.41	121.67	8.55
Ala	A	140	53.80	20.23		131.00	8.02

A.8 Backbone assignment of mouse T53A-N87S at 15 °C and pH 7.4.

Res		Number	CA	CB	CO	^{15}N	HN
Met	M	1					
Asp	D	2	54.32	41.45	176.03		
Val	V	3	62.57	32.52	176.00	120.35	8.25
Phe	F	4	57.96	39.31	175.91	123.49	8.36
Met	M	5	55.38	32.72	176.01	122.28	8.24
Lys	K	6	56.67	32.81	177.19		
Gly	G	7	45.27		174.22		
Leu	L	8	55.16	42.52	177.68	121.60	8.07
Ser	S	9	58.39	63.69	174.59	116.74	8.34
Lys	K	10	56.46	32.92			
Ala	A	11	52.60	19.07	177.94	125.38	8.32
Lys	K	12	56.41	32.95	176.71	120.93	8.36
Glu	E	13					
Gly	G	14	45.23		174.05		
Val	V	15	62.45	32.72	176.49	120.15	8.01
Val	V	16	62.33	32.90	176.03	125.32	8.32
Ala	A	17	52.59	19.16	177.70	128.52	8.47
Ala	A	18	52.67	19.14	177.94	123.75	8.34
Ala	A	19	52.75	19.00	178.22	123.13	8.29
Glu	E	20	56.74	30.18	176.97	120.15	8.36
Lys	K	21	56.70	32.90	177.18	122.32	8.36
Thr	T	22	62.36	69.77	174.72	115.30	8.15
Lys	K	23	56.78	32.83	176.71	123.81	8.37
Gln	Q	24	56.16	29.52	176.62	121.81	8.45
Gly	G	25	45.18		174.28	110.59	8.51
Val	V	26	62.59	32.90	176.40	119.85	8.04
Ala	A	27	52.81	19.10	178.16	127.47	8.45
Glu	E	28	56.85	30.19	176.69	120.63	8.43
Ala	A	29	52.67	19.31	177.77	125.12	8.33
Ala	A	30	52.79	19.00	178.50	123.10	8.26
Gly	G	31	45.34		174.24	107.84	8.34
Lys	K	32	56.24	33.20	177.03	120.75	8.13
Thr	T	33	62.06	69.91	174.68	115.64	8.26
Lys	K	34	56.58	32.84	176.53	123.81	8.46
Glu	E	35	56.87	30.13	177.00	122.21	8.47
Gly	G	36	45.26			110.06	8.47

Res		Number	CA	CB	CO	^{15}N	HN
Val	V	37	62.33	32.81	175.94	119.60	7.93
Leu	L	38	54.96	42.56	176.68	125.87	8.31
Tyr	Y	39	58.05	38.84	175.61	122.51	8.29
Val	V	40	62.18	32.84	176.18	123.37	8.10
Gly	G	41	45.18		173.97	112.21	8.07
Ser	S	42	58.31	63.75			
Lys	K	43	56.41	32.97	176.90		
Thr	T	44	61.96	69.91	174.63	115.53	8.20
Lys	K	45	56.41	33.16		123.89	8.49
Glu	E	46					
Gly	G	47	45.19		173.88		
Val	V	48	62.43	32.79	176.03	120.00	7.94
Val	V	49	62.20	32.74	175.88	125.26	8.31
His	H	50	56.42	31.07	175.84	124.78	8.51
Gly	G	51	45.25		173.83	110.57	8.44
Val	V	52	62.04	32.91	175.97	119.60	8.05
Ala	A	53	52.49	19.23	177.87	128.22	8.51
Thr	T	54	61.92	69.99	174.58	114.89	8.24
Val	V	55	62.32	32.80	175.88	123.12	8.26
Ala	A	56	52.52	19.06	177.81	128.16	8.46
Asp	E	57	56.67	30.37	176.73	120.95	8.40
Lys	K	58	56.58	33.07	177.01	122.86	8.46
Thr	T	59	62.09	69.77	174.67	115.99	8.23
Lys	K	60	56.71	32.98		123.73	8.41
Glu	E	61					
Gln	Q	62	55.85	29.51	176.00	121.81	8.45
Val	V	63	62.37	32.90	176.37	121.99	8.31
Thr	T	64	61.91	69.82	174.07	118.14	8.33
Asn	N	65	53.13	38.93	175.27	121.78	8.55
Val	V	66	62.69	32.44	176.89	120.77	8.26
Gly	G	67	45.35		174.69	112.67	8.58
Gly	G	68	45.09		173.76	108.88	8.26
Ala	A	69	52.32	19.40	177.68	123.82	8.19
Val	V	70	62.41	32.62	176.36	120.54	8.24
Val	V	71	62.20	32.78	176.32	125.44	8.42
Thr	T	72	61.93	69.91	174.93	118.68	8.33
Gly	G	73	45.27		174.05	111.40	8.46
Val	V	74	62.30	32.81	176.58	119.56	8.10
Thr	T	75	62.06	69.91	174.11	118.98	8.32

Res		Number	CA	CB	CO	^{15}N	HN
Ala	A	76	52.43	19.24	177.60	127.45	8.40
Val	V	77	62.20	32.80	176.05	120.11	8.16
Ala	A	78	52.51	19.13	177.66	128.19	8.44
Gln	Q	79	55.75	29.61	175.98	120.38	8.42
Lys	K	80	56.45	33.16	176.71	123.32	8.46
Thr	T	81	61.90	69.82	174.47	116.96	8.32
Val	V	82	62.30	32.74	176.18	123.09	8.33
Glu	E	83	56.76	30.37	177.06	125.39	8.59
Gly	G	84	45.35		174.18	110.76	8.54
Ala	A	85	52.92	19.31	178.52	124.01	8.29
Gly	G	86	45.35		174.33	108.23	8.52
Ser	S	87	58.32	63.90	174.75	115.75	8.17
Ile	I	88	61.29	38.54	176.30	122.82	8.22
Ala	A	89	52.58	19.13	177.59	128.11	8.38
Ala	A	90	52.53	19.11	177.75	123.39	8.23
Ala	A	91	52.61	19.05	178.16	123.47	8.31
Thr	T	92	61.95	69.77	175.18	112.67	8.11
Gly	G	93	45.21		173.64	110.74	8.33
Phe	F	94	57.81	39.65	175.50	120.34	8.10
Val	V	95	62.01	33.11	175.44	123.77	8.08
Lys	K	96	56.39	33.07	176.52	126.40	8.41
Lys	K	97	56.41	33.09	176.42	123.90	8.49
Asp	D	98	54.49	41.02	176.29	121.23	8.43
Gln	Q	99	56.06	29.37	176.13	120.19	8.37
Met	M	100	55.80	32.90	176.84	120.98	8.43
Gly	G	101	45.31		174.12		
Lys	K	102	56.36	32.98	177.33	120.88	8.29
Gly	G	103	45.33		174.34	110.64	8.56
Glu	E	104	56.44	30.33	176.78	120.67	8.35
Glu	E	105	56.96	30.04	176.94	121.79	8.61
Gly	G	106	45.03		173.47	109.61	8.40
Tyr	Y	107	55.80	38.10	174.08	121.30	8.05
Pro	P	108	63.22	31.99	176.90		
Gln	Q	109	55.85	29.59	176.08	121.31	8.56
Glu	E	110	56.67	30.63	176.88	122.28	8.55
Gly	G	111	45.18		173.75	110.26	8.50
Ile	I	112	60.90	38.57	176.27	120.15	8.00
Lue	L	113	54.99	42.27	177.18	127.07	8.43
Glu	E	114	56.39	30.46	175.91	122.30	8.45

Res		Number	CA	CB	CO	^{15}N	HN
Asp	D	115	54.32	41.16	175.80	121.45	8.38
Met	M	116	53.36	32.55	174.09	122.05	8.27
Pro	P	117	62.80	32.05	176.77		
Val	V	118	61.94	32.91	175.83	120.97	8.33
Asp	D	119	51.98	41.29	174.87	126.16	8.57
Pro	P	120	63.66	32.06	177.66		
Gly	G	121	45.32		174.59	108.99	8.57
Ser	S	122	58.55	63.88	174.82	115.70	8.12
Glu	E	123	56.80	30.01	176.18	122.97	8.54
Ala	A	124	52.29	19.23	177.18	124.43	8.22
Tyr	Y	125	57.66	38.88	175.35	119.93	8.03
Glu	E	126	55.65	30.76	175.47	123.84	8.16
Met	M	127	53.30	32.46	174.26	123.89	8.44
Pro	P	128	63.03	32.12	176.92		
Ser	S	129	58.22	63.79	174.83	116.84	8.51
Glu	E	130	56.54	30.32	176.55	123.26	8.60
Glu	E	131	56.84	30.13	177.00	122.05	8.49
Gly	G	132	45.16		173.87	110.00	8.43
Tyr	Y	133	58.22	38.83	175.77	120.36	8.09
Gln	Q	134	55.36	29.85	174.89	122.81	8.25
Asp	D	135	54.25	41.11	175.54	121.77	8.26
Tyr	Y	136	57.53	39.06	175.10	120.55	8.06
Glu	E	137	53.57	30.29	173.72	125.50	8.28
Pro	P	138	62.96	32.23	176.90		
Glu	E	139	56.60	30.37	175.43	121.66	8.54
Ala	A	140	53.80	20.23		130.99	8.02

Curriculum Vita

Lijuan Kang

Education

9/2002 – 7/2006 B.S. in Chemistry, Sun Yat-Sen University, Guangzhou, China

8/2006 – 10/2012 Ph. D. in Chemistry and Chemical Biology, Rutgers, the state university of New Jersey, Piscataway, NJ

Experience

8/2006 – 9/2012 Graduate and Teaching assistance, Rutgers, the State University of New Jersey, Piscataway, NJ
6/2009 – 6/2012 Lab Safety Officer, Rutgers, the State University of New Jersey, Piscataway, NJ

Publications

Lijuan Kang, Kuen-Phon Wu, Michele Vendruscolo and Jean Baum (2011)
"The A53T mutation is key in defining the differences in the aggregation kinetics of human and mouse α-synuclein." J. Am. Chem. Soc. 133, 13465–13470

Lijuan Kang, Gina M. Moriarty, Lucy A. Woods, Alison E. Ashcroft, Sheena E. Radford and Jean Baum (2012)
"N-terminal acetylation of α-synuclein induces increased transient helical propensity and decreased aggregation rates in the intrinsically disordered monomer", Protein Science 21, 911-917 (highlighted)

Lijuan Kang and Jean Baum
"Secondary structure propensity, not global conformation, play a key role in modulate the growth rate of human and mouse α-Synuclein variants", Manuscript in Preparation

Kuen-Phon Wu, Maria Janowska, Lijuan Kang, Lucy A. Woods, Alison E. Ashcroft, Sheena E. Radford and Jean Baum
"Release of head-to-tail intramolecular and inter-chain contacts of α-synuclein leads to rapid aggregation", Manuscript in Preparation